University of Trento
Università of Brescia
University of Bergamo
University of Padova
University of Trieste
University of Udine
University IUAV of Venezia

Ivan Giongo

ROLE OF TIMBER DIAPHRAGMS IN THE SEISMIC RESPONSE OF UNREINFORCED MASONRY (URM) BUILDINGS

Prof. Maurizio Piazza

Prof. Jason Ingham

April, 2013

UNIVERSITY OF TRENTO

Engineering of Civil and Mechanical Structural Systems

Ph. D. Head's prof. Davide Bigoni

Final Examination 29 / 04 / 2013

Board of Examiners

Prof. Egidio Rizzi (University of Bergamo)

Dr. Dennis Kochmann (California Institute of Technology)

Prof. Spyros Karamanos (University of Thessaly)

Dr. Giovanna Concu (University of Cagliari)

ACKNOWLEDGEMENTS

I would like to gratefully thank my supervisors Maurizio Piazza and Jason Ingham for the support and trust that they have provided to me. I would like to express my sincere gratitude to Roberto Tomasi for his help and advice during these years.

I am also grateful to the members of the Timber Research Group of the University of Trento for their friendship: Ermanno Acler, Mauro Andreolli, Daniele Casagrande, Paolo Grossi, Cristiano Loss, Andrea Polastri, Simone Rossi and Tiziano Sartori.

I am thankful to the former undergraduate students Daniele Bertoldi, Lorenzo Dallavalle, Alfredo Rizzardi, Carlo Rodegher e Francesca Pintarelli for their precious help.

Many thanks are also extended to Dmytro Dhizur. Without his support it would not have been possible for me to conduct any experimental test at the “other side of the World”. Adolfo Preciado Quiroz and Kevin Walsh are thanked for their help with the diaphragm testing. Thanks are extended to Yuri Dhizur and Igor for their tireless assistance during almost all the Whanganui experience. New Zealand Natural Hazards Research Platform is gratefully acknowledged for providing funds for the diaphragm project.

Part of the research presented in this thesis has been carried out within the framework of the RELUIS Project which is financed by the Italian Emergency Management Agency.

Rothoblaas Company and Heco Company are thanked for providing the mechanical fasteners used in the campaign on the screw pressure. The assistance of the technicians of the Laboratory for Material testing of the University of Trento is also sincerely appreciated.

SUMMARY

The research presented in this thesis was focused on timber floor diaphragms in unreinforced masonry (URM) buildings. The work was divided into two phases. The first phase was aimed at the investigation of the effects of the in-plane behavior of timber diaphragms on the global seismic response of URM buildings. The second phase was dedicated to the assessment and retrofit of timber floors, with particular attention to the out-of-plane behavior.

A study on the equivalent frame method, which is a more and more appreciated masonry modeling technique, is presented. Both as-built and strengthened timber floors were addressed. In order to understand the influence of the masonry modeling method on the seismic response of URM structures when flexible diaphragms are concerned, a simplified elastic no tension method was proposed. Such method is able to describe the characteristic nonlinear behavior of masonry (due to extremely low tensile strength) by means of a series of linear analyses based on a Rankine failure criterion.

An *in-situ* testing campaign on full-scale 100 year old timber diaphragms is presented. Both mechanical and dynamic in-plane properties of wood diaphragms were investigated. Cyclic and snap back tests were carried out thanks to an innovative *ad hoc* loading system, developed by means of wire ropes and steel pulleys. The loading system was designed to reproduce a realistic inertial load distribution and to be lightweight, versatile and easily relocatable from one diaphragm section to the next. The effect of different refurbishment techniques was also probed during the experimental campaign.

The outcomes of a testing campaign regarding out-of-plane refurbishment techniques of existing timber floors by means of timber to timber composite structures are described. A numerical model based on the theory of composite beams with incomplete interaction, was calibrated to take into account the real load distribution and connector spacing.

An original procedure to camber timber beams by employing the compression pressure generated by screw fasteners is presented. The camber deflection is attained by superposing a timber reinforcement element on top of a beam and then connecting the two elements by means of screws inserted at 45° to the beam axis. Such method which is currently patent pending, was validated using data obtained from experimental testing. A mathematical formulation was also developed to describe the cambering procedure. A specific experimental campaign was therefore performed to precisely evaluate the amount of pressure that each screw is capable of yielding. Many parameters supposed to affect the compression force, were explored through 170 tests.

INDEX

1 INTRODUCTION

Earthquakes have constantly highlighted in several parts of the World (e.g. Italy, Turkey, Greece, Portugal, New Zealand), that unreinforced masonry structures are a major source of life-loss and damage, particularly when timber diaphragms are present. Historic city centers of most Countries, are in fact comprised of URM buildings with timber diaphragms. Although each Country has its own peculiar typology of timber floors and different refurbishment techniques, it is possible to identify common behaviors and similar problems, especially when seismic hazard is concerned.

The seismic response of a masonry structure in fact is strictly related to the ability to behave as “box” with all its components which collaborate in resisting to the horizontal actions. Such behavior depends on the quality of the connections between the different structural elements and on the horizontal diaphragm in-plane stiffness. When the connection system between floor diaphragms and adjacent walls is deficient, the walls behave independently and local out-of-plane collapse mechanisms which involve overturning of the walls may be observed (Fig. 1.1).

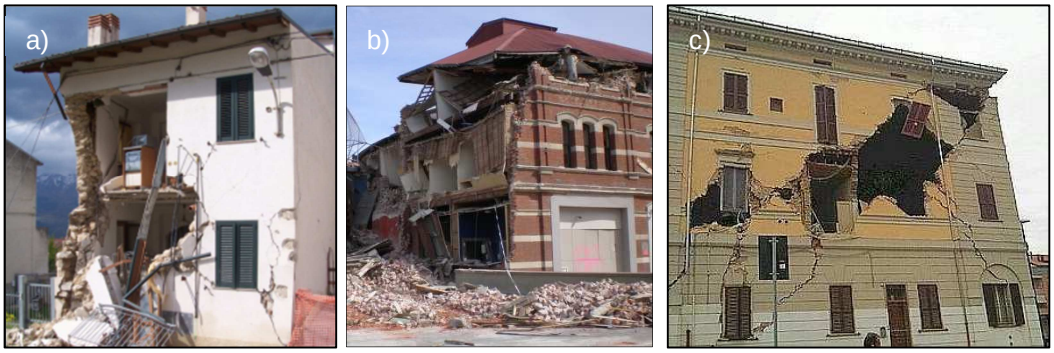

Fig. 1.1 Out-of plane failure of masonry walls: a) L’Aquila Earthquake, Italy (2009) [Bursi et al. (2009)]; b) Christchurch Earthquake, New Zealand (2011) [Dizhur (2011)]; Emilia, Italy Earthquake (2012) [www.adnkronos.com].

If the diaphragm-to-wall connections are adequate, then it is the in-plane stiffness that becomes the governing parameter in determining the global behavior of masonry buildings. By considering two limit cases, quite different seismic responses can be registered. In the presence of rigid diaphragms, the horizontal forces are distributed on

the resisting walls accordingly to the wall stiffness and to the wall position. In case of infinitely flexible diaphragms the horizontal force component that is transferred on a masonry pier, depends on the wall tributary area with respect to vertical loads. Therefore, it is a matter of basic importance to understand where the real condition falls.

The need to increase timber diaphragm stiffness and strength has generated, in the past times, strengthening solutions which recent earthquakes have demonstrated to be inadequate or, in some cases, even unfavorable. As a matter of fact, the substitution of timber floors with concrete ones and the insertion of a concrete curb “inside” the wall thickness, could yield significant self-weight increase and weakening of the existing masonry walls (Fig. 1.2).

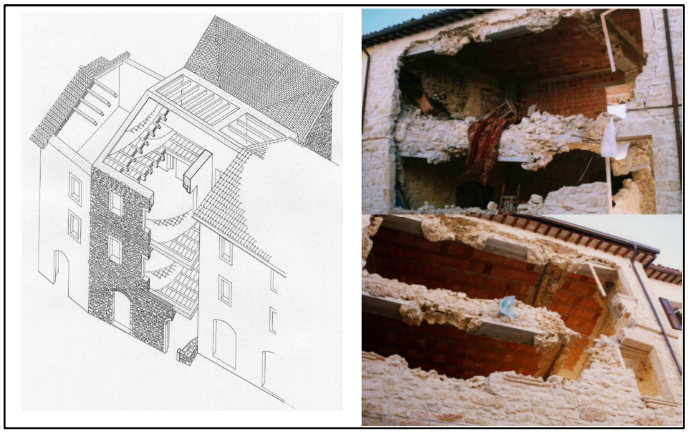

Fig. 1.2 Umbria Marche Earthquake, Italy (1997): Collapse mode observed in masonry building reinforced by substituting existing timber floors with new concrete ones. [Borri, (2007)]

Therefore, after recent earthquakes, some floor refurbishment techniques have been reconsidered. Currently the Italian standard code on existing buildings, bans the possibility of inserting a concrete curb in the depth of the existing walls, and suggests alternative strengthening methods to be used for horizontal diaphragms. Among such methods, those which permits to improve both in-plane and out-of plane behaviors should be preferred.

Old timber floors in fact, were designed to bear moderate loads and may suffer from excessive deflections with respect to current requirements. In the past, the stiffening and strengthening of wooden floors has been often achieved by using a reinforced concrete slab over the timber decking with a steel mesh connected to the timber joists. The

aforementioned technique has some shortcomings concerning mainly the increase of dead load and the need for an additional structural depth over the existing decking. Moreover, it does not meet the requirement of “reversibility”, coming from the heritage administration agencies. Therefore, recently the interest in “dry”, “reversible” strengthening techniques (where the existing timber beams are coupled with thick timber planks, connected with different kinds of connection systems) has been aroused.

1.1 Thesis Outline

As mentioned in the summary, the research work has been organized into two parts. The first part pertains to the assessment of the timber diaphragm in-plane behavior and the analysis of the influence of flexible diaphragms on the global seismic response of traditional URM structures. In the second part of the thesis the out-of-plane behavior of wood floors is addressed, with keen attention to timber to timber refurbishment techniques.

PART 1

Pushover analysis of traditional masonry buildings: influence of refurbished timber-floors stiffness

The main purpose of Chapter 2 is to evaluate the effects that in-plane stiffness of different types of wooden diaphragms, yield on the capacity curve of a traditional masonry building, obtained by means of a nonlinear static (pushover) analysis. In order to determine it, an equivalent-frame modeling is employed to schematize a two-story building, the like of which is fairly common in the Italian building legacy. Both as-built and retrofitted wood floor types is taken into account. As to better understand and control all the aspects that rule the global seismic behavior of a masonry construction, a general-purpose finite element (FE) software is adopted. Therefore every "feature" is manually implemented.

Proposal of a simplified Elastic No Tension method for the seismic evaluation of URM buildings with flexible diaphragms

The goal of Chapter 3 is to deepen the understanding of the influence of the modeling technique on the evaluation of the seismic response of URM structures with timber diaphragms. For this purpose a simplified elastic no-tension (ENT) method for modeling masonry structures is proposed and adopted in order to perform push-over nonlinear analysis in function of different parameters of the building. According to such ENT-like method, after each load step all the finite elements which are outside a Rankine failure

surface are eliminated, and the analysis is repeated with an updated geometry of the model. A “globally nonlinear” behavior is therefore depicted through a series of linear analyses. Another aspect that is analyzed, is whether timber diaphragm can be treated as “linear materials” when it comes to the global seismic analysis of a masonry building. Therefore a procedure to take into account wood diaphragm nonlinear behavior is proposed and validated on experimental data pertaining to both as-built and retrofitted timber floor typologies.

Parametric analyses on timber diaphragm in-plane behavior

A parametric study on single straight sheathed diaphragms is reported in Chapter 4. The structural analysis software SAP2000 [CSI 2004] is employed to develop a nonlinear model which is validated on experimental data from tests previously carried out at the University of Trento. Special attention is paid to the floorboard disposition and to the diaphragm deformed shape. To evaluate diaphragm deformations, an analytical formulation based on the revision of existing approaches is proposed and validated through the finite element model.

Experimental campaign on the in-plane properties of timber diaphragms

Despite the evaluation of both mechanical and dynamic in-plane properties of existing timber diaphragms is a crucial point when assessing URM buildings, extremely few data are available in the literature, since realizing full-scale tests in an ancient building means extra difficulties usually not present in a laboratory environment. To address the paucity of available in-situ test data, an experimental campaign was executed to investigate the as-build cyclic and dynamic behavior of full-scale vintage flexible timber floor diaphragms with the outcomes being presented in Chapter 5. The campaign was conducted during an exchange period at the University of Auckland. Two sections of a diaphragm located in a vintage URM building in the city of Whanganui, were subjected to a series of cyclic and snap back tests in the direction orthogonal to the floor joists. In order to reproduce a realistic inertial load distribution to the test specimens, an ad hoc loading system was developed. The test results are compared to the provisions contained in international seismic assessment documents [FEMA 356, ASCE 41-06, NZSEE (2011)]. A method of estimating the natural period of timber flexible diaphragm is proposed in order to improve the evaluation of the diaphragm shear transfer.

PART 2

Experimental tests on timber-to-timber strengthening methods for improving the out-of-plane behavior of existing wood diaphragms

In order to address the issue of improving the strength and the stiffness of timber floor diaphragms not only to face in-plane forces but also to bear out-of plane loads, an experimental campaign on timber-to-timber strengthening solutions, is presented in Chapter 6. The reinforcement elements consisted of thick timber planks which were arranged on top of the timber flooring and secured to the beam joists by using screw fasteners. Four different configurations of the connection system were tested. Experimental data are compared with theoretical values obtained through the theory of composite beams with incomplete interaction developed by [Newmark et al.] and through the approach suggested by [EN 1995]. A specific numerical model is realized in order to take into account both the real load distribution and the connectors spacing. Parametric analyses were performed in order to investigate the influence of these parameters on the global behavior. With regards to the Serviceability Limit State, particular attention was paid to the midspan deflection of the tested floors.

Proposal of a new method for cambering timber composite beams by means of sole screws

The possibility of cambering a timber beam by simply putting another beam on top of it and inserting screws inclined at 45° relative to the beam axis is investigated in Chapter 7. To this purpose, three experimental tests were performed at the Laboratory of the Department of Mechanical and Structural Engineering (DIMS) of the University of Trento and the results are reported. After the calibration of a numerical model to help in understanding the "cambering phenomenon", an analytical formulation is proposed. The cambering procedure proved to be more effective when the fastener are inserted starting from the internal part of the beam, permitting to obtain significant values of upward deflection.

Experimental campaign on the compression pressure developed by screw fasteners

The effectiveness of the original cambering method presented in Chapter 7 is based on the capability of self-tapping screws to induce an internal stress-state in timber elements during the drilling procedure. The horizontal component of the resultant pressure yielded by the inclined screws is directly related to the possibility to hog the composite system. An extensive experimental campaign aimed at determining the values of the internal stresses induced by different type of screw fasteners is described in Chapter 8. The

influence of different parameters such as screw size, screw angle, initial pressure, connector typology, wood density and time-dependence is studied.

1.2 References

ASCE-SEI 41/06, (2007) *Seismic rehabilitation of existing buildings*, American Society of Civil Engineers, Reston, Va.

Bursi O. S., Dusatti T., Pucinotti R., (2009) *A Reconnaissance report. The April 6, 2009, L'Aquila Earthquake. Italy*

CSI [Computers and Structures Inc.], (2004), *CSI Analysis Reference Manual For SAP2000*®, ETABS®, and SAFE®. CSI, Berkeley

Dhizur D., (2012) *In-situ testing of Unreinforced Masonry Building in Whanganui*, Research Symposium, University of Auckland, 12/11/2012

EN 1995-1-1, (2004), Eurocode 5: Design of timber structures - Part 1-1: General – Common rules and rules for buildings.

FEMA 356, (2000), *Prestandard and Commentary for the Seismic Rehabilitation of Buildings,* American Society of Civil Engineers and Federal Emergency Management Agency, Reston, VA

NZSEE, (2011), *Assessment and Improvement of Unreinforced Masonry Buildings for Earthquake Resistance*, New Zealand Society for Earthquake Engineering, Wellington, New Zealand

Newmark N.M., Siess C.P., Viest I.M., (1951), *Tests and Analyses of Composite Beams with Incomplete Interaction. Proceedings, Society for Experimental Stress Analysis, Vol. 9, No. 1, 75-92*

PART 1

2 PUSHOVER ANALYSIS OF TRADITIONAL MASONRY BUILDINGS: INFLUENCE OF REFURBISHED TIMBER-FLOORS STIFFNESS

2.1 Introduction

It is utterly acknowledged (with no need to mention the effects of recent seismic phenomena) how important it is for structural designers to know and master a reliable, simplified method able to analyze the global seismic response of masonry buildings. Several studies have shown that masonry is highly nonlinear, even for low levels of stress. As a result, linear elastic methods are not fit to represent it. Recently, new techniques are getting more and more widespread, i.e. the so-called macro-elements methods. The main advantage of these methods, with respect to techniques based on shell or solid nonlinear finite-elements, is the decrease in run-time analysis due to the concentration of all the nonlinearities in some specific points. Furthermore, referring to equivalent-frame structures allows designers to deal with simplified constitutive laws and failure criteria. In order to "capture" the real global behavior of a traditional building, it is necessary to optimize these numerical models through parametric analyses which investigate numerous aspects that might affect the seismic performance, from frames geometry to lateral loads distribution etc.. Once one has defined how to schematize the masonry skeleton he/she needs to model horizontal diaphragms, whose in-plane stiffness plays an undeniable key-role in distributing seismic lateral loads to the resisting walls. As a matter of fact it is expected that the more the in-plane stiffness grows, the more the collaboration between systems of piers increases. In addition, earthquake damages have demonstrated that the in-plane stiffness of horizontal diaphragms often influences the out-of-plane walls response, by determining the type of local mechanism occurring (II mode mechanisms). Nevertheless, as this chapter regards the global seismic performance, no results are reported concerning this matter.

2.2 The modeling

2.2.1 The building

The numerical model used to investigate the effects that the real in-plane stiffness of wooden floors yields on seismic behavior of masonry buildings, is based on the so-called "equivalent frame" method. Consequently every pier and every spandrel is schematized with an elastic frame element. The mechanical nonlinearities are concentrated in particular cross-sections (plastic hinges) placed both in the middle and in the ends of the elastic frames. Since the analysis of real “post-earthquake” masonry buildings has shown that most of the damages do not involve the intersections between piers and spandrels, rigid offsets are inserted where the vertical elements meet the horizontal ones. The length of these offsets depends on the geometry of the openings (windows and doors). In particular the effective height of a pier (correspondent to the elastic part of the frame) has been deduced from a formula developed by Dolce in 1989 [Dolce (1989)]. Referring to the in-plane behavior of walls, the bottom ends of the vertical frames (piers) have been modeled as fixed (FEMA 356). On the other hand, considering the global seismic performance of masonry buildings, the out-of plane stiffness of the walls has been regarded as negligible and therefore moment releases have been introduced at both ends of the piers (FEMA 356).

2.2.1.1 Piers

According to Magenes and Calvi [Magenes and Calvi (1997)], three different failure criteria have been considered: rocking, sliding and shear cracking. The following formulae have been used:

- Rocking:

$$M_u = \frac{P \cdot D}{2}\left(1 - \frac{p}{k \cdot f_u}\right) \qquad \textit{(Eq. 2.1)}$$

where M_u = moment of resistance, P = axial load (concentrated), D = pier length, p = P/Dt, t = pier thickness, f_u = compressive strength of masonry, k = parameter depending on the stress distribution assumed at the pier base (k = 0.85).(Eq. 2.1), is the same proposed in the Italian Code NTC 2008.

- Sliding:

$$V_d = Dt\left[\left(1{,}5c + \mu p\right) / \left(1 + 3\frac{c\alpha_v}{p}\right)\right] \qquad \textit{(Eq. 2.2)}$$

where V_d = "the ultimate load of a wall" [Magenes and Calvi (1997)], c,μ = mechanical parameters related to the Mohr-Coulomb criterion, α_v = *M/VD (shear ratio)*, *M,V* = moment and shear forces acting on the pier.

- Shear cracking:

$$V_u = \frac{f_{tu} \cdot D \cdot t}{b}\sqrt{1 + \frac{p}{f_{tu}}} \qquad \textit{(Eq. 2.3)}$$

where $V_u = V_d$, f_{tu} = tensile strength of masonry, b = coefficient depending on the shear distribution at the central cross-section of the pier (b = 1 for uniform shear distribution, b = 1.5 for parabolic distribution). The tensile strength f_{tu} is assumed to be equal to 1.5 times the mean shear strength of masonry f_{mv0} (under zero compressive stress). (Eq. 2.3) is consistent with the formula suggested by the former Italian code O.P.C.M. 3431 for existing buildings.

In accordance with the suggestions contained in D.M. 14-01-2008 an elastic-perfectly plastic law has been assumed for both flexural and shear behavior. The post-elastic state has been modeled by means of rigid-perfectly plastic hinges [Pasticier et al. (2007)]. A "rocking hinge" has been inserted at each end of the elastic part of the frames (their activation occur when moments acting on these extremities reach M_u), with no limits on deformation. Although the Italian Code [D.M. 14-01-2008] prescribes an ultimate rotation corresponding to a lateral deflection of 0.8% of the height of the pier, an indefinitely plastic behavior has been preferred. This choice is due to two reasons. First of all one should determine *a priori* which quota of the ultimate lateral deflection has to be assigned to each hinge. Moreover, this presupposes that the ratio between the bending moments acting on the ends of the elastic part of the walls is known at every step. Secondly, a lateral deflection of 0.8% of the height of the piers, means a displacement greater than 20 mm (for walls higher than 2.5 m) which is unlikely to be attained. As a matter of fact, the same Code proposes that in case of shear mechanisms, the maximum lateral deflection has to be limited to 0.4% of the height of the pier. This implies that, for the case study analyzed (two-story building), when one wall reaches the target of 0.8%, the total base shear has already diminished of more than 20% (owing to shear failure) and therefore [D.M. 14-01-2008] the pushover analysis has already been stopped. A shear hinge has also been introduced at the mid-

span of the frames (as the external loads have been applied to the nodes of the frame, the shear diagrams are uniform). The hinge is activated by the minimum value between $V_{d,top}$, $V_{d\ bottom}$, and V_u ($V_{d,\text{top}}$/ $V_{d\ bottom}$ corresponds to V_d with α_v calculated at the top/bottom section of the elastic part of the pier). According to the Italian Code, the shear plastic phase has been limited to a maximum drift of 0.4% of the pier-height.

The values of p and α_v, maintained constant during the analyses, have been deducted from a linear static procedure.

2.2.1.2 Spandrels

Two "rocking hinges" without any limits to deformation have been added to the elastic ends of the spandrels. The ultimate moment M_u that activates the hinges, has been determined as suggested in NTC 2008:

$$M_u = H_p \frac{h}{2}\left[1 - H_p / \left(0{,}85ht\right)\right] \qquad \text{(Eq. 2.4)}$$

where H_p = $0.4f_{hm}ht$, f_{hm} = mean compressive strength of masonry in the horizontal direction, h = height of the spandrel, t = thickness of the spandrel. Like for the piers, a "shear hinge" has been inserted at the center of the frames schematizing the spandrels. This hinge (indefinitely plastic) is activated when the shear force reaches the minimum value between the following two criteria:

$$V_p = \frac{2M_u}{l} \qquad \textit{(Eq. 2.5)}$$

$$V_t = h \cdot t \cdot f_{vm0} \qquad \textit{(Eq. 2.6)}$$

where f_{mv0} = the mean shear strength of masonry (under zero compressive stress), l = length of the spandrel.

2.2.1.3 Reinforced Concrete Stringcourses

Reinforced concrete stringcourses have been modeled at the top of every level, with a bi-linear elastic perfectly-plastic constitutive law. As like piers and spandrels, so RC beams have been schematized through elastic frames with rigid offsets at the extremities. Two "rocking hinges" (rigid, perfectly- plastic, without any restrictions on deformation) have consequently been added at the ends of the elastic part of the

beams. The failure criterion has been deducted from European Standard: Eurocode 2 [UNI EN 1992-1-1].

2.2.2 The wooden floors

In order to study the influence that the in-plane stiffness of wood diaphragms has on the global behavior of a masonry building under seismic condition, different types of unreinforced/reinforced floors have been modeled. The mechanical properties of floors have been derived from an experimental campaign previously carried out at the Laboratory of the Department of Mechanical and Structural Engineering (DIMS) of the University of Trento [Piazza et al. (2008), Baldessari et al. (2009)]. Only the membrane behavior of floors has been taken into account, by means of nonlinear, two-dimensional finite elements. Considering the test set-up (Fig. 2.3), an equivalent shear stiffness G_{eq} has been calculated from the experimental data, regarding the diaphragm deformation as equal to the shear deformation of a simply supported beam under a uniform load distribution.

$$G_{eq} = \frac{\chi \cdot \Delta W \cdot L}{8 \cdot B \cdot t \cdot \Delta f} \qquad \textit{(Eq. 2.7)}$$

where χ = the shear factor = 1, L = floor span perpendicular to the load direction, B = floor span parallel to the load direction, t = floor (membrane) thickness, ΔW = lateral load applied [N], Δf = mid span deflection.

2.3 The experimental data

The experimental data pertain to a campaign conducted on six different types of wooden diaphragms (Fig. 2.1). Both monotonic and cyclic tests were been carried out on full scale specimens (5×4 m). The overall test set-up is shown in Fig. 2.3, while in Fig. 2.4 the experimental results are reported in terms of a total load Vs. mid-span displacement curve, for every type of tested floor. Every shear stress/strain law has been validated through FEM models of the tested specimens, based on nonlinear shell elements (with just membrane behavior). In Fig. 2.2 it is depicted, e.g. for the double floor, the good agreement between experimental and numerical behavior (external load Vs. mid-span displacement).

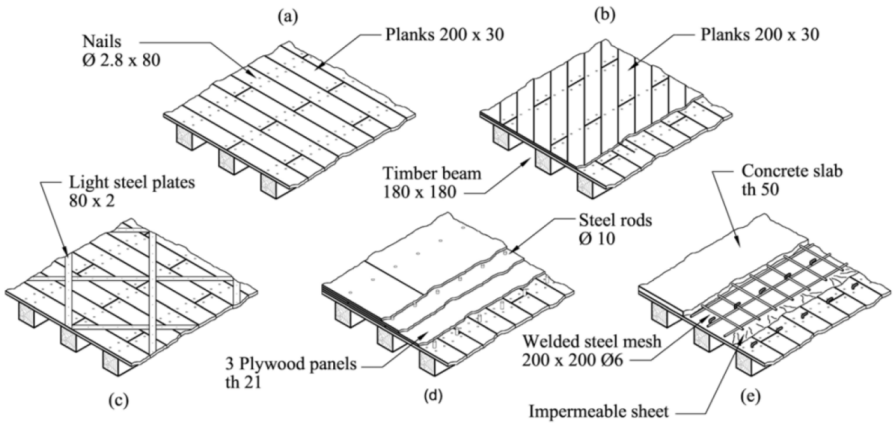

Fig. 2.1 Different timber-floor in-plane-shear strengthening techniques: (a) existing simple layer of wood planks on the timber beams; (b) second layer of wood planks crossly arranged to the existing one and fixed by means of steel studs; (c) diagonal bracing of the existing wood planks by means of light steel plates or FRP laminae; (d) three layers of plywood panels glued on the existing wood planks; (e) a stud−connected reinforced concrete slab (all measures in mm)

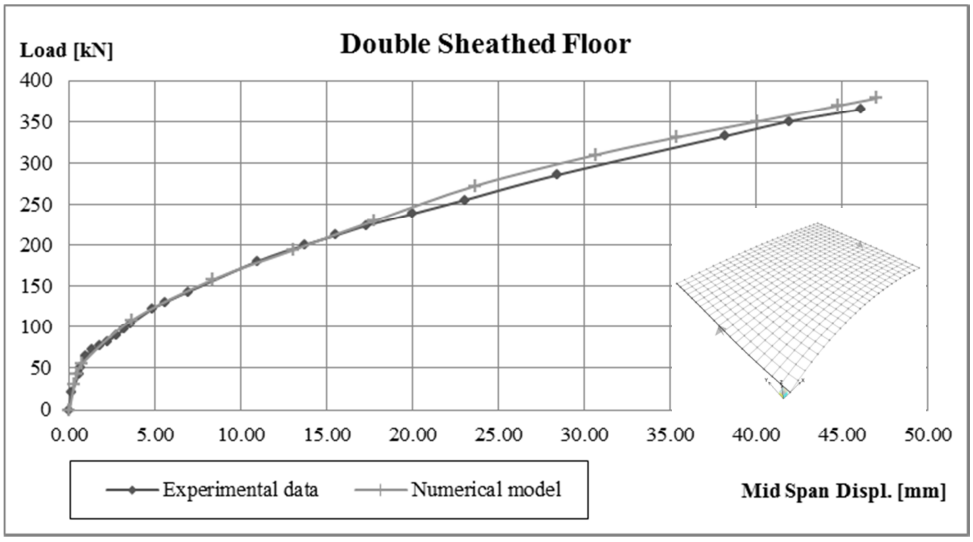

Fig. 2.2 Validation of numerical floor-models

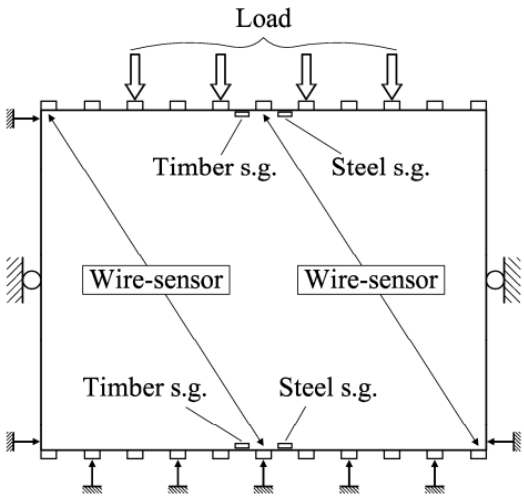

Fig. 2.3 The test apparatus

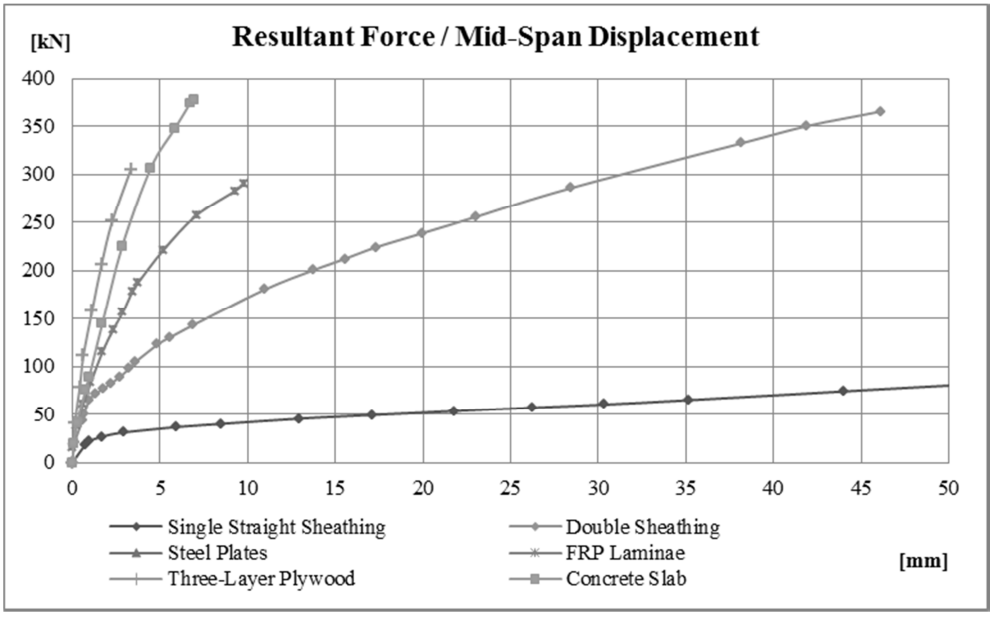

Fig. 2.4 In-plane behaviour of tested floors

2.4 Case study building

The masonry building selected for the parametric analyses has been found in the literature [Righetti and Bari (1993)]. The choice has been prompted by the need of analyzing a masonry construction neither extremely irregular (the results would have been too dependent on the specific structure studied), nor particularly regular (as not to be too dissimilar from "real buildings"). Furthermore, since the structure is a two-story building, it is possible not to consider the variation in axial forces that the development of the pushover analysis yields; as suggested by the Italian Code in its former version [OPCM 3431].

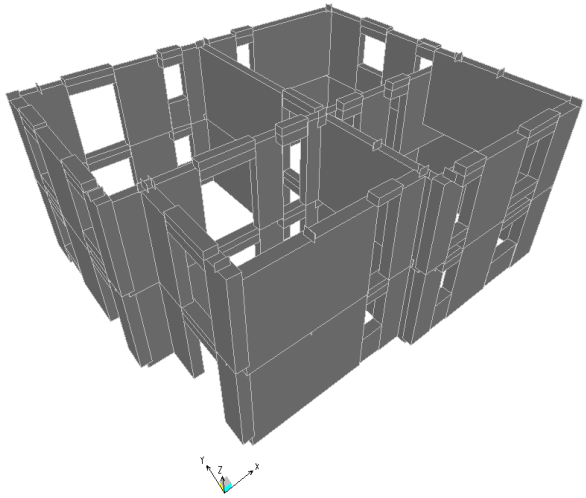

Fig. 2.5 Analyzed building

Weight density of masonry	γ_m	18	kN/m^3
Characteristic compressive strength of a brick	f_{bk}	10	MPa
Characteristic compressive strength of masonry	f_k	4.5	MPa
Characteristic shear strength of masonry (under zero compressive stress)	f_{vk0}	0.2	MPa
Elastic modulus of masonry	E	4500	MPa
Shear modulus of masonry	G	1800	MPa
Mean compressive strength of masonry	f_m	6.5	MPa
Mean shear strength of masonry (under zero compressive stress)	f_{vm0}	0.3	MPa
Mean compressive strength of masonry (horizontal direction)	f_{hm}	2.0	MPa

Friction parameter	μ	0.4	

Tab. 2.1 Mechanical properties of masonry

Weight density of concrete	γ_c	24	kN/m^3
Characteristic compressive strength of concrete	R_{ck}	30	MPa
Elastic modulus of concrete	E	30	GPa

Tab. 2.2 Mechanical properties of concrete

2.5 The analyses

2.5.1 The parametric analyses

Together with the in-plane stiffness of wooden floors, many other parameters that affect the global seismic behavior of a traditional building, have been analyzed. As to evaluate the influence of spatial variability of the seismic ground motions, the mass center has been moved into different positions ($\Delta x = \pm 0.54$ m, $\Delta y = \pm 0.66$ m) as counseled by the Italian Code. No differences have been observed in the static pushover curves related to different positions of the mass center (hypothesis of rigid diaphragm).

Two different lateral load patterns have also been applied during the pushover analyses: an inverted triangle (first mode) load pattern and a mass proportional one. While in the *y* direction the two patterns have produced no effects on the capacity curve, in the *x* direction the maximum base shear shows a difference greater than 30%. As one can see from Fig. 2.6, the mass proportional pattern stresses the first story more than the other (there are more active hinges), delaying the formation of plastic hinges in the upper story. This, considering that the global failure (*x* direction) is always a second-story mechanism, generates an increase in resistant base shear. It would appear that the following sentence contained in the ASCE Standard [ASCE/SEI 41-06]: *"Recent research [FEMA 440 (FEMA 2005)] has shown that multiple load patterns do little to improve the accuracy of nonlinear static procedures and that a single pattern based on the first mode shape is recommended"* does not fit the studied building.

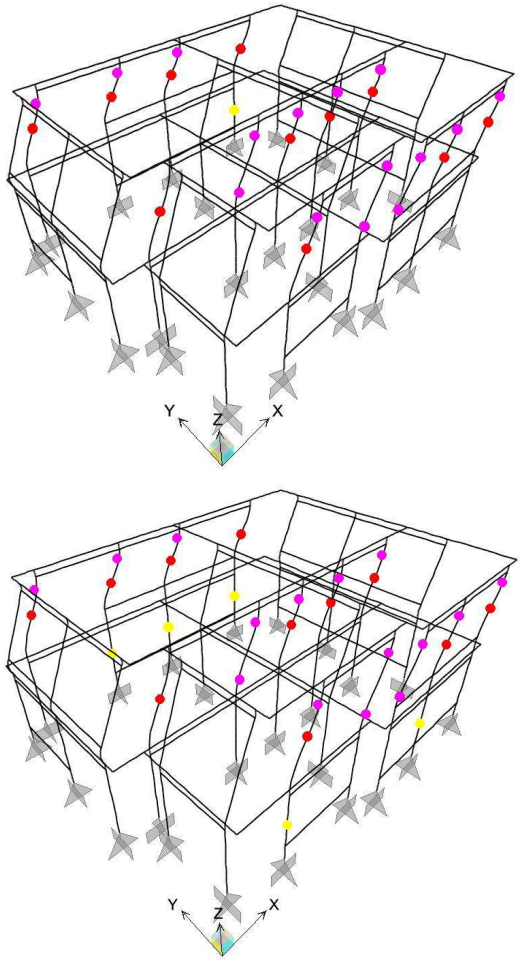

Fig. 2.6 X direction deformed shape - (Inverted triangular load pattern on the left; mass proportional load pattern on the right) - Plastic hinges: purple = rocking hinge, red = hinge that has reached the deformation limit, yellow = bottom shear hinge, orange = top shear hinge

In order to determine the effects that the stiffness of the stringcourses induces on the seismic performance of an existing building, the elastic modulus of concrete has been varied, from the one of un-cracked material (30 GPa) to zero (the MOE used in all the other models has been 15 GPa, corresponding to the cracked material). Neither the base shear, nor the control point displacement have shown appreciable sensitivity to stringcourses stiffness. Only a predictable reduction in "global elastic stiffness" has been observed as the MOE value has decreased (Fig. 2.7).

Another aspect to be stressed is the different "plastic demand" related to the spandrels. When concrete stiffness is that of cracked material, the global failure occurs with all the

spandrels in the elastic phase. On the other hand (as expected) if one neglects stringcourses stiffness, "rocking hinges" are activated at the ends of some spandrels. On the contrary, regarding stringcourses as un-cracked, yields the activation of plastic hinges in the stringcourses themselves.

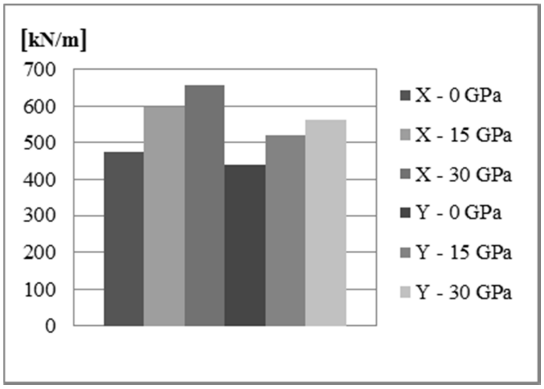

Fig. 2.7 Global secant elastic stiffness vs. concrete MOE

It has also been studied what happens when the coupling actions of both spandrels and stringcourses is not taken into account and the masonry walls are modeled as cantilever beams (Fig. 2.8). These simplifying assumptions are frequently employed in Linear Static Procedures by designers and it is commonly believed that they lead to a higher level of safety than that attainable with a frame model. From a "resistance point of view" this is certainly true, in fact (as one might expect) a decrease of more than 35% in maximum base shear has been observed in both directions. Nevertheless, the application of a Non Linear Static Procedures requires a displacement check. Since the "cantilever beams" hypothesis produces an increase of almost 200% in ultimate displacement of control point (Fig. 2.9), it would appear that disregarding the coupling effect of spandrels could induce to overestimate the ductility resources of a masonry building.

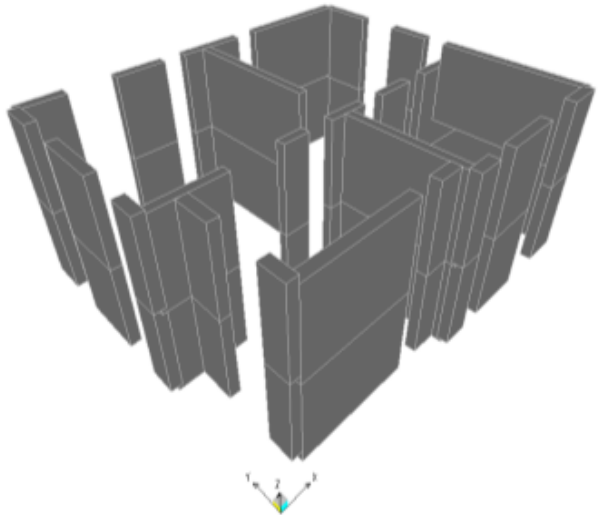

Fig. 2.8 Cantilever beams model (soft spandrel hypothesis)

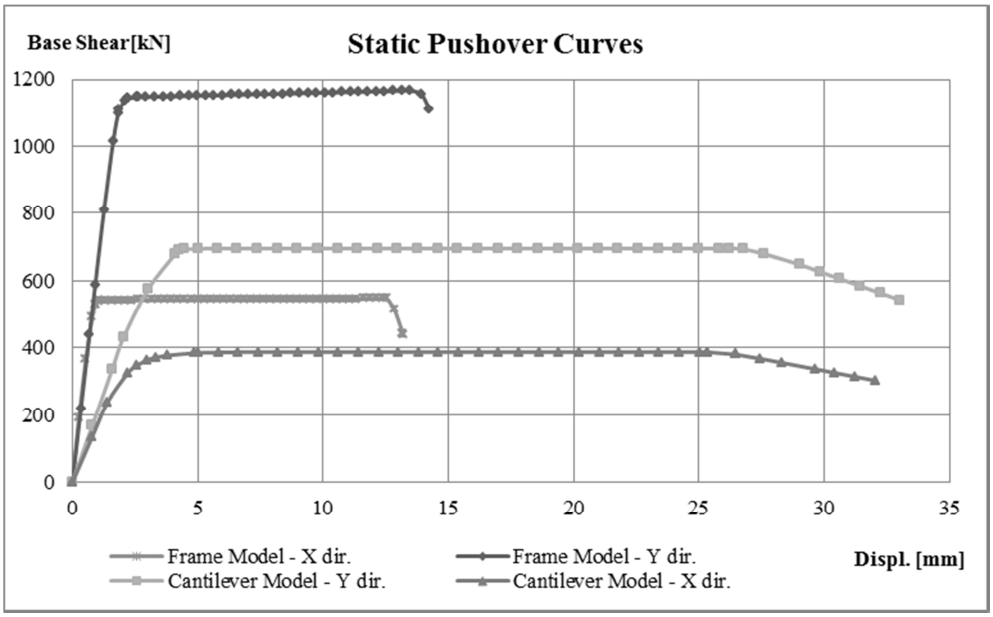

Fig. 2.9 Comparison between the seismic performance of equivalent-frame model and cantilever-beams model

Another aspect subjected to investigation has been the possible birth of fictitious internal forces, owing to the rigid links that connect orthogonal systems of walls. So as to seek the effects of these links, a model of the building with none of them has been created (rigid diaphragm hypothesis, Fig. 2.11). From the results (Fig. 2.12) it is possible to see that in *y* direction the removal of the links, reduces both the global elastic stiffness and the maximum base shear. As one might expect, it would appear that those reductions are due to a less restrained building. Nonetheless, in *x* direction, an increase in total shear resistance has been observed. A reason may be that if one eliminates the coupling action generated by the links, then the bending stresses at the top of the piers grow (under the same level of lateral loads); this leads to an extension of the effective length of compression, strictly related to a variation of α_v, that makes the shear resistance ($V_{d,top}$) raise. Since the global failure mechanism, in *x* direction, is associated with the formation of shear hinges at the top of the second-story piers, an increase in maximum base shear should therefore be considered plausible.

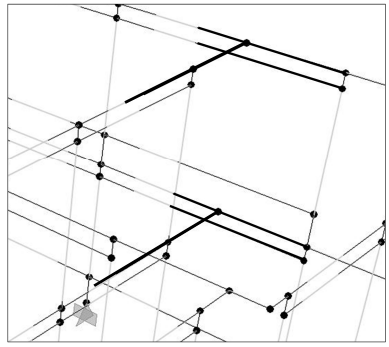

Fig. 2.10 Rigid links connecting orthogonal systems of walls

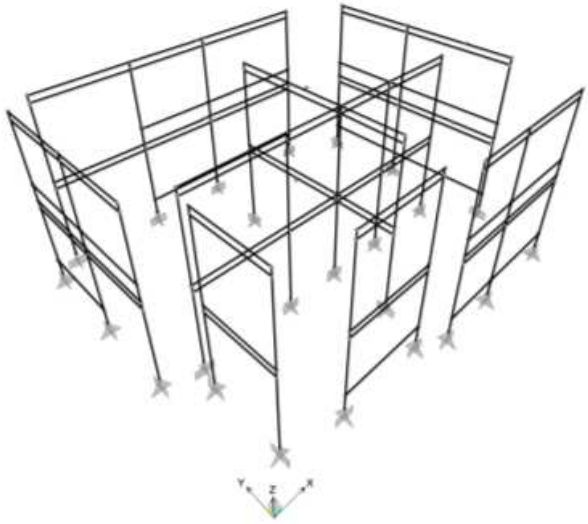

Fig. 2.11 Model without any link between perpendicular systems of walls

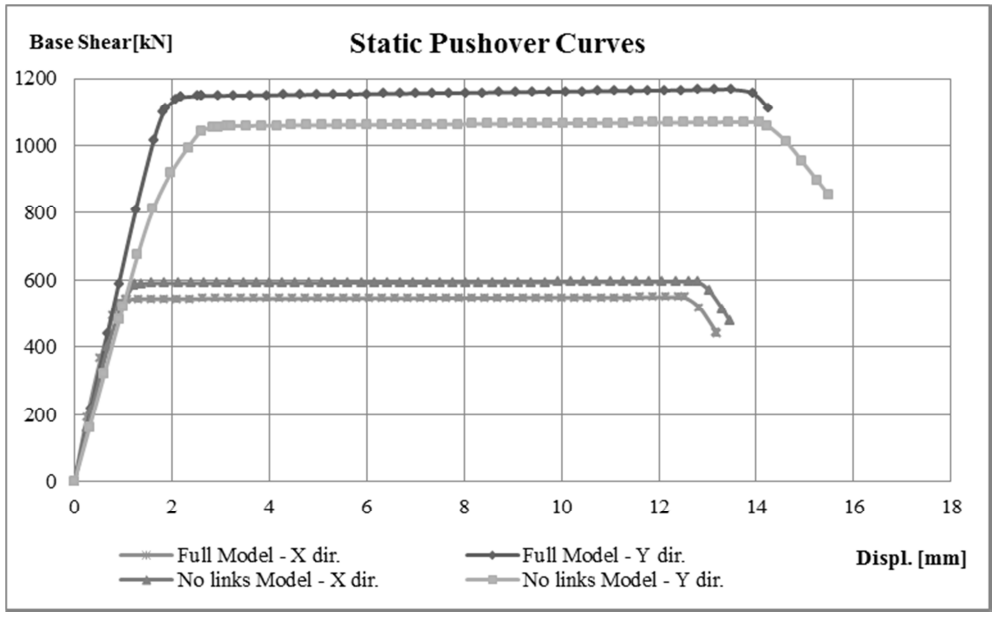

Fig. 2.12 Comparison between full model and no-links model

2.5.2 Influence of diaphragms stiffness

In Fig. 2.13 and Fig. 2.14 the results of static pushover analyses with the different wooden floors are reported. It is quite evident that, in terms of displacement capacity, the most common as-built traditional floor (single straight-sheathing) embodies a poor solution for a masonry building placed in a seismic zone (even though the tested one was very well-made, far beyond the common standard). Furthermore one can see that modeling single straight-sheathed floors with rigid diaphragms leads to overestimate both the shear resistance and the ultimate displacement of approximately 20% and 100% respectively. The reason is that rigid floors are capable of involving in the failure mechanism almost all the walls (story mechanism). Actually when the building reaches the collapse point (80% of the shear resistance) nearly all the piers, directed along the earthquake direction, have already gone beyond the plastic threshold (Fig. 2.16). On the other hand, quite a low in-plane stiffness means that there is little "collaboration" between the systems of walls. That is to say, the failure occurs when a single system of walls attains its ultimate displacement (Fig. 2.15). As a result, the analysis ends with many of the piers in the elastic phase, preventing the structure from obtaining the performance observed under the rigid diaphragms hypothesis.

Apart from the single straight-sheathed floor (whose in-plane stiffness is almost negligible), it appears that the maximum base shear is not affected by variation of the in-plane stiffness of diaphragms. In addition, in both directions the global stiffness does not show appreciable differences changing the type of floor refurbishment.

When the earthquake action is directed along *y* axis, the ultimate displacement of the pushover curve seems to be highly sensitive to the floor stiffness (Fig. 2.14). As a matter of fact, the stiffer the floors, the bigger the displacement capacity becomes. Nevertheless, with the rigid-diaphragms hypothesis the ultimate displacement is smaller than that obtained considering any other type of refurbished floor. A possible reason may be found analyzing the deformed shape of the structure. It has been observed that there is a sort of torsion movement that, starting from a certain point onwards (corresponding to the activation of a rocking hinge on a specific pier), significantly raises the stress level of the external walls (directed perpendicularly to the seismic action), leading the structure to failure. This "trigger point" has proved to be postponed if the floors stiffness increases and, consequently, the analysis can go further too. On the other hand if this torsion movement is entirely stopped (rigid-floors hypothesis) many more piers reach their ultimate displacement simultaneously (shear failure), calling the analysis to a premature halt.

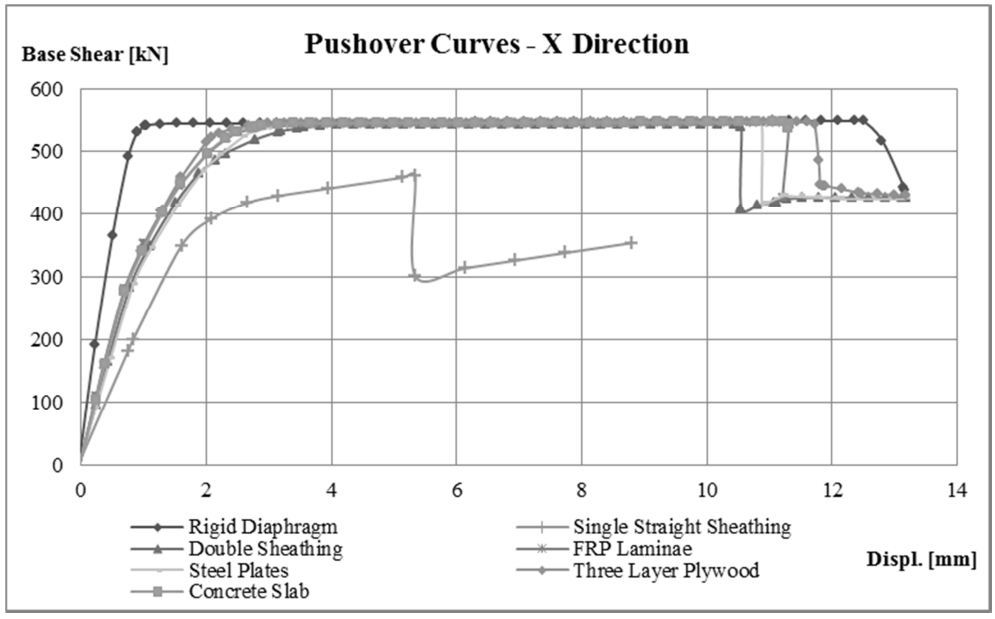

Fig. 2.13 Nonlinear static analyses: capacity curves

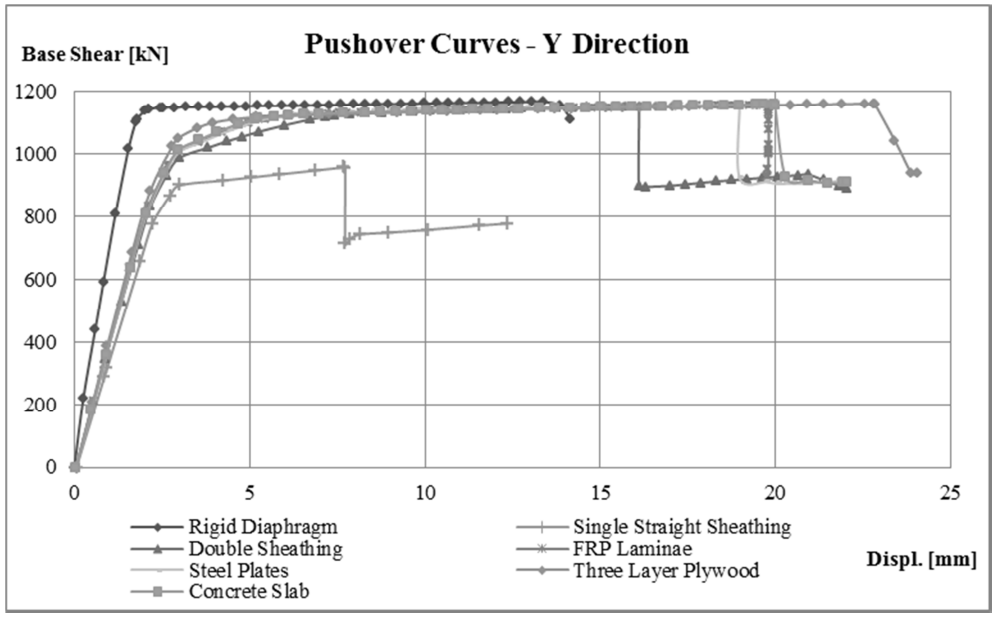

Fig. 2.14 Nonlinear static analyses: capacity curves

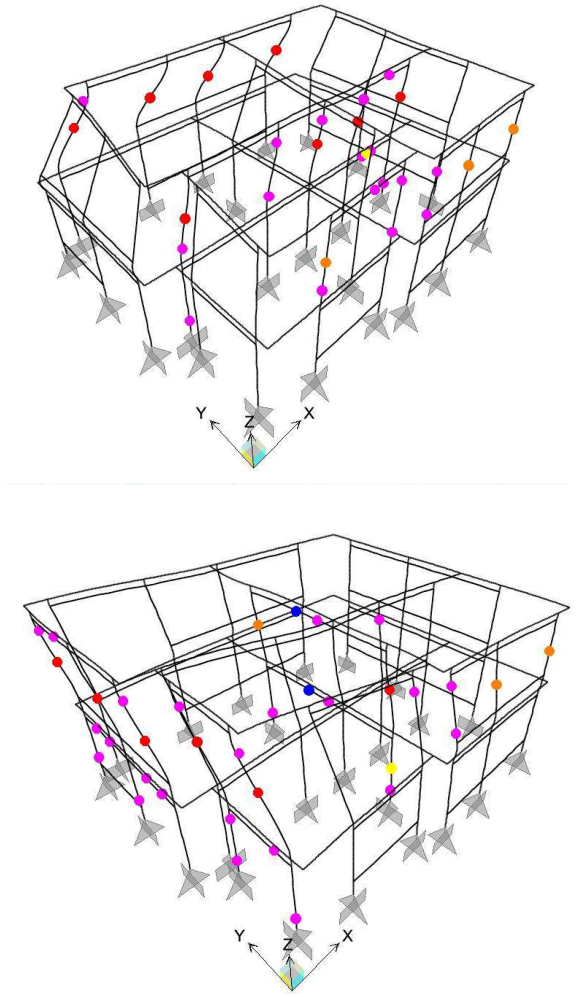

Fig. 2.15 Deformed shape (single straight-sheathing hyphothesis): x dir. on the top, y dir. on the bottom

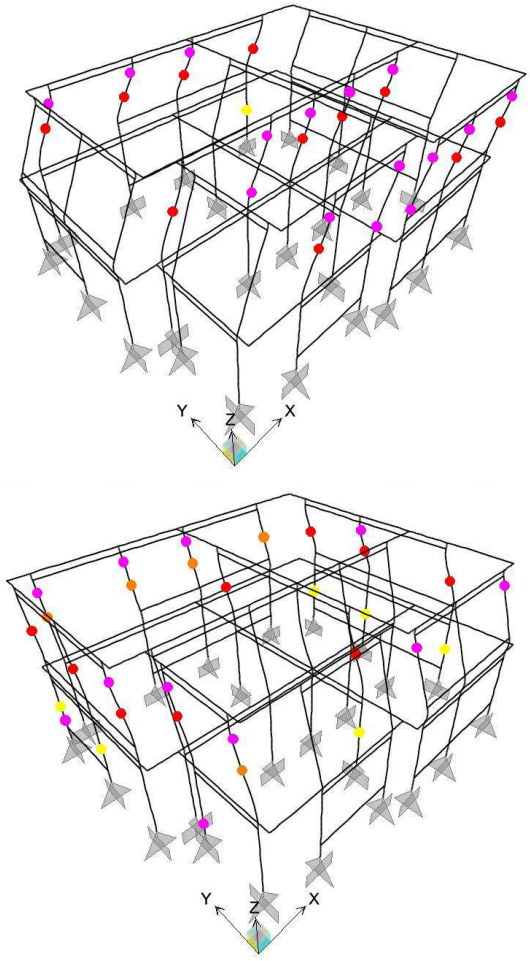

Fig. 2.16 Deformed shape (rigid diaphragm hyphothesis): x *dir. on the top,* y *dir. on the bottom*

2.6 Conclusions

From the presented results it would appear that a floor strengthening and stiffening is quite basic to the improvement of the seismic response of a masonry construction. Yet, the choice of the type of refurbishment does not seem to be of any relevance at all. Nonetheless, before leap to conclusion one should consider that the capacity curve is strictly linked to the building geometry and to the load distribution. Moreover, although the global behavior could be not affected by the in-plane floor stiffness, not so is the local one.

An interesting aspect that ought to be more deeply studied, is the possibility of updating failure criteria of piers by determining step by step the values of p and α_v.

2.7 References

Baldessari, C., Piazza, M., Tomasi, R., (2009). *The refurbishment of existing timber floors: characterization of the in-plane behaviour.* ISBN: 978-0-415-55804-4. Protection of Historical Buildings. PROHITECH 09, London: Taylor & Francis, 255-260.

Calderini, C., Cattari, S., Lagomarsino, S., (2009). *In-plane strength of unreinforced masonry piers.* Earthquake Engineering and Structural Dynamics, 38(2), pp. 243-267.

Cattari, S., Curti, E., Galasco, A., Resemini, S. (2005). *Analisi sismica lineare e non lineare degli edifici in muratura: teoria ed esempi di applicazione secondo OPCM 3274/2003 e 3431/2005*. – collana Edilizia-Progettare e costruire, Ed. Esselibri-Simone, Naples. (in Italian).

Dolce, M., (1989). *Schematizzazione e modellazione per azioni nel piano delle pareti, Corso sul consolidamento degli edifici in muratura in zona sismica.* Ordine degli Ingegneri, Potenza. (in Italian)

Magenes, G., Calvi, G. M., (1997). *In-plane seismic response of brick masonry walls.* Earthquake Engineering and Structural Dynamics, 26, 1091-1112.

Magenes, G., Bolognini, D., Braggio, C. (2000) *Metodi semplificati per l'analisi sismica non lineare di edifici in muratura.* CNR-Gruppo Nazionale per la Difesa dai Terremoti. Rome. (in Italian).

Pasticier, L., Amadio, C., Fragiacomo, M., (2008). *Non-linear seismic analysis and vulnerability evaluation of a masonry building by means of the SAP2000 V.10 code.* Earthquake Engineering and Structural Dynamics, 39, 467-485.

Piazza, M., Baldessari, C., Tomasi, R., Acler, E. (2008). *Behaviour of refurbished timber floors characterized by different in-plane stiffness*. Structural Analysis of Historical Constructions, Bath, U.K., Dina D'Ayala, E. Fodde (Eds.).

Righetti, G., Bari, L. (1993). *L'edificio in muratura. La muratura portante in laterizio normale e porizzato: caratteristiche e prestazioni*. Consorzio Poroton, Ed. Lambda, Padua. (in Italian).

ASCE/SEI 41-06. (2007). *Seismic Rehabilitation of Existing Buildings.* American Society of Civil Engineers, Virginia.

D.M. 14-01-2008. (2008). *Norme Tecniche per le Costruzioni*. NTC 2008. (in Italian).

FEMA 356. (2000). *Prestandard and Commentary For the Seismic Rehabilitation of Buildings.* Federal Emergency Management Agency.

FEMA 440. (2005). *Improvement of Nonlinear Static Seismic Analysis Procedures*. Federal Emergency Management Agency.

NZSEE. (2006). *Assessment and Improvement of the Structural Performance of Buildings in Earthquakes.* Recommendations of a NZSEE Study Group on Earthquake Risk Buildings.

O.P.C.M. 3431. (2005). *Ulteriori modifiche ed integrazioni all'O.P.C.M. 20 marzo 2003 n. 3274, recante «Primi elementi in materia di criteri generali per la classificazione sismica del territorio nazionale e di normative tecniche per le costruzioni in zona sismica».* (in Italian).

UNI EN 1996-1-1. (2006). *Eurocode 6 : Design of Masonry Structures. Part 1-1 : General Rules for Buildings—Rules for Unreinforced and Reinforced Masonry*.

UNI EN 1992-1-1. (2005). *Eurocode 2: Design of concrete structures Part 1-1: General rules and rules for buildings.*

3 PROPOSAL OF A SIMPLIFIED ELASTIC NO TENSION METHOD FOR THE SEISMIC EVALUATION OF URM BUILDINGS WITH FLEXIBLE DIAPHRAGMS

3.1 Introduction

The main purpose of this chapter is to deepen the understanding of the effects of different modeling techniques when evaluating the seismic response of URM buildings with timber diaphragms. The results of the analyses reported in Chapter *2* showed that the capacity curves obtained by employing an equivalent frame method, are characterized by a clear *plateau* which is related to the assumptions behind the plastic hinges property definition. Another issue that is addressed in the present chapter, is to determine whether the wood diaphragms (both as built and refurbished ones) are to be treated as linear materials or not. Several studies have shown that timber floors, when subjected to significant lateral loads, exhibit a highly nonlinear behavior. Since a yielding point is not always clearly identifiable [Piazza et al. (2011)], one cannot easily fit the experimental data with a bilinear curve nor can define, *a priori* a target displacement in which determining an equivalent secant stiffness. As a matter of fact, the diaphragm requirements in terms of displacement are related to the masonry skeleton the floor is connected to. In order to sort all these issues out, a simplified elastic no-tension (ENT) method for modeling masonry structures was proposed.

3.2 Modeling of masonry

Masonry is known for its low tensile strength and therefore a numerical model based on plane, linear elastic finite elements (the simplest choice) could not be able to reproduce the real behavior of a historical building. On the other hand, employing refined constitutive laws could be very time consuming and not easily manageable in case of large structures. In addition, the mechanical properties of masonry are extremely variable and differ from one building to one other. Therefore the benefits achievable through a very detailed modeling can be vanished by the approximation level related to the materials, since in most occasion is not possible to perform a thoroughly exhaustive material testing.

Elastic no tension models (ENT) represent a first step towards finer modeling approaches and could be considered a reasonable compromise between accuracy and feasibility.

Unfortunately ENT materials are highly sensitive to boundary conditions and prone to lack of solution and excessive displacements. One famous example of this, is described by [Como (2010)]. The author considers a panel (unit depth) loaded as in Fig. 3.1, with both ends free to deform. Applying the Hooke's law it can be seen that the extremities of the uniform loaded portion of the panel, shorten of a quantity Δ_a equal to:

$$\Delta_a = \frac{pa}{Ea}\frac{L}{2} = \frac{p}{E}\frac{L}{2} \qquad \textit{(Eq. 2.1)}$$

The right portion of the panel is subjected to compression ($N = pb/2$) and also bending ($M = pb^2/12$) which makes its top section rotate anticlockwise. Thanks to the Navier's formula it can be demonstrated that the left fiber of this portion undergoes a displacement Δ_b:

$$\Delta_b = \frac{pb}{2}\frac{L}{2Eb} + M\frac{12L}{2Eb^3}\frac{b}{2} = \frac{p}{E}\frac{L}{2} = \Delta_a \qquad \textit{(Eq. 2.2)}$$

Along the line between the two portions, fractures inevitably develop. If b is sufficiently small, the maximum amplitude Δ' of these openings can be determined relying on the beam theory:

$$\Delta' = \frac{M}{8}\frac{L^2}{EJ} = \frac{pL^2}{8E}\frac{1}{b} \qquad \textit{(Eq. 2.3)}$$

When the zone which the triangular part of the load is applied to, gets smaller and smaller or in other words when $b \to 0$, Δ' becomes:

$$\lim_{b\to 0} \Delta' = \infty \qquad \textit{(Eq. 2.4)}$$

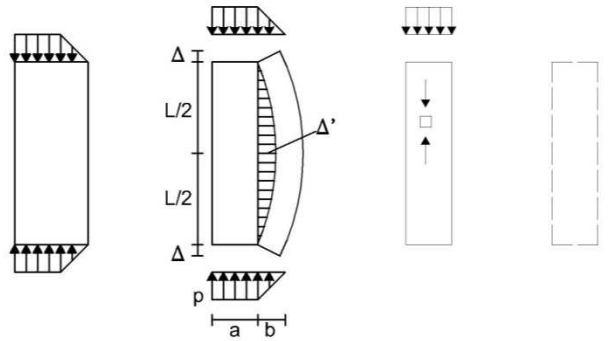

Fig. 3.1 Example of singularity in the displacement field of a ENT panel

Hence a simplified method was formulated in order to take into account a very limited tensile strength and avoid the typical problems related to ENT models. So as to achieve this, a "global" Rankine failure criterion (with no limits in compression, Fig.3.2) was adopted, maintaining though an infinite linear elastic behavior throughout all the various steps the analysis was comprised of. To make it clearer, let us consider a displacement controlled analysis on a simple masonry pier, modeled with planar linear elastic finite elements, as in Fig.3.3a. The pushover analysis has been divided into five steps (from *A* to *E*). After the first step a check on the principal stresses has to be made: if one of the principal stresses (σ_I, σ_{II}) of a generic element exceeds the masonry tensile strength, then the element is eliminated and the external force needed to maintain the structure at a displacement equal to ΔA decreases (Fig.3.3b). Thanks to the linear elastic behavior of the material, it is possible to stop the analysis right after the first step, do the stress check, unload the structure, eliminate the elements that are outside the failure surface and then reload up to the ΔA displacement being confident to reach the A' point. Repeating this procedure for every step and connecting the points A',B'…E' (Fig.3.3d,e), one obtains the capacity curve of the structure.

A "globally nonlinear" behavior has thus been depicted through a series of linear analyses. The level of accuracy is related to the number of steps the analysis has been divided into. The greater the number of steps, the lower the probability that some elements, at the time of the stress check, are far beyond the failure surface keeping the adjacent elements from being eliminated. Consequently, in case of coarse steps, the structure response tends to be stiffer. Assuming an infinite resistance in compression, is quite a strong hypothesis (not on the safe side) borrowed from the limit analysis [Heyman, (1995)] so as to keep the method as much easy to handle as possible.

The method implementation was accomplished by means of SAP2000 and the CSI's Open Application Programming Interface that guaranteed the complete automation of the procedure.

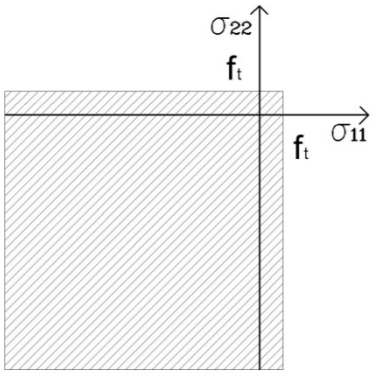

Fig.3.2 Failure criterion in terms of principal stresses (f_t = tensile strength of masonry)

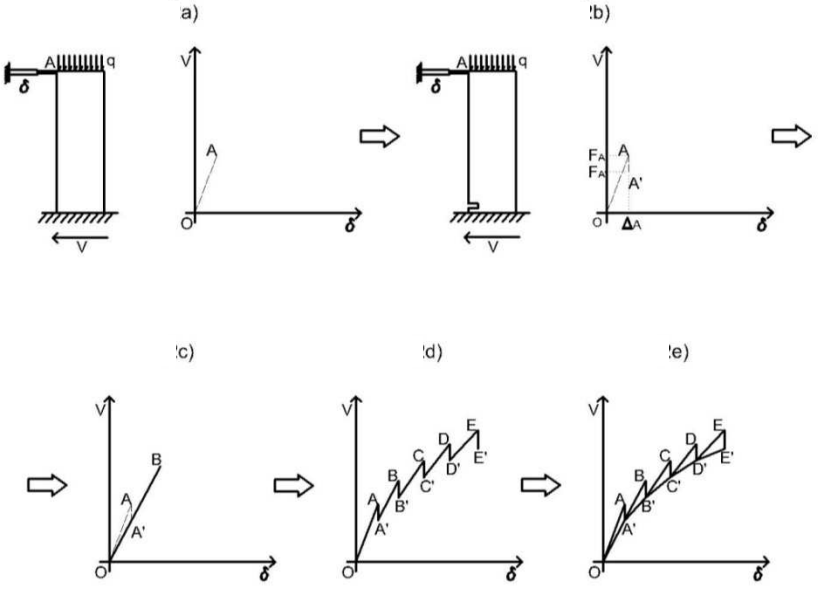

Fig.3.3 Simplified ENT procedure

The general flow diagram of the procedure is given in Fig.3.4.

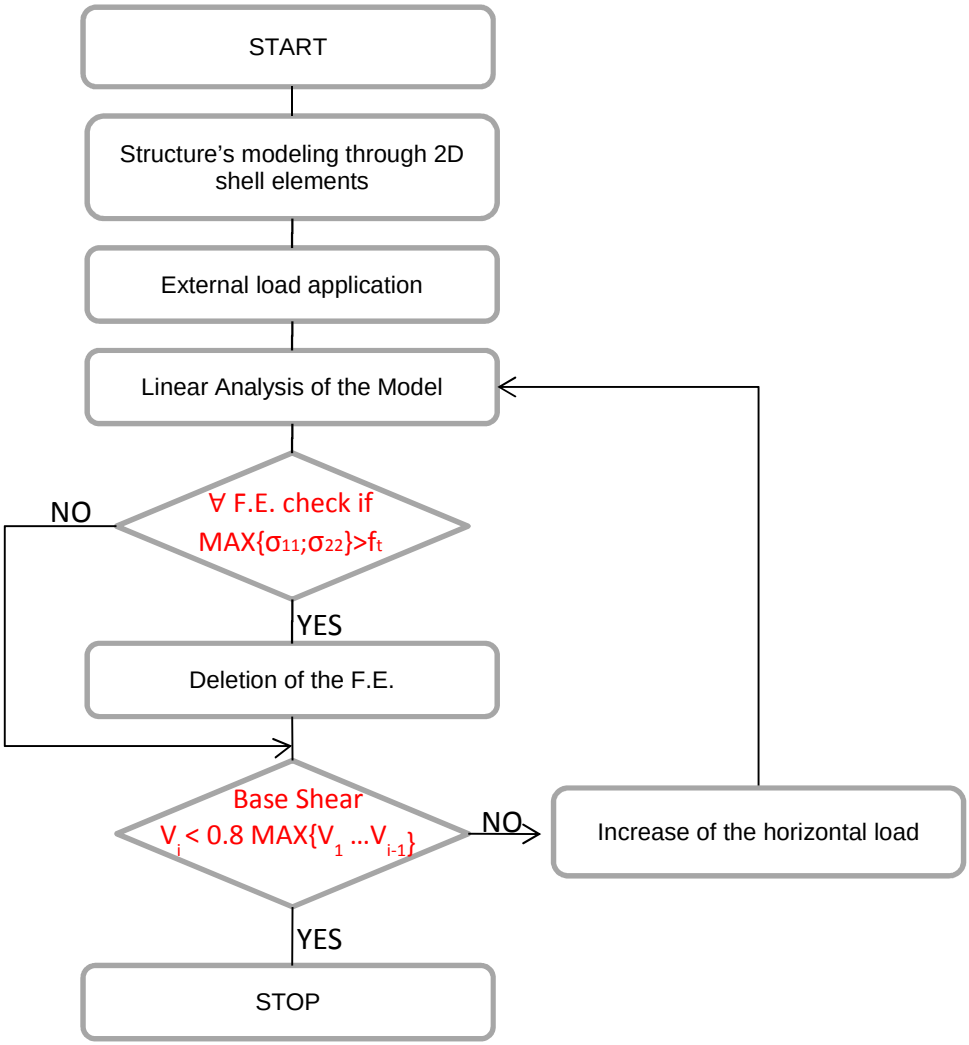

Fig.3.4 Flow diagram

3.2.1 Method validation

In order to validate the proposed method a case study was selected from the literature. The choice fell on the "Catania Project" [Liberatore (2000)], an Italian research project involving several research groups, proposed by the *National Group* for *Earthquake Defence.* In particular the attention was focused on the internal wall of the building sited in *Via Martoglio* (Catania, Italy,Fig.3.5), whose mechanical parameters are reported in Table 1. According to the Italian Standards [C.M.617 (2009)], a value equal to 1.5 times

the shear strength, was assumed for the tensile strength of masonry ($f_t = 1.5\tau_k = 0.24$ *MPa*).

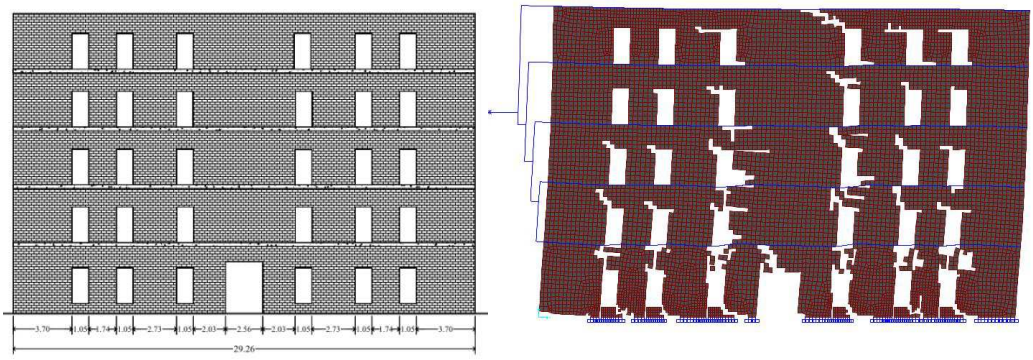

Fig.3.5 Via Martoglio wall – Unloaded condition (on the left), ultimate condition (on the right)

With the aim of applying a prescribed load distribution (e.g. mass proportional, first mode proportional) in a displacement controlled analysis, an equivalent isostatic loading system was adopted [Anthoine (2006)]. The horizontal forces were introduced into the model at the story level, in correspondence with the concrete curbs, together with the vertical loads (so as to avoid any mass loss when an element is deleted due to excessive traction). The meshing of the wall was performed through four-node (2x2 Gauss points), two-dimensional finite elements (with just membrane behavior) whose maximum size (0.2x0.2 m^2) was determined after a sensitivity analysis. It should be noted that the mesh dependence is related to the analysis step dimension.

Weight density of masonry	γm	17	kN/m3
Tensile strength of a brick	fbt	1	MPa
Compressive strength of masonry	fu	6.0	MPa
Shear strength of masonry	τk	0.16	MPa
Elastic modulus of masonry	E	1600	MPa
Shear modulus of masonry	G	300	MPa
Cohesion	c	0.15	MPa
Friction parameter	μ	0.5	
Elastic modulus of concrete curbs	Ec	20000	MPa

Table 3.1 Mechanical properties of masonry

From the study of the damage evolution it can be stated that the first cracks appeared on the lintel above the main door at the ground floor. Then, a progressive reduction of the coupling effect offered by the spandrels was observed (starting from the lower stories) and consequently the formation of rocking mechanisms at the base of the ground story piers. The shear resistance of the wall is given in Fig.3.6 (*V = 1002 kN*). With respect to the data reported in Table 2 (there is a significant scatter in the results of the different research groups) the shear resistance obtained through the proposed method is somewhat on the safe side. It should be underlined that the ultimate load is strictly related to the f_t value. If $f_t = 2\tau_k$ had been used, a shear resistance close to *1300 kN* would have been obtained. As far as displacements are concerned, the proposed method exhibited the collapse point at 1.96 cm, very close to when the research group of Pavia detected the formation of a soft-story (Fig.3.6). On the other hand, as expected, it was quite distant from the ultimate displacement shown by the POR based methods (L'Aquila research group) which do not consider any damages of the spandrels.

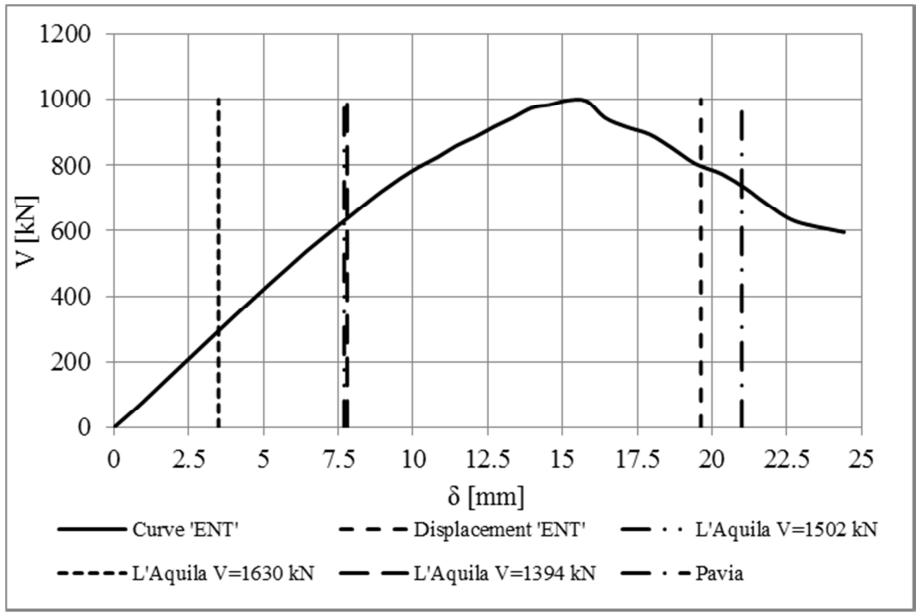

Fig.3.6 Capacity curve of the Via Martoglio wall

Model	Research Units	V (kN)
	Basilicata	2050
Elastic curbs E = 20000MPa	Genova	1492
	Pavia	1227
Elastic curbs E = 20000MPa (rigid offsets)	Basilicata	2226
	Basilicata	2050
Elastic curbs E = 4000MPa	Genova	1263
	Pavia	848
POR, piers' height = interstorey height	L'Aquila	1502
POR, piers' height = openings' height	L'Aquila	1630
POR90, piers' height = interstorey height	L'Aquila	1394

Tab. 3.2 Catania Project results

3.2.2 Case study building

Fig.3.7 shows the structure selected for the analyses regarding the in-plane behavior of timber diaphragms. It is a four story building (15.60 m high) with a rough size of 10.60x15.60 m^2. The thickness of the walls is 0.6 m for the first two stories and 0.5 m for the others. There is also an internal spine wall whose thickness is equal to 0.3 m. As already mentioned, the loading system is able to maintain a prescribed load pattern throughout the displacement controlled analysis, required to depict the post peak phase. In other words, at the "actuator", the analysis is a proper displacement controlled analysis, while on the building it becomes a force-controlled one. This means that the nodal displacement of the frame representing the actuator, is an increasing monotonic function. On the other hand, some points of the building could show a reduction in displacement in order to counterbalance (due to the isostatic loading system) the decreased stiffness of part of the structure. The ratio between the forces acting at the same level was worked out thanks to a force-controlled elastic analysis in which, all the inertial forces were applied exactly where they were supposed to be. That is to say, for example, that the forces generated by the floor mass were introduced at the nodes of the cells modeling the diaphragms. It should be noted that this distribution, representative of the undamaged condition, was kept unchanged for the entire analysis. To determine whether this aspect yields remarkable effects on the determination of the peak point, some force-controlled analyses were performed following a procedure similar to that exposed in paragraph 2 (no effects were registered).

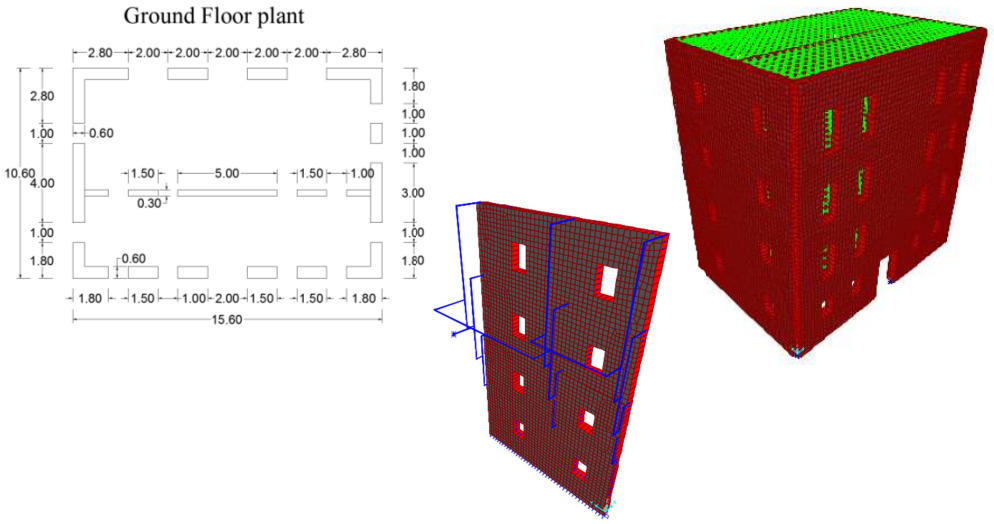

Fig.3.7 Case study building (on the left and on the right) and the isostatic loading system (in the middle)

It is known that the choice of the control point has a great influence on the determination of the capacity curve. In addition, owing to the features of the loading system, it was not rare to observe a decrease (from a certain time onwards) in the displacement of the monitored point. Therefore it was chosen of monitoring the building displacement in correspondence with the frame element representing the actuator. Considering that this element is positioned at about two third of the building height, the resulting capacity curves are on the safe side in terms of ultimate displacement.

3.3 Modeling of wood diaphragm

Data pertaining to wood diaphragms were taken from [Baldessari et al. (2009)] where an extensive experimental campaign on *5x4* m^2 timber floors is presented. A fitting of the backbone force-displacement curves was carried out following the procedure proposed by [ABK (1984)]:

$$F(\delta) = \frac{F_u \cdot \delta}{F_u / k_i + |\delta|} \qquad \textit{(Eq. 2.5)}$$

where δ is the midspan displacement, $F(\delta)$ is the force at the diaphragm's end, k_i is the initial stiffness and F_u is the ultimate force. F_u is obtained multiplying the unit shear strength of the diaphragm v_u by its width [Paquette & Bruneau (2006)]. With reference to every floor typology tested by Baldessari et al., all the parameters required for determining the backbone curves are given in Table 3.

	v_u [kN/m]	F_u [kN]	k_i [kN/mm]
Single Straight Sheathing	52.0	208.0	1.1
Double Sheathing	67.6	270.4	11.2
Steel Plates	59.8	234.4	23.2
FRP Laminae	51.8	207.2	45.1
Concrete Slab	85.4	341.6	60.0
Plywood Layers	64.8	259.2	106.1

Tab. 3.3 Parameters for ABK formula

Both the experimental tests and the parametric analyses performed on FEM models (Fig.3.9) showed that the deformed shape of the diaphragms are extremely close to that of a uniformly loaded shear beam. Consequently an equivalent shear stiffness G_{eq} was calculated regarding the diaphragm deformation as equal to the shear deformation of a simply supported beam under a uniform load distribution.

$$G_{eq}(\delta) = \frac{2F(\delta) \cdot L}{8 \cdot B \cdot t \cdot \delta} \qquad \textit{(Eq. 2.6)}$$

where L = floor span perpendicular to the load direction, B = floor span parallel to the load direction, t = floor (membrane) thickness, $2F(\delta)$ = lateral load applied, δ = mid span deflection. It is worth noting that the secant stiffness curve calculated in (Eq. 2.6), is a function of the midspan displacement of the specimen and therefore could not be representative of floors with different geometries. To solve this problem, might be useful referring to a non-dimensional quantity such as the shear strain γ. On the other hand the shear strain is not uniform and varies along the equivalent-beam axis. Since the diaphragms were modeled with a series of reference mehses (Fig.3.10) consisting of an

external frame of rigid rods and two internal diagonal rods whose stiffness is equal to G_{eq} multiplied by the floor thickness, a mean value of shear strain γ^* was calculated for every δ (Fig.3.8). So as to take into account the nonlinear behaviour of the floors, the following iterative procedure was developed. The analysis begins with the shear stiffness of the floors equal to G_1 (Fig.3.8). At the end of the first step, the angular deformation of each cell is calculated: if the maximum γ is equal or smaller than γ^*_1, it is possible to proceed with the stress check and the element deletion, otherwise the stiffness has to be changed and the step rerun. This process must be repeated after each step.

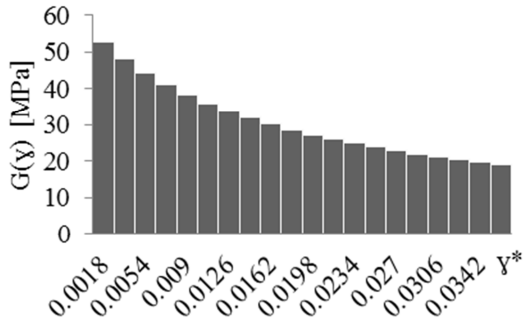

Fig.3.8 Equivalent shear stiffness (Double sheathing)

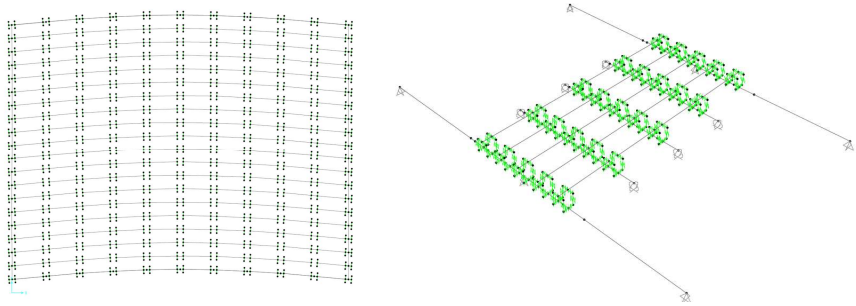

Fig.3.9 Numerical model employed in the parametric study of the deformed shape

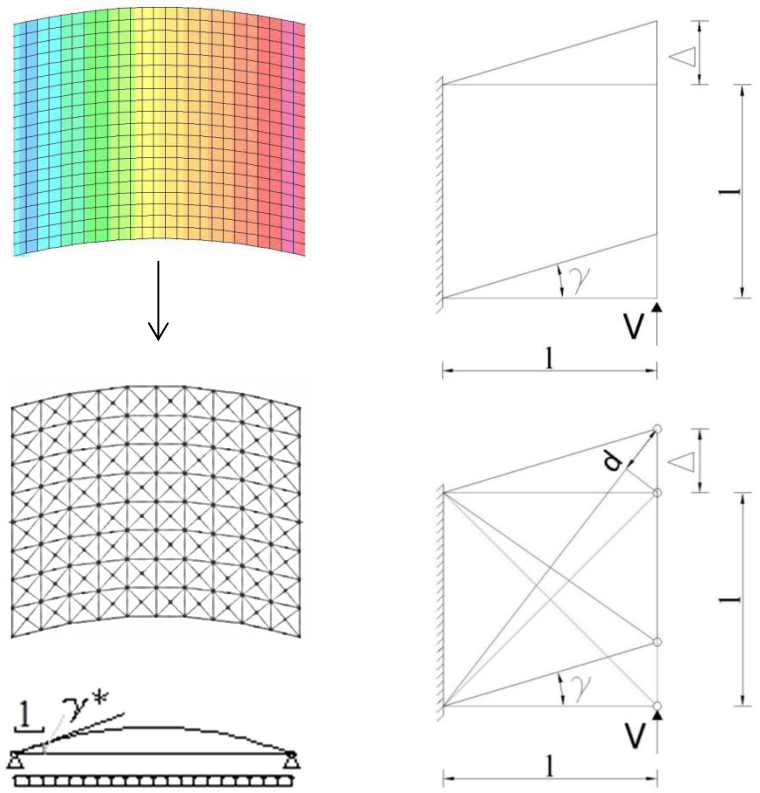

Fig.3.10. Diaphragm modeling

For the analyses where the diaphragm behaviour was considered linear elastic, the target point needed to determine the secant shear stiffness, was chosen in accordance with the results presented by [Paquette & Bruneau (2003)] which carried out pseudo-dynamic tests on a URM building with flexible floor of size very similar to the specimens tested by [Baldessari et al. (2009)].

3.4 Analysis results

Fig.3.11 presents the capacity curves of the case study building for the analyzed diaphragms. It can be seen that the in-plane stiffness of floors plays a negligible role in determining the global response of the structure (all the curves are practically the same). A probable reason can be found in the distance between the mass center and the center of stiffness which is smaller than *0.5 m*. In order to increase the stress state of the diaphragms, the model was modified by halving the thickness of the north wall (moving therefore the center of stiffness). As a result, a very slight difference was registered, denoting an increase in the performance as the floor stiffness grew (Fig.3.12). It should be noted that in masonry buildings the bulk of the structure is represented by the walls. Consequently, the north-wall's stiffness-variation generated by the halving of the thickness, was somehow counterbalanced by the reduction in horizontal force (acting on the north wall) due to the mass diminishing. Therefore it was decided to apply an additional eccentricity of *2 m* to the mass center, even if that was not consistent with the building geometry. From Fig.3.13 it is possible to observe that the higher the floor stiffness, the greater the shear resistance and the ultimate displacement. This result seems not to be in good agreement with chapter 2 where, apart from the single straight sheathing, it appears not to be any significant variations in the pushover curves between the different floor typologies. The causes might be found in the different method adopted for modeling masonry (equivalent frame method) and in the building characteristics.

With reference to the issue of assuming for diaphragms a linear behavior rather than a nonlinear one, many analyses were carried out: no appreciable differences were observed. The only small difference was registered for single square sheathing solution when the aforementioned additional eccentricity was considered (Fig. 3.14). So it seems that a linear elastic behavior could be adequate to reproduce the global seismic response of a URM building with timber floors. Further analysis is however recommended.

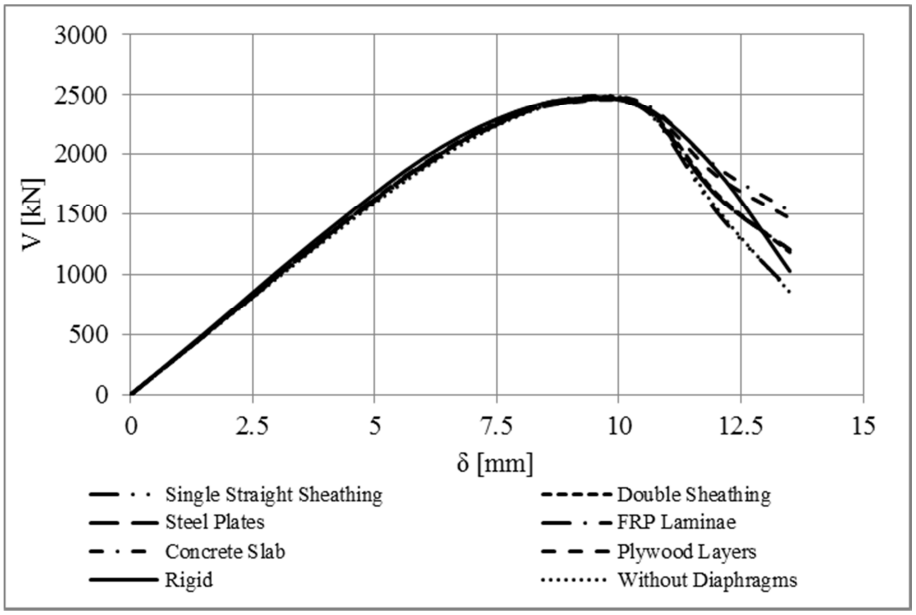

Fig.3.11 Capacity curves (different floor-typologies)

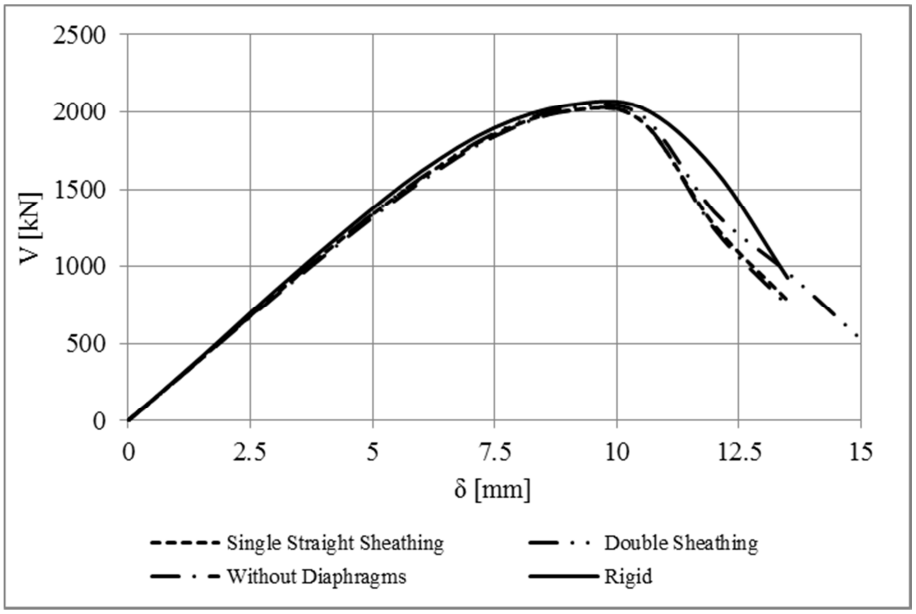

Fig.3.12 Capacity curves (North wall with halved thickness)

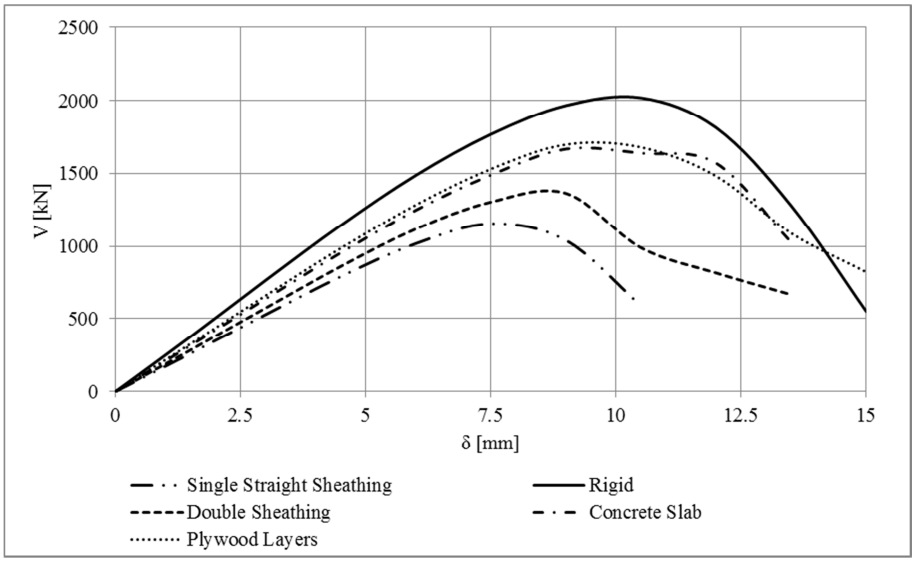

Fig.3.13 Capacity curves (2 m of additional eccentricity to the mass centre)

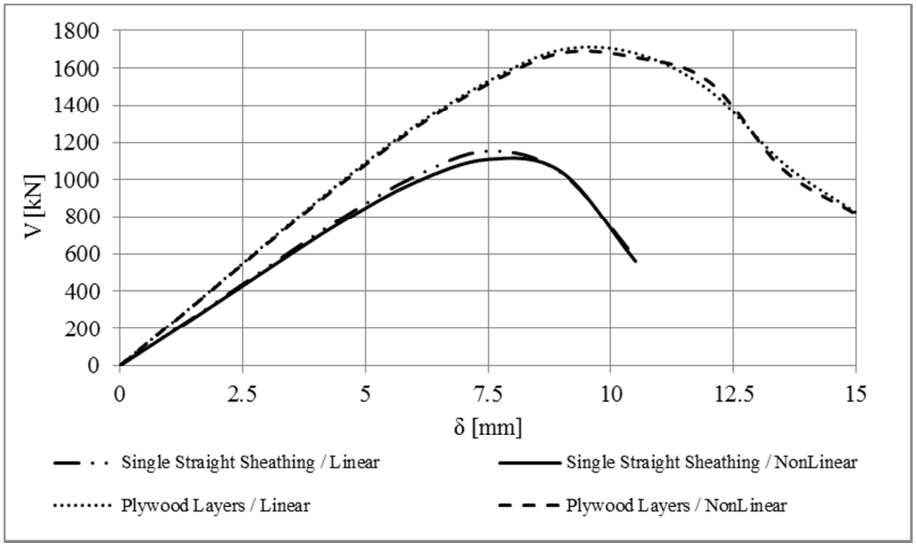

Fig. 3.14 Floors with linear constitutive law Vs. Floors with nonlinear constitutive law

3.5 Conclusions

From the presented results it would appear that modeling the real in-plane stiffness of diaphragms becomes quite important only in presence of remarkable eccentricity between the mass center and the center of stiffness. However, it should be taken into account that in URM buildings, the seismic mass associated with floors is very small in comparison with the mass of the walls. Therefore the position of the center of mass is related to that one of the center of stiffness.

In addition, it seems that modeling wood diaphragms with a linear elastic in-plane behavior is sufficient to describe the global seismic response of URM buildings.

As far as the proposed simplified ENT method is concerned, it has shown to be quite easy to handle and able to follow the damage evolution. Since after each step of the analysis, a copy of the up-to-date model is automatically saved, it is possible to check the stress distribution step by step

A future development could be to adopt the proposed method to perform the building safety checks for vertical loads.

3.6 References

Piazza M., Polastri A., Tomasi R., (2011), *Ductility of timber joints under static and cyclic loads. Proceedings of the Institution of Civil Engineers,* Structures and Buildings, v. 164, n. SB2 (2011), 79-90

Heyman J., (1995), *The stone skeleton*, Cambridge University Press

Liberatore D., (2000), *Progetto Catania: Indagine sulla risposta sismica di due edifici in muratura (Project Catania: Investigation on the seismic response of two masonry buildings)*, GNDT – *National Group for Seismic Protection*: Rome, (in Italian)

Baldessari C., Piazza M., Tomasi R., (2009), *The refurbishment of existing timber floors: characterization of the in-plane behaviour*, Protection of Historical Buildings PROHITECH 09, LONDON: Taylor & Francis, 2009, 255-260

Agbabian & Associates, S.B. Barnes & Associates, and Kariotis & Associates, (1984), *(ABK) A Joint Venture; Methodology for mitigation of seismic hazards in existing unreinforced masonry buildings: The methodology*. El Segundo, Calif.

Como M., (2010), *Statica delle costruzioni storiche in muratura*, Aracne editrice S.r.l.

C.M. 617: 02-02-2009, *Istruzioni per l'applicazione delle «Nuove norme tecniche per le costruzioni» di cui al decreto ministeriale 14 gennaio 2008*. (*In italian*)

CSI [Computers and Structures Inc.], (2004), *CSI Analysis Reference Manual For SAP2000*®, ETABS®, and SAFE®. CSI, Berkeley

Anthoine A., (2006), *A simple displacement control technique for pushover analyses*, Earthquake Engineering and Structural Dynamics 35, 851-866

Paquette J., Bruneau M., (2003), *Pseudo-dynamic testing of unreinforced masonry building with flexible diaphragm*, *Journal of Structural Engineering* 129,708.

4 PARAMETRIC ANALYSIS ON TIMBER DIAPHRAGM IN-PLANE BEHAVIOR

4.1 Introduction

In the previous chapters diaphragm modeling was based on experimental data which inevitably are affected by a certain degree of "particularism". Therefore, in order to develop a general formulation which can be adopted for various diaphragm configurations, a thorough parametric analysis was conducted by means of a numeric model. The analysis was focused on single straight-sheathed diaphragms. A summary of the most significant results produced by such analysis is reported in the present chapter.

4.2 Finite Element Model

The numerical model employed for the parametric study on single straight sheathed wooden floors relies on relatively consolidated assumptions which are quite common in literature [Brignola et al. (2008), Peralta et al. (2003), Wilson (2012)]. The first one of which is that the timber elements (boards and joists) are considered as linear-elastic. As a result, all the nonlinearities are concentrated in the fastener (nail) behavior. Secondly, no material penetrations or contact issues are taken into account. Friction phenomena are also neglected. The *Finite Element Model* (FEM) was realized by means of SAP2000 [CSI (2004)], a quite widespread software for structural analysis and design. Timber joists and planks were modeled by *linear el*astic *frame* elements, while nails were represented by *nonlinear (multi-linear elastic) link* elements connected to the timber frame elements through *rigid link* elements. In case of an interrupted board, a "physical discontinuity" was introduced in the frame element representing the board (Fig. 4.1).

The nonlinear behavior assigned to the nails was derived from the curve proposed by McLain [McLain (1975)]:

$$F' = \underline{A} \cdot log_{10}\left(1 + \underline{B}\delta\right) \qquad \textit{(Eq. 4.1)}$$

Where *F'* is load applied to the nail, *δ* is the nail slip, *A and B* are experimentally derived parameters. Parameter *A* is a function of the specific gravity of the timber elements constituting the joint. Parameter *B* [Pellicane et al. (1991)] was determined in accordance with the procedure proposed by Wilkinson [Wilkinson)1971)] which relies on the research carried out by Kuenzi (1955) where the nail is regarded as a beam on elastic foundations. Since each degree of freedom (DoF) of the multi-linear element behaves independently, such nonlinear curve (Eq. 4.1) was assigned to the translational DoFs *U2* and *U3*. The DoFs *U1*, *R2* and *R3* were fully restrained (no flexural or axial nail deformations were allowed) while *R1* (torsional) was set free (Fig. 4.1).

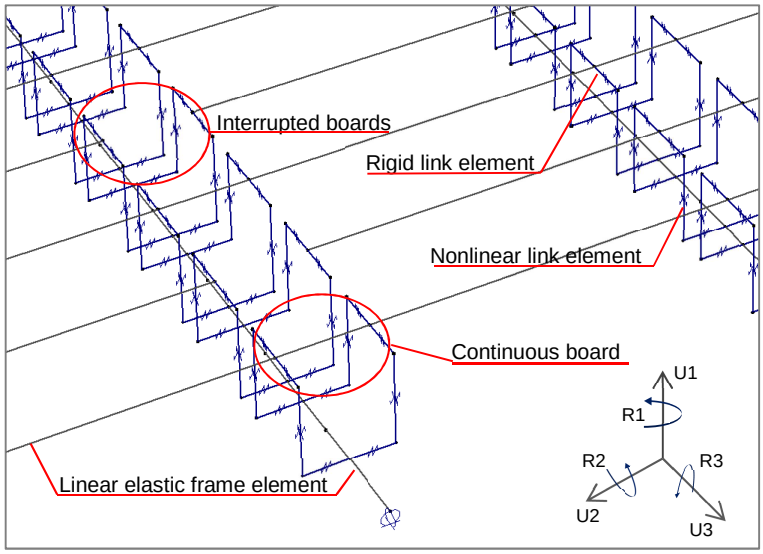

Fig. 4.1 Numeric modeling details (two nail-couples for each joist)

4.2.1 Model validation

The numerical model was validated through the data obtained from the experimental campaign carried out at the University of Trento in 2007 (Laboratory of the Department of Mechanical and Structural Engineering) [Piazza et al. (2008), Baldessari et al. (2009)]. Two different sized specimen were available for the validation: *1* small scale (*2.0 m x 1.0 m*, Fig. 3) and *1* full scale (*5.0 m x 4.0 m*, Fig. 4.2). The steel chord present on the full scale floor was modeled through *linear elastic frame* elements connected to the joists and floorboards by means of *rigid link* elements (the stiffness of the torsional spring R1 was assumed equal to zero). Boundary conditions and loading pattern reproduced those adopted in the testing campaign by Baldessari et al.. Consequently,

hinges were introduced at the mid length of the lateral joists (tests were carried out only in the direction parallel to the joists) and the external force was applied through a *1* point load (small scale specimen) and *4* point loads (full scale specimen). Fig. 4.3 shows the good agreement registered between the experimental curve and the pushover curve obtained from the numeric model.

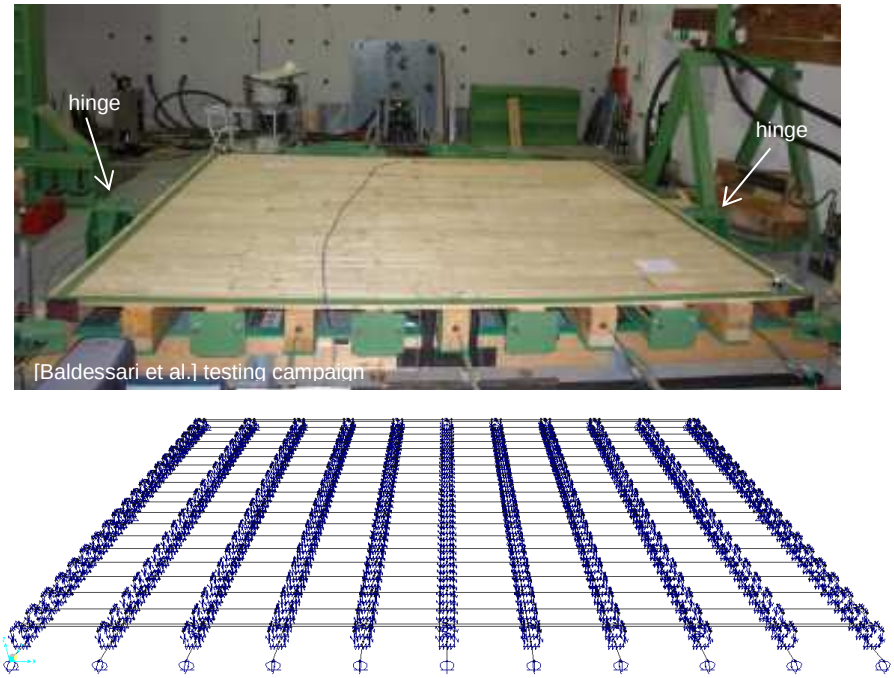

Fig. 4.2 FEM validation (5.0 m x 4.0 m specimen)

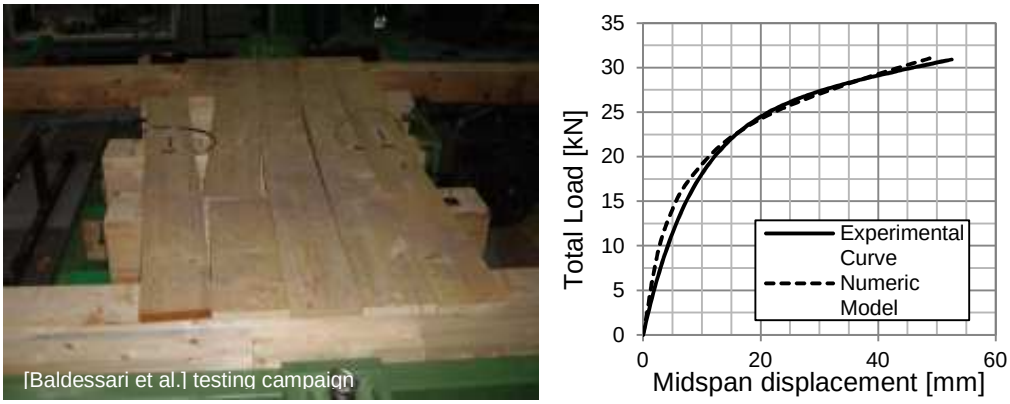

Fig. 4.3 FEM validation (2.0 m x 1.0 m specimen)

4.3 Parametric Analyses

Two different case-study diaphragms were taken into consideration for each aspect which was investigated in the parametric analyses. The first one was exactly the same size as the full-scale floor (labeled *B_5*x4, aspect ratio *r = 1.25*) used for the model validation. The second one was instead a *10.0 m x 5.0 m* diaphragm (labeled *A_10x5*, aspect ratio *r = 2.0*). Both case studies were analyzed taking into consideration the flooring disposition presented in Fig. 4.4, [NZS 3603:1993,].
The external force was applied following the parabolic load distribution suggested by [FEMA 356] so as to reproduce the inertia forces:

$$f_d = \frac{1.5F_D}{L}\left[1-\left(\frac{2x}{L}-1\right)^2\right] \qquad \textit{(Eq. 4.2)}$$

where F_D is the total inertial load, L is the distance between the lateral support points of the diaphragm and x is the distance from the diaphragm's end. In order to understand the influence on the diaphragm response produced by different horizontal components of the seismic action, the load distribution was alternatively applied both parallel and orthogonal to the joists direction. Many parameters were investigated such as:

- material deformability;
- nail pattern, number and spacing;
- joist size and spacing;
- board size;
- boundary conditions.

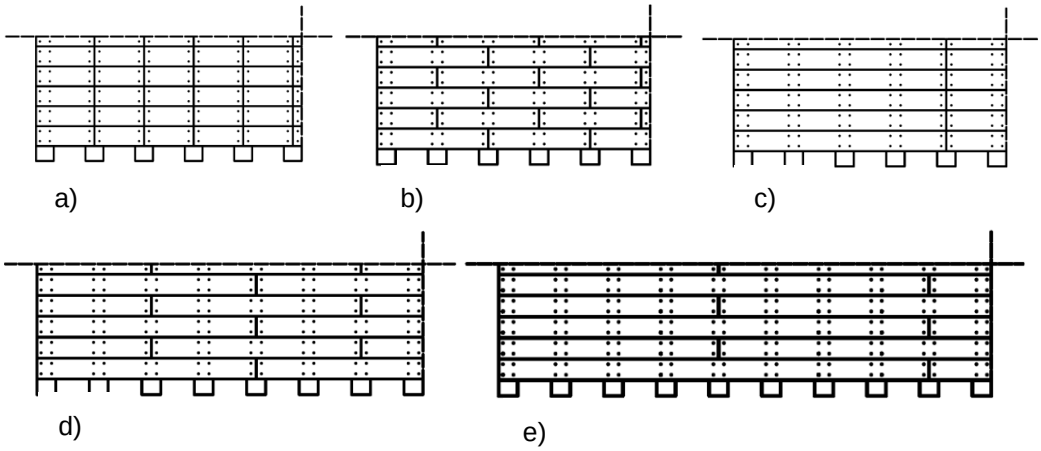

Fig. 4.4 Flooring lay-up: a) single span (0.5 m) boards; b) two span (1m) staggered boards; c) four span (2 m) boards; d) four span staggered boards; e) eight span (4 m) staggered boards (A_10x5)

In Fig. 4.5, some of the pushover curves obtained varying the floorboard behavior are reported. With reference to the floorboard configuration labels presented in Fig. 4.4, it was observed that configurations *a*, *b* and *c* were not sensitive to the "constitutive law adopted" for the modeling. In other words, the boards behaved as rigid bodies with all the deformations concentrated in the nails. The behavior of diaphragms with longer boards was instead significantly affected by the flexural deformability of the planks (Fig. 4.5c). In all conditions, the influence of the board shear deformability appeared to be negligible.

The influence of the different floorboard configurations is presented in Fig. 4.6. It can be seen that the use of long boards in a staggered disposition increased the diaphragm in-plane stiffness. This appears to be in contrast with what observed by [Brignola et al. (2008)] where no actual difference was observed between single span disposition, two span staggered disposition and four span staggered disposition. It can also be noticed that a very important role in determining the floor response was played by the nails. In fact a variation in the nailing pattern (adopting *1* nail couple where the board was continuous) produced almost the same effect registered when going from a single span configuration to an eight span staggered disposition. Consequently it is not surprising that a reduction in the floorboard width produced an increase in the diaphragm stiffness, due to the extra nail couples related to the increased number of boards (Fig. 4.7). As one might expect, by considering that the floorboards behaved almost rigidly without involving their deformability (with the exception of configuration *e)*), it was observed that

a variation in the board thickness did not generate appreciable changes in the pushover curve unless quite long planks were adopted.

As regards boundary conditions, analyses (with load acting parallel to the joists) were conducted varying the constraints applied to the external joists. In order to be able to appreciate a possible flexural beam-like behavior, a solution that prevented the external joists from rotating and another one with just a hinge positioned at the joist midspan were investigated. It was observed that model *B_5x4* was scarcely affected by such changes in the constraints. The response of model *A_10x5*, showed that in case of single span flooring (where the boards behave like rigid bodies) the external joists tend to rotate, while in presence of long staggered boards (which exploit their own flexural deformability) the pushover curve was not influenced by the lateral constraint mutation (Fig. 4.8) conversely to what could be expected. Some analyses were also performed hindering the nail deformability in the direction parallel to the load direction. No effects were registered in case of single span floorboards. This means that the nails deformed mainly in the direction orthogonal to the joists. On the other hand when the floorboards were arranged in a staggered configuration the "parallel component" of the nail deformation became significant, even for *2* span boards.

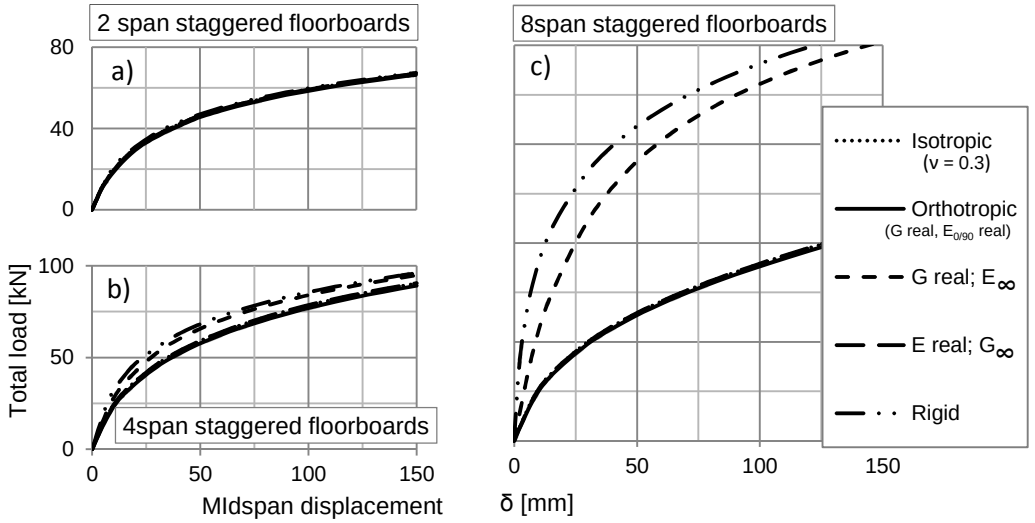

Fig. 4.5 Effect on the pushover curve produced by different assumptions on the plank behavior (E_{real} = 10 GPa, G_{real} = 0.63 GPa)

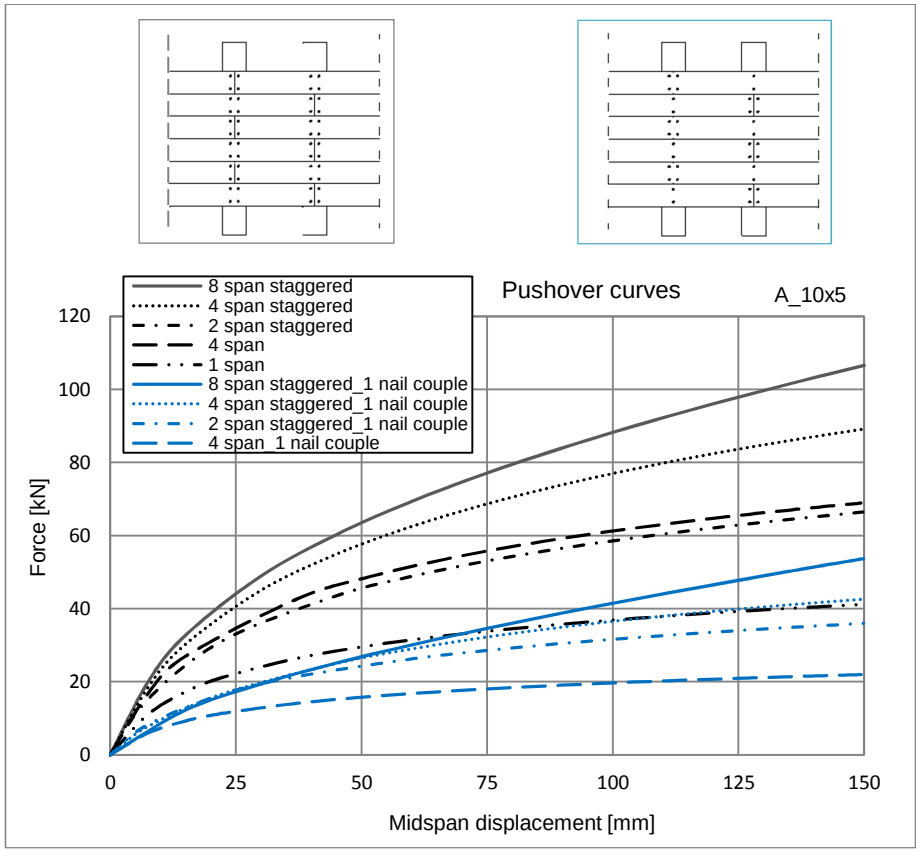

Fig. 4.6 Pushover curves (load direction parallel to the joists, target displacement = 150 mm)

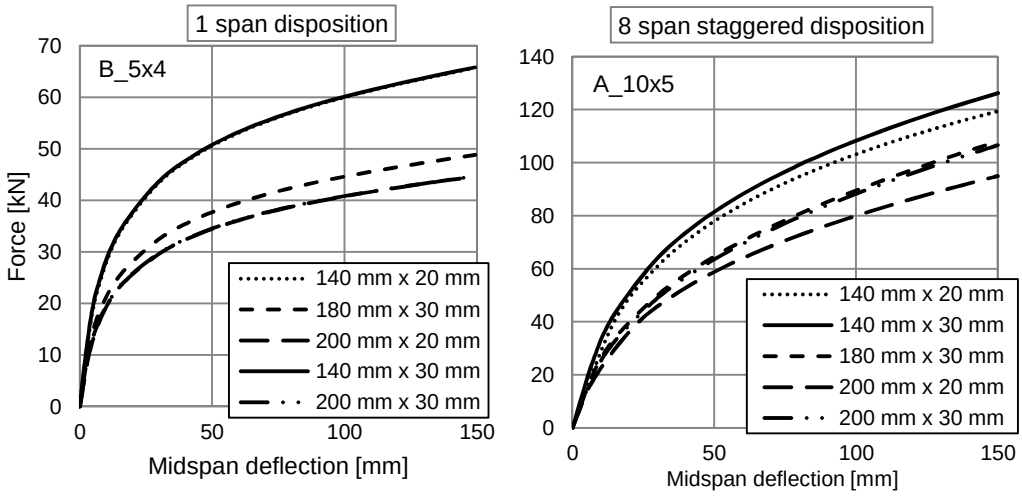

Fig. 4.7 Influence of the floorboard size on the diaphram behavior

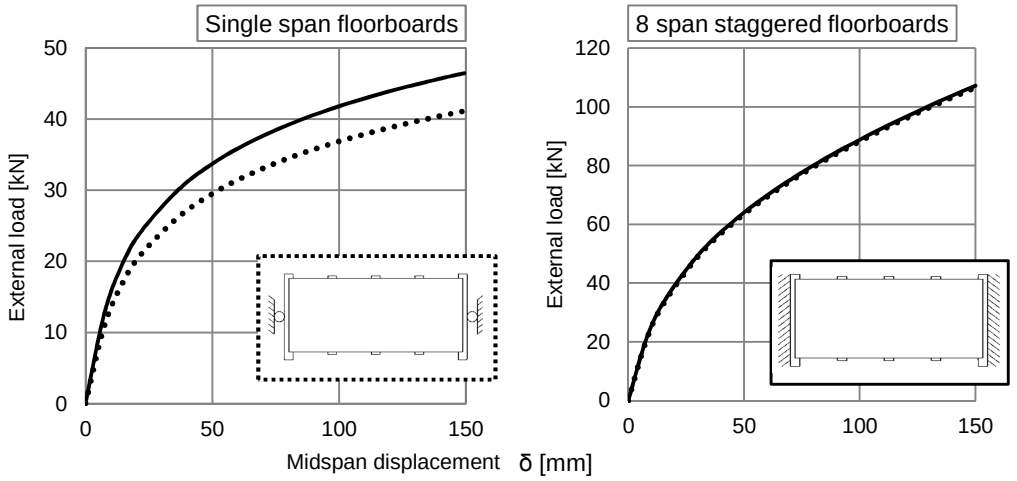

Fig. 4.8 Pushover curves: effects of the lateral constraint variation (A_10x5)

In order to determine the static scheme that better approximate the behavior of a timber floor subjected to lateral inertial loads, the deformed shape of the FE model was analyzed. The ideal beams taken into account were: a flexural beam with both ends fixed and subjected to uniformly distributed load; a shear beam under a parabolic load distribution (which has the same behavior of a pinned flexural beam under uniformly distributed load) and a shear beam loaded with a uniform load distribution. It should be noted that even if the shapes of the two ideal shear beams seem very similar, the G_d values derived adopting the two schemes vary of approximately 40%.

Single span floor diaphragms exhibited a clear variation in the deformed curve slope adjacent to the external bays (Fig. 4.9), which might be a prompt to think to a fixed flexural-beam behavior. This was due to the presence on the external joists of *4* nails acting together (in parallel) while, on the internal joists, there were *2* nail couples working in series. The use of *2* nails instead of *4* on the outer joists (this means that every board had *1* nail couple on each of its ends) changed the deformed shape significantly, showing a way more pronounced sag.

It is interesting to notice that, for the “big size” case study (*A_10x5*), a reduction of the joist spacing from 500 mm to 300 mm, made the deformed shape extremely similar to that of a shear beam under a parabolic load distribution. In case of longer boards (*4* span, not staggered), the pronounced sag just mentioned was observed even in presence of 2 nail couples on the outer joists (*A_10x5,* Fig. 4.10a). Conversely the passage to a deformed shape like that of shear beam under parabolic load was

registered when the joist spacing was doubled (Fig. 4.10b). In most of the analyses, the specimens with *2* span staggered floorboards were better represented by a shear beam under parabolic load (Fig. 4.10c). However when the analyses concerned floors with 1 nail couple on the external joists or diaphragms with 1 nail couple on those joists where the boards are continuous, the deformed shape were slightly better approximated by a uniformly loaded shear beam (Fig. 4.10d). Diaphragms with *8* span/ *4* span staggered floorboards showed a deformed shape highly sensitive to the parameter variations, which oscillated from that of a shear beam under uniform load to that of a shear beam under parabolic load.

As concerns the deformations orthogonal to the joist direction, it was observed that the deformed shape was mainly dependent on the joist section slenderness (Fig. 4.11). To describe the behavior of diaphragms with “thin” joists (where the restoring couple offered by the nails has a more significant influence), it appears to be a better choice referring to an ideal shear beam under uniformly distributed load, rather than a shear beam under parabolic load which should, however, be formally more consistent with the applied load distribution. In particular, the numeric models exhibited a more pronounced “sagged shape” than the ideal beams.

It is interesting to note that in case of a smaller floor (*B_5x4,* Fig. 4.11*b*), the deformed shape varied during the analysis showing a profile which got closer to the ideal shape of a shear beam under uniform load as the analysis went on. Thicker joists meant, on the other hand, a deformed shape more similar, or even coincident, to that one of a shear beam under parabolic load (or a pinned flexural beam under a uniform load distribution). In this case, no size-effect was registered.

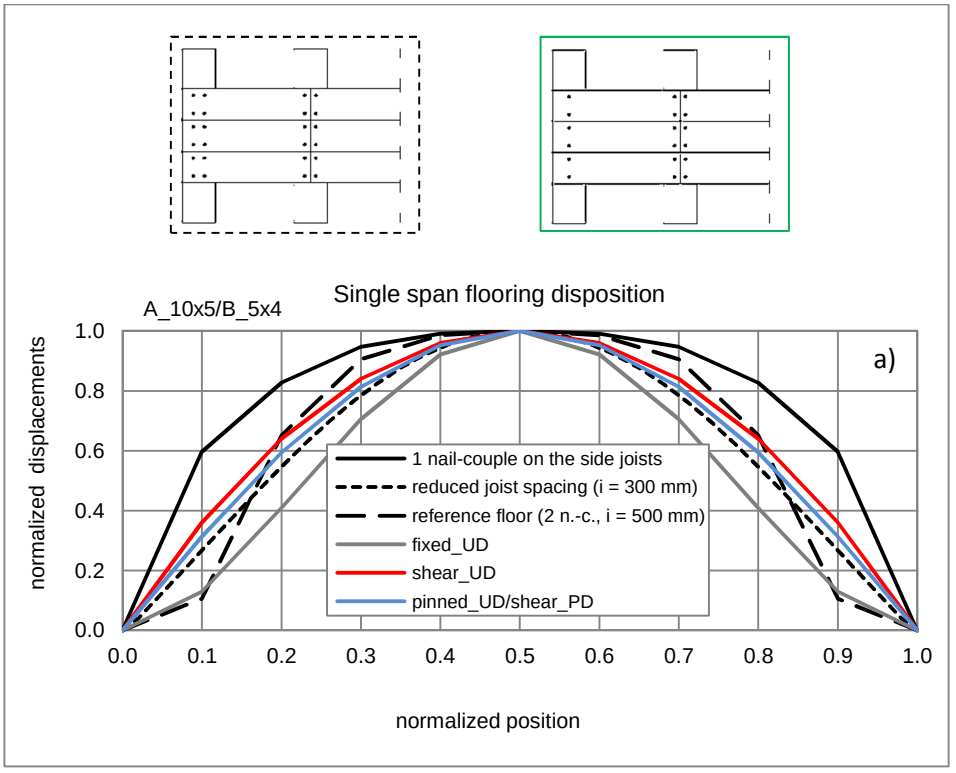

Fig. 4.9 Floor deformed shapes (load applied parallel to the joist, target displacement = 150 mm)

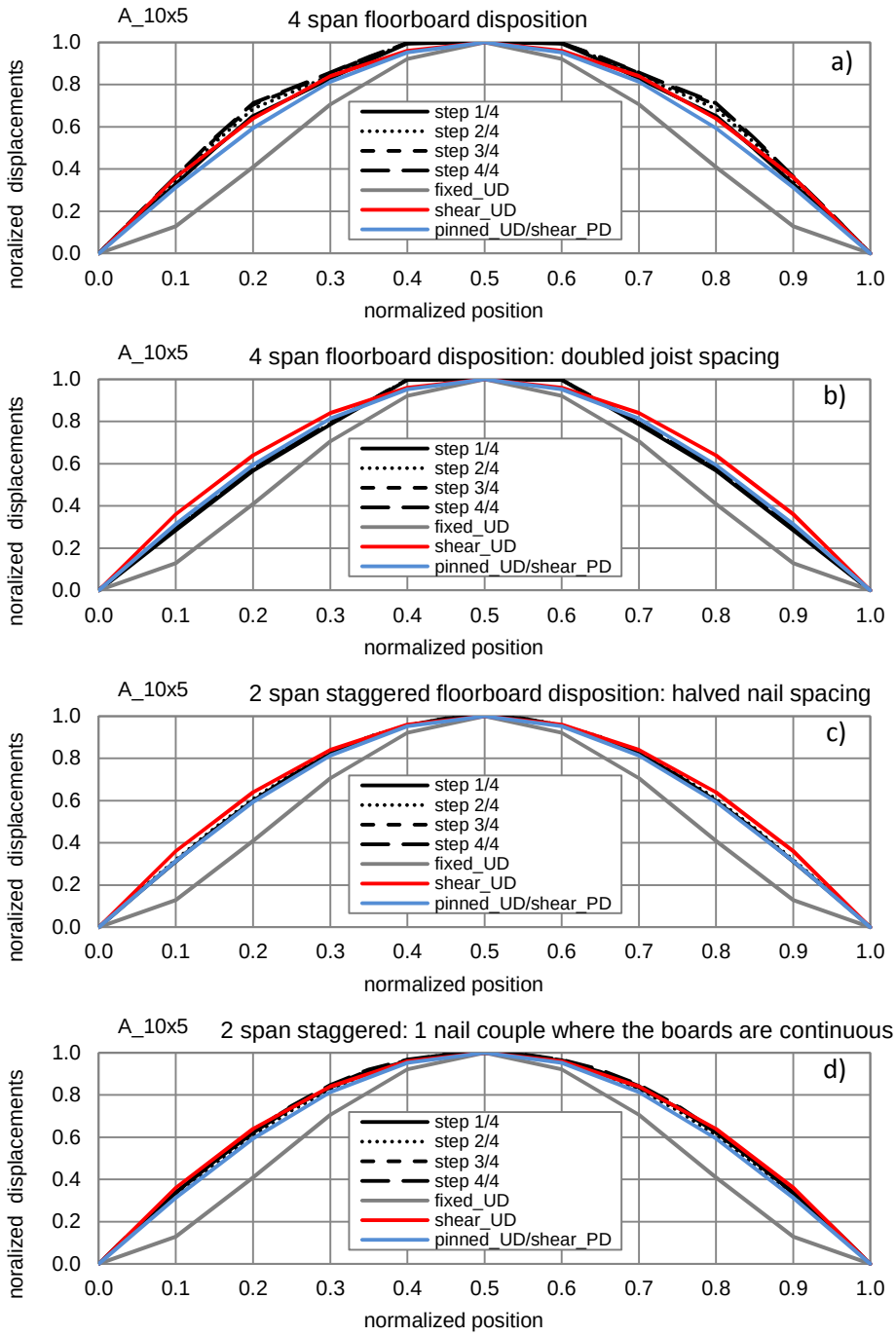

Fig. 4.10 Floor deformed shapes (load applied parallel to the joist, target displacement = 150 mm). To depict the deformation evolution, the analyses have been reported divided in 4 steps

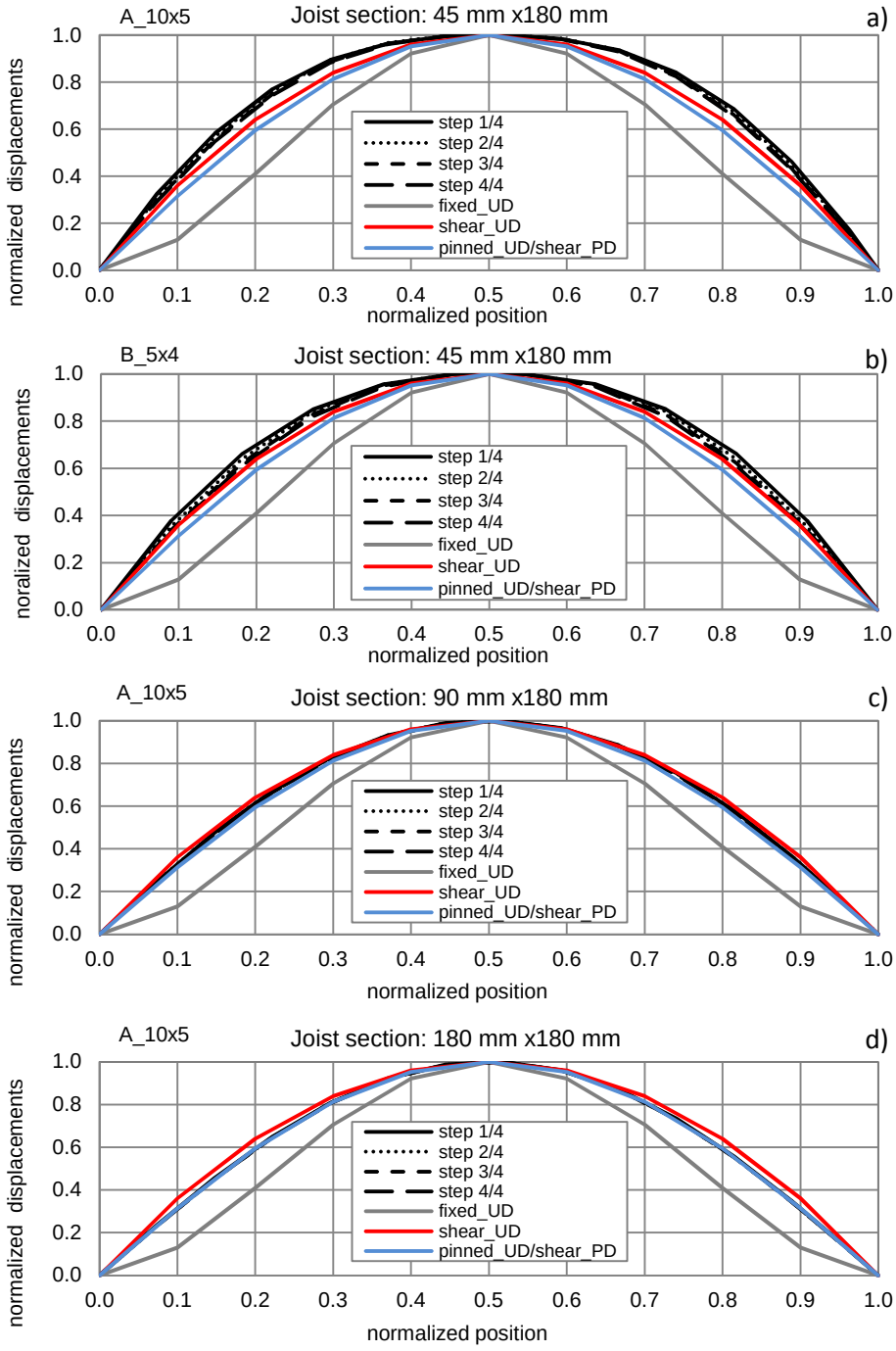

Fig. 4.11 Deformed shape under load acting orthogonal to the joists (target displacement = 150 mm). To depict the deformation evolution, the analyses have been reported divided in 4 steps

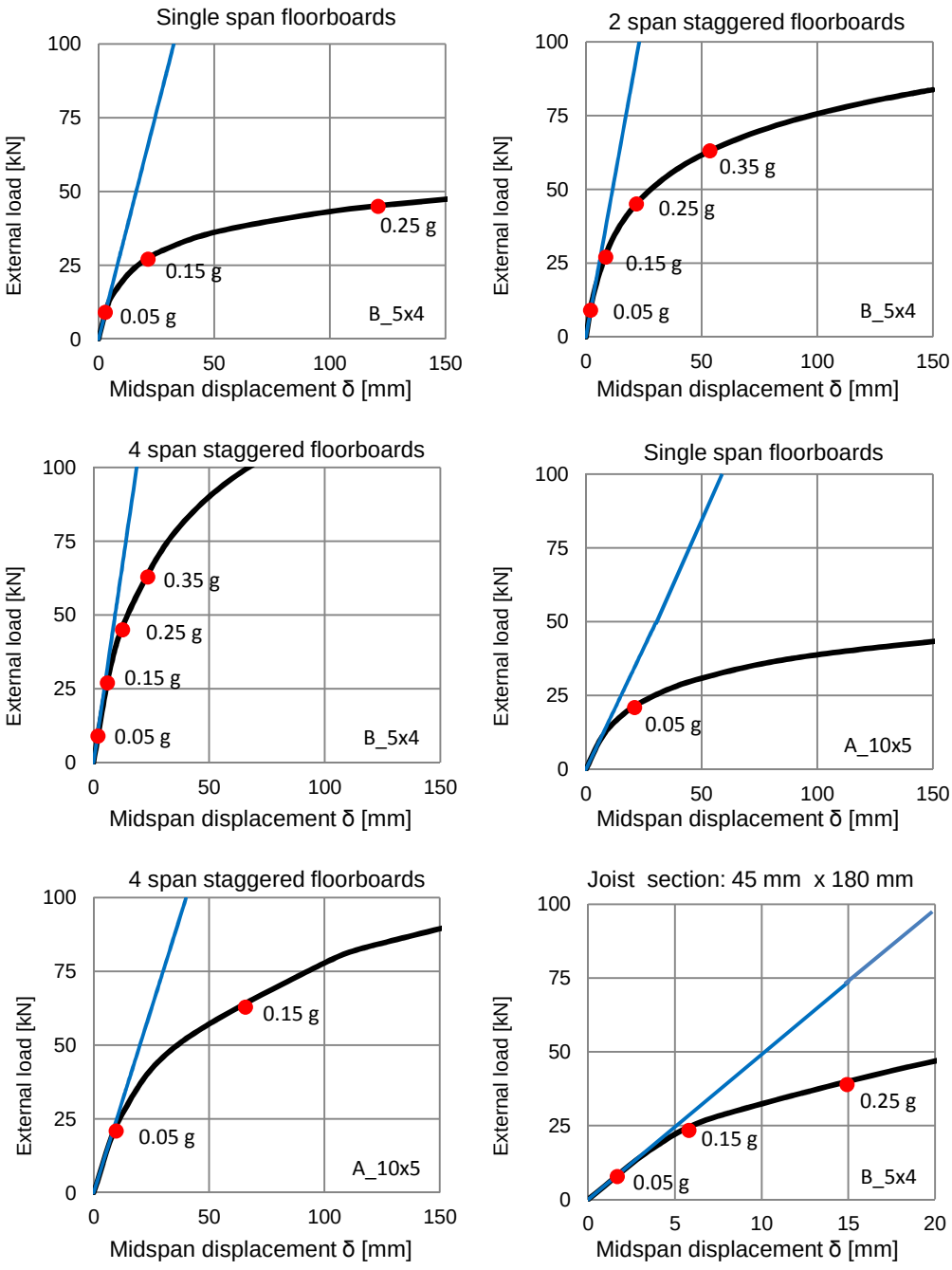

Fig. 4.12 Seismic design load: Linear modelling Vs. Nonlinear modelling

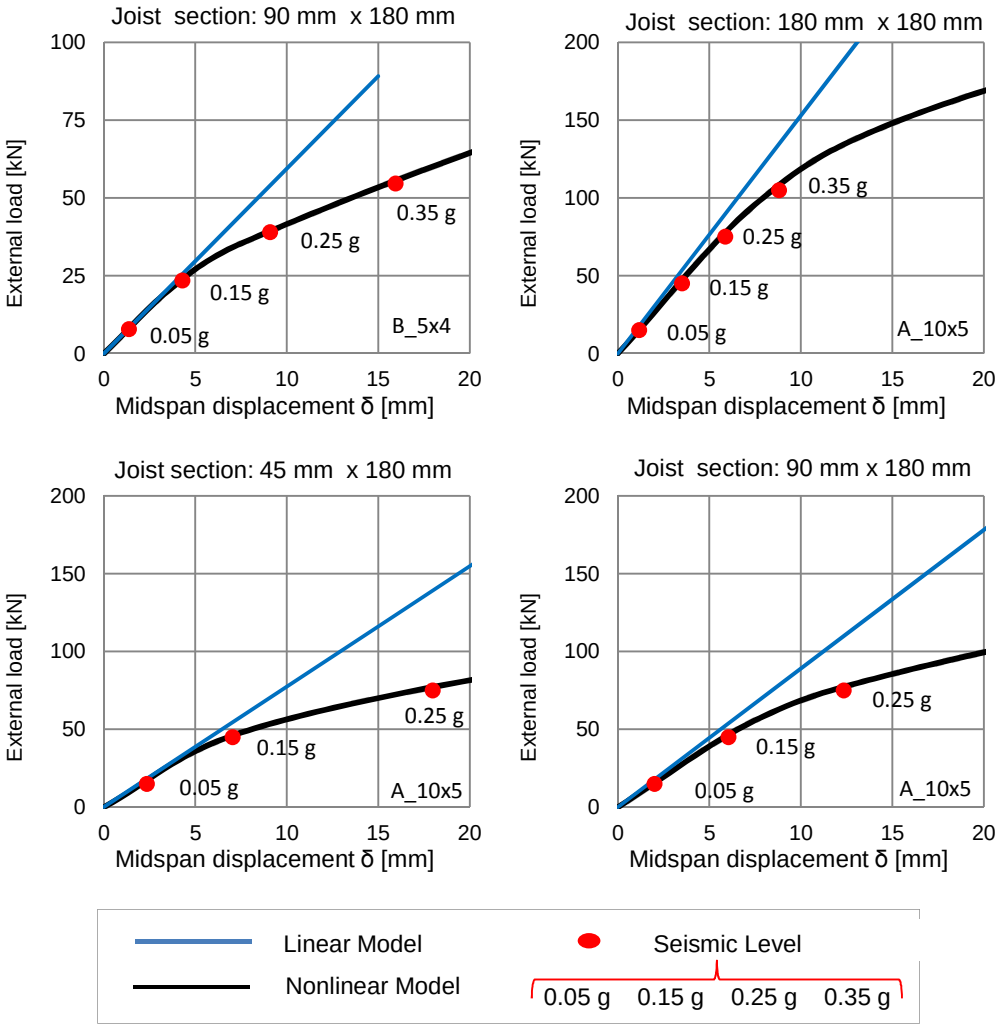

Fig. 4.13 Seismic design load: Linear modelling Vs. Nonlinear modelling

Fig. 4.12 and Fig. 4.13 report the comparison between the diaphragm pushover curves and the diaphragm responses obtained through linear modeling (nails have a linear elastic behavior). The red dots represent different load levels[1] corresponding to various seismic accelerations. First of all it can be appreciated the orthotropic behavior of single square sheathed diaphragms[2]. Secondly it can be noted how for single span flooring

[1] The "out-of-plane wall" contribution was considered in the determination of the seismic mass.

[2] While comparing the displacements in the two load directions produced by same levels of seismic action, it has to be kept in mind that the span is different.

disposition, the diaphragm response cannot be schematized through a linear model even for moderate seismic action. One might object that single span floorboards are not realistic. However it should be noted that several international standards base their assessment approaches (which are linear) on that assumption. Solely in case of very long staggered boards (when the load acts parallel to the joists) and very thick joists (when the load is orthogonal to the joist direction) the error made employing a linear model can be deemed as acceptable even in case of severe seismic condition. It should not be forgotten that in the FE model, the mechanical properties of materials were adopted in accordance with “new diaphragm” condition.

4.4 Proposal of a formulation to determine the equivalent shear stiffness

In the following paragraph a procedure to evaluate the timber diaphragm stiffness when it is loaded in the direction parallel to the joists is presented. A brief description of some of the available approaches which are relevant to understand the “background” of the proposed formulation is also given.

4.4.1 Standard & Literature approaches

The Italian guideline [CNR DT-201] suggests an approach based on the Virtual Work Principle. In particular, it considers just single span floorboards which are treated as rigid frames connected to the joists (rigid as well) by means of rotational springs (Fig. 10). Every board has one nail couple on each of its extremities. Nail deformation in the load direction is not taken into account.

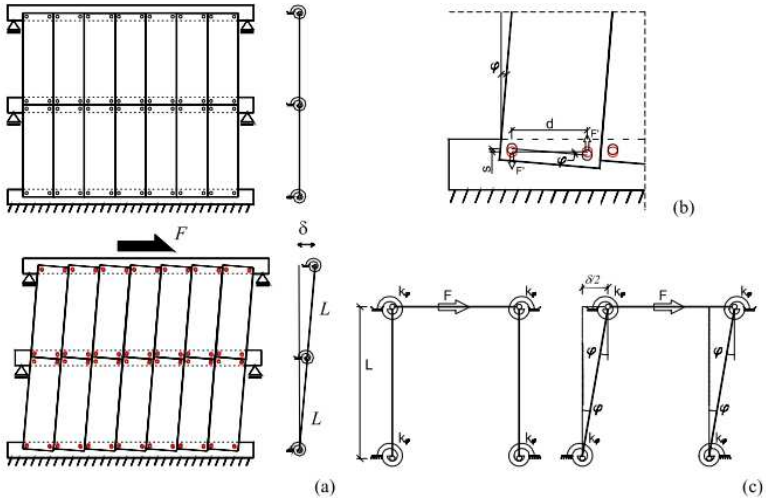

Fig. 4.14 [CNR DT-201] a) Floor scheme; b) single nail-couple stiffness; c) equivalent static scheme

The application of a force F_D to the floor reported in Fig. 11, produces a rotation angle equal to φ which is the same for all the floor bays. The nail slip value is determined assuming a linear elastic behavior:

$$e_n = \frac{s}{2} \cdot tan(\varphi) = \frac{F'}{K_{ser}} \qquad \textit{(Eq. 4.3)}$$

where K_{ser} is the nail slip modulus. By writing the moment resisting force M' exerted by the nail couple it is possible to isolate the rotational stiffness of a nail couple (k_φ):

$$M' = F' \cdot s = \left(\frac{s^2}{2} K_{ser} \right) tan(\varphi) = k_\varphi \, tan(\varphi) \approx k_\varphi \varphi \qquad \textit{(Eq. 4.4)}$$

On each board there are two nail couple working in parallel:

$$M_{board} = 2 \cdot M' = 2 \cdot k_\varphi \varphi \qquad \textit{(Eq. 4.5)}$$

Where M_{board} is the moment resistance of a floorboard. The employment of the Virtual Work Principle permits to define a relation between the external load and the midspan displacement:

$$F_D \cdot \delta = \sum_{n^\circ board} M_{board} \varphi = \sum_{n^\circ board} 2 k_\varphi \varphi^2, \quad with \quad \varphi = 2 \frac{\Delta}{L} \qquad \textit{(Eq. 4.6)}$$

$$F_D = \left(\sum_{n^\circ board} 8\frac{k_\varphi}{L^2} \right) \Delta = k_{glob} \Delta \qquad \textit{(Eq. 4.7)}$$

where k_{glob} is the global floor stiffness. By making the summation in (Eq. 4.7) explicit one obtains:

$$k_{glob} = \sum_{n^\circ board} 8\frac{k_\varphi}{L^2} = 8mn\frac{k_\varphi}{L^2} = 8mn\frac{s^2}{2}\frac{k_{ser}}{L^2} = 4\frac{BK_{ser}s^2}{hLb} \qquad \textit{(Eq. 4.8)}$$

Where m is number of floor bays ($m = \lfloor L/h \rfloor$), n is the number of floorboards along a joist ($n = \lfloor B/b \rfloor$), b is the board thickness and h is the joist spacing.

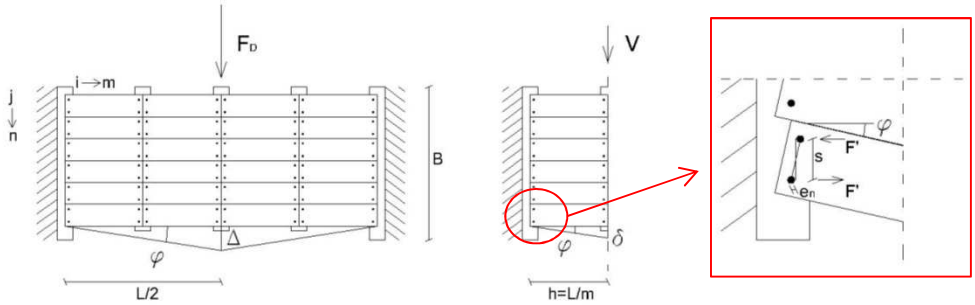

Fig. 4.15 Timber floor behavior according to [CNR-DT 201]

The same result of (Eq. 4.8) could have been achieved by considering the floorboards as springs working in series or in parallel according to their position.

The generic *j-th* board located in the *i-th* bay is subjected to the force $V_{i,j}$ which makes the board deflect of a quantity equal to δ_i.

$$\varphi = \frac{\delta_i}{L/m} = \frac{e_n}{s/2} \quad \rightarrow \quad \delta_i = \frac{2e_n L}{ms} \qquad \textit{(Eq. 4.9)}$$

The board stiffness can be written as:

$$k_b = \frac{V_{i,j}}{\delta_i} \qquad \textit{(Eq. 4.10)}$$

Acknowledging that the shear force is constant from a bay to the next, $V_{i,j} = V_j$. All the boards within the same bay work in parallel. Therefore:

$$V_j = \frac{V}{n} = \frac{F_D}{2n} \quad \rightarrow \quad k_b = \frac{F_D}{2n}\frac{ms}{2e_n L} = \frac{F_D ms}{4ne_n L} \qquad \textit{(Eq. 4.11)}$$

Consequently the stiffness associated to an entire bay (k_{bay}) is given by the sum of the stiffnesses of the boards in the bay:

$$k_{bay} = \sum_{j=1}^{n} k_b = nk_b = \frac{F_D ms}{4nLe_n} \qquad \textit{(Eq. 4.12)}$$

On the other hand the floor bays from *i = 1* to *i* = $\lfloor m/2 \rfloor$ work in series. As a result the stiffness of half diaphragm (k_{diaph}) is:

$$k_{diaph} = \frac{1}{\sum_i^{m/2}\left(\frac{1}{k_{bay}}\right)} = \frac{k_{bay}}{\frac{m}{2}} = \frac{F_D s}{2Le_n} \qquad \textit{(Eq. 4.13)}$$

The two diaphragm halves work in parallel, hence the total stiffness is:

$$k_{glob} = 2k_{diaph} = \frac{F_D s}{Le_n} \qquad \textit{(Eq. 4.14)}$$

By applying the equilibrium condition to a single board, it is possible to determine the expression of the nail slip (linear elasticity constitutive law):

$$\left(\frac{V}{n}\right)\left(\frac{L}{m}\right) = 2F's \quad \rightarrow \quad F' = \frac{F_D L}{4mnsK_{ser}} \qquad \textit{(Eq. 4.15)}$$

$$e_n = \frac{F'}{K_{ser}} = \frac{F_D L}{4mnsK_{ser}} \qquad \textit{(Eq. 4.16)}$$

By substituting (Eq. 4.16) into (Eq. 4.14), the same expression for k_{glob} as in (Eq. 4.8) it is derived:

$$k_{glob} = \frac{4mns^2 K_{ser}}{L^2} = \frac{4BK_{ser}s^2}{lLb} \qquad \textit{(Eq. 4.17)}$$

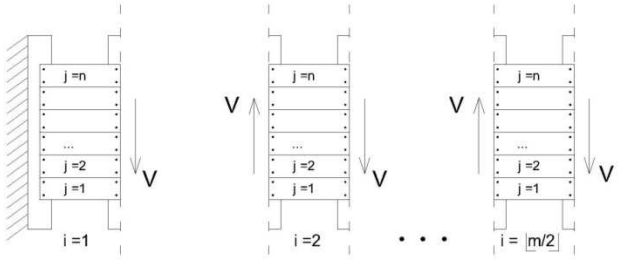

Fig. 4.16 Shear transfer mechanism in the [CNR-DT 201] approach

New Zealand Standard [NZSEE (2006)], similarly to [CNR-DT 201], regards the floorboards as rigid bodies and assumes that all the diaphragm deformation is due to the nail slip. To determine the midspan deflection, [NZSEE (2006)] suggests the following formula:

$$\Delta = \frac{Le_n}{2s} \qquad \textit{(Eq. 4.18)}$$

where L is the diaphragm span, s is the nail spacing and e_n is the nail slip resulting from the shear force V.

[Brignola et al. (2008)] allows for a more general "deformative behavior" by adding the board shear deformation and the board flexural deformation (fixed beam static scheme) to the deformation due to rigid rotation (Fig. 4.17).

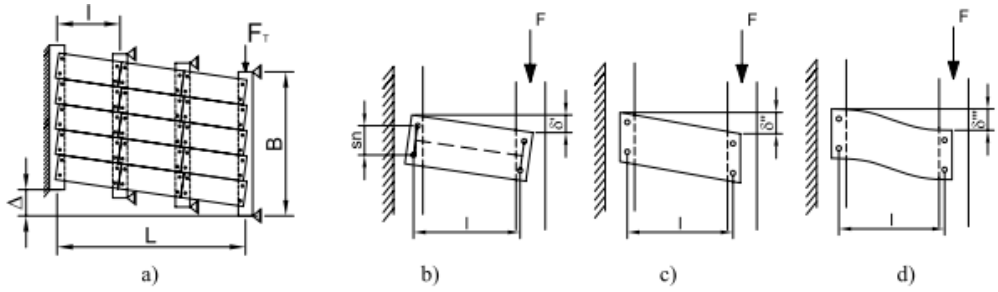

Fig. 4.17 [Brignola et al. (2008)] a) in-plane deformation of a single straight sheathing timber floor. Contributions of deformability; b) rigid rotation of the board due to nail slip; c) board shear deformation; d) board flexural deformation

The board deflection can be evaluated as follows:

$$\delta = \delta' + \delta'' + \delta''' = \left(\frac{2F'}{K_{ser} s} + \frac{\chi F}{Gbt} + \frac{Fl^2}{12EJ} \right) l \qquad \textit{(Eq. 4.19)}$$

where χ is the shear factor, G is the board shear modulus, E is the board modulus of elasticity, J is the board moment of inertia and F is the force applied to the board, which can be expressed as:

$$F = \frac{F_T b}{B} \qquad \textit{(Eq. 4.20)}$$

where F_T is the total shear force on the diaphragm. For each deforming mechanism, an equivalent shear strain γ can be obtained by simply diving the corresponding deflection component by the board length:

$$\gamma = \gamma' + \gamma'' + \gamma''' = \frac{F_T}{B}\left(\frac{bl}{K_{ser}s^2} + \frac{\chi}{Gt} + \frac{bl^2}{12EJ}\right) \qquad \textit{(Eq. 4.21)}$$

The total displacement of the diaphragm (Δ) is:

$$\Delta = \gamma L = \frac{F_T L}{B}\left(\frac{bl}{K_{ser}s^2} + \frac{\chi}{Gt} + \frac{bl^2}{12EJ}\right) \qquad \textit{(Eq. 4.22)}$$

Subsequently the same authors [Brignola et al. (2012)] proposed a different approach valid in case of sufficient interlocking between boards or in case of boards that span the full diaphragm length. The presence of a steel chord along the diaphragm perimeter is also required. Provided such conditions, the internal floorboards are treated as simple flexural beams, while the external boards and the chords are considered as fixed flexural beams. According to the authors the fixed end condition is guaranteed by the presence of the chord in the direction orthogonal to the joists. Therefore the diaphragm stiffness is given by the sum of these contributions (internal boards, external boards and chords work in parallel):

$$k_{diaph} = \frac{32}{5L^3}\left(Eb^2tB + 8Eb^3t + 10E_c b_c t_c\right), \quad \Delta_{mid} = \frac{F_{tot}}{k_{diaph}} \qquad \textit{(Eq. 4.23)}$$

where E_c is the modulus of elasticity of the steel chord elements, t_c is the chord thickness, b_c is the chord width and F_{tot} is the total lateral load on the diaphragm. The equivalent shear stiffness is then determined assuming as static scheme a shear beam under uniformly distributed load:

$$G_{eq} = \frac{4}{5}\frac{Eb^2t}{L^2} + \frac{32}{5}\frac{Eb^3t}{BL^2} + 8\frac{E_c b_c^3 t_c}{BL^2} \qquad \textit{(Eq. 4.24)}$$

4.4.2 Analytical formulation

The basic FE model configuration employed for deriving the shear stiffness evaluation formula, had a single span flooring with *1* nail couple at each board extremity. The midspan displacement (Δ_{mid}) can be determined by summing the relative displacements (δ_i) measured on two adjacent joists from the diaphragm end to the "midspan joist":

$$\Delta_{mid} = \sum_{i=1}^{\lfloor m/2 \rfloor} \delta_i = \sum_{i=1}^{\lfloor m/2 \rfloor} \vartheta_i \cdot h = \sum_{i=1}^{\lfloor m/2 \rfloor} \vartheta_i \cdot \frac{L}{m} \qquad \textit{(Eq. 4.25)}$$

where *m* is the number of "floor bays", ϑ_i is the board rotation, *h* is the joist spacing and L is floor length. From the analysis of the deformed shape, it appeared that the boards of a single span flooring rotate rigidly. Therefore, under the "small displacements hypothesis" ($\theta_i \approx tan\ \theta_i$), the rotation of each board in the *i-th* bay can be expressed as:

$$\vartheta_i = \frac{e_n \cdot 2}{s} \qquad \textit{(Eq. 4.26)}$$

where e_n is the nail slip and *s* is the nail spacing. The nail slip can be obtained from Mclain's curve rearranging (Eq. 4.1):

$$e_n = \frac{10^{F'/\underline{A}} - 1}{\underline{B}} \qquad \textit{(Eq. 4.27)}$$

By applying the equilibrium principle to the floorboards, it is possible to derive the force (F'_i) acting on the single nail:

$$\frac{V_i}{n} \cdot \frac{L}{m} = 2F' \cdot s \rightarrow F' = \frac{V_i}{n} \cdot \frac{L}{m} \cdot \frac{s}{2} \qquad \textit{(Eq. 4.28)}$$

where V_i is the shear force in the *i-th* bay (assuming that the external load is applied to the joists) and *n* is the number of boards along the joist. Consequently (Eq. 4.26) becomes:

$$\vartheta_i = \frac{2}{\underline{B}s} \cdot 10^{\frac{V_i L}{nm} \frac{s}{2\underline{A}} - 1} \qquad \textit{(Eq. 4.29)}$$

Bearing in mind the parabolic load distribution suggested by FEMA, each joist is subjected to a force equal to:

$$F_i = \int_{(x_i+x_{i-1})/2}^{(x_{i+1}+x_i)/2} f_d(x)dx, \quad i \geq 2, \quad F_1 = \int_0^{(x_2+x_1)/2} f_d(x)dx \qquad \textit{(Eq. 4.30)}$$

Where x_i is the *i-th* joist position, measured from the diaphragm end. Therefore, the shear force in the *i-th* bay is (Fig. 10):

$$V_i = V_{i-1} - F_i, \quad i \geq 1, \quad V_0 = F_D / 2 \qquad \textit{(Eq. 4.31)}$$

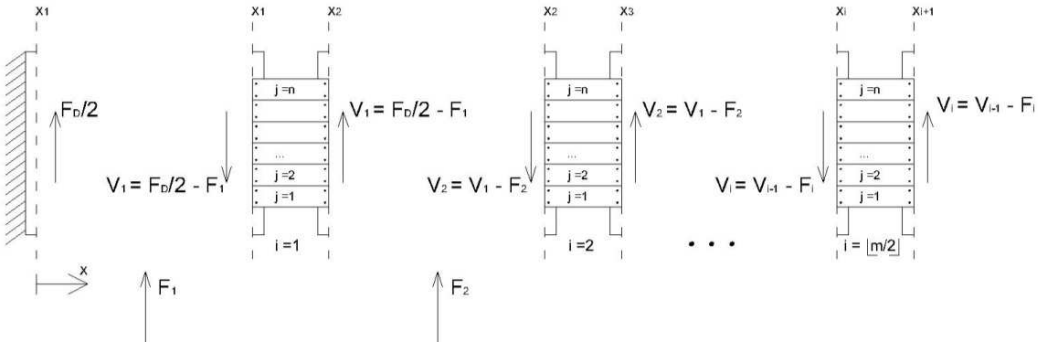

Fig. 4.18 Schematization of the shear load transfer

Hence, the nail load can be written as:

$$F' = \frac{V_{i-1} - F_i}{n} \cdot \frac{L}{m} \cdot \frac{s}{2} \qquad \textit{(Eq. 4.32)}$$

The midspan displacement is:

$$\Delta_{mid} = \sum_{i=1}^{\lfloor m/2 \rfloor} \frac{2L}{\underline{B}sm} \cdot 10^{\frac{(V_{i-1}-F_i)L}{nm} \cdot \frac{s}{2\underline{A}} - 1} \qquad \textit{(Eq. 4.33)}$$

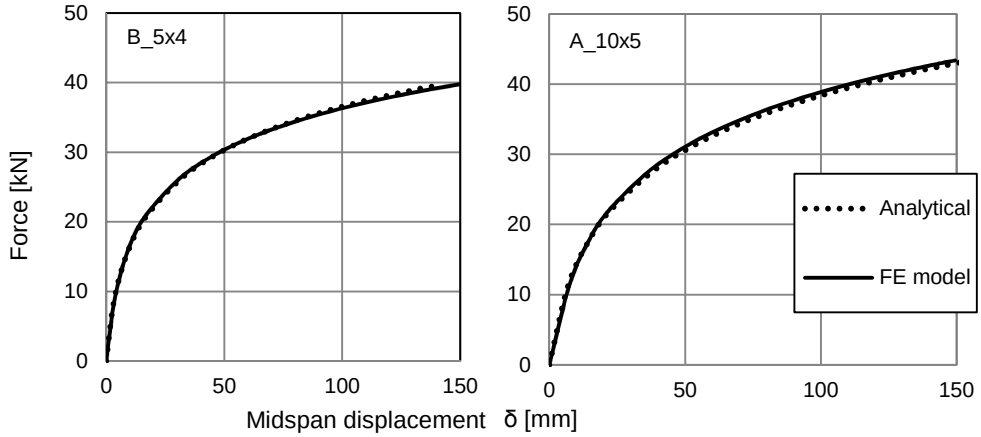

Fig. 4.19 Diaphragm deflection evaluation: comparison between FE model and analytical procedure (single span flooring disposition)

The comparison between the midspan deflection Vs. external load curve obtained from the FE model and that one derived from (Eq. 4.33) is reported in Fig. 11. Finally it is possible to determine the equivalent shear stiffness value:

$$G_{eq} = k\frac{F_D L}{A\sum_{i=1}^{\lfloor m/2 \rfloor}\frac{2L}{\underline{B}sm}\cdot 10^{\frac{(V_{i-1}-F_i)L}{nm}\cdot\frac{s}{2\underline{A}}-1}} \qquad \textit{(Eq. 4.34)}$$

where A is the floor section ($A = Bt$, B = *floor depth*, t = *flooring thickness*) and k is a parameter depending on the static scheme adopted to represent the floor behavior ($k = 1/8$ for the shear beam under uniformly distributed load, $k = 5/32$ for the shear beam under parabolic distributed load).

(Eq. 4.34) is based on the assumption/approximation that floorboards rotate rigidly. Consequently, in order to take into account flooring dispositions other than single span, a modification factor $\omega(F_D, \lambda)$ is proposed:

$$\omega(F_D,\lambda) = -2.4\cdot 10^{-3}F_D + \lambda\left(\frac{L}{l}\right), \quad if\ \frac{L}{l} > 3 \qquad \textit{(Eq. 4.35)}$$

where λ is a parameter depending on the ratio between the diaphragm length and the floorboard length.

$$\lambda\left(\frac{L}{l}\right) = 1.3\cdot 10^{-3}\left(\frac{L}{l}\right)^2 + 10^{-2}\left(\frac{L}{l}\right) + 0.63 \qquad \textit{(Eq. 4.36)}$$

In case *L/l ≤ 3*, another modification factor *ξ(l/h)* is introduced:

$$\xi\left(\frac{l}{h}\right)=0.062\frac{l}{h}+\Omega\left(\frac{L}{l}\right),\quad \frac{L}{l}\leq 3 \qquad \textit{(Eq. 4.37)}$$

with:

$$\Omega\left(\frac{L}{l}\right)=-0.065\left(\frac{L}{l}\right)^{2}+0.55\left(\frac{L}{l}\right)-0.45 \qquad \textit{(Eq. 4.38)}$$

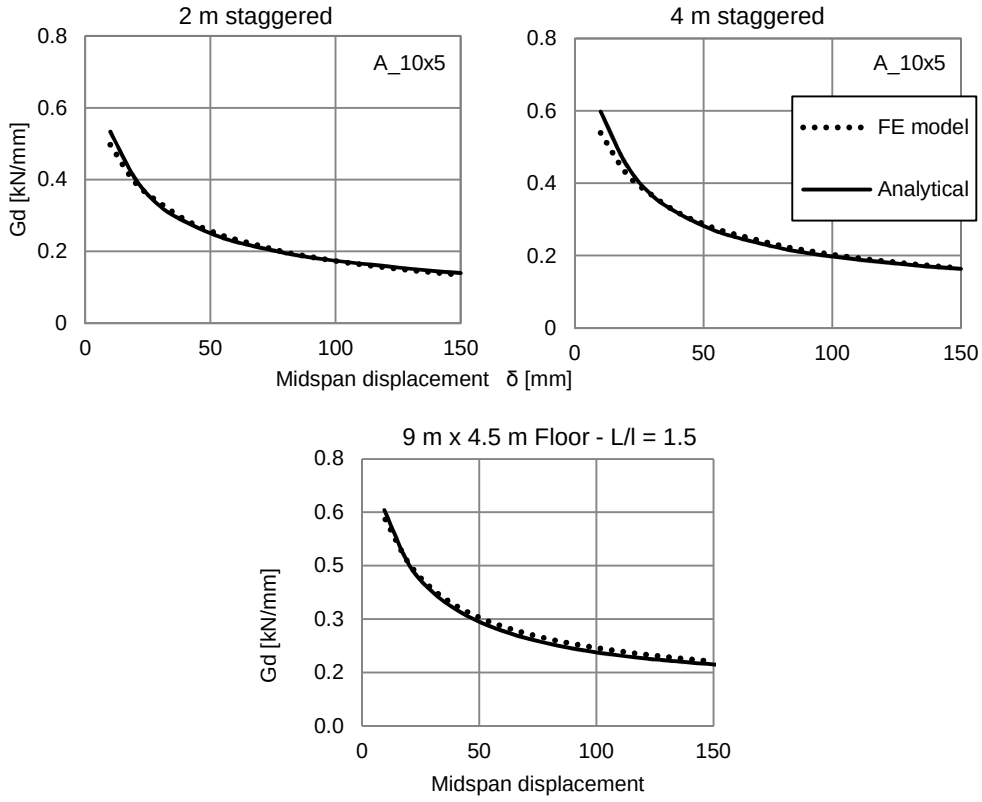

Fig. 4.20 Diaphragm stiffness evaluation: comparison between FE model and analytical

procedure Fig. 12 shows the comparison between the G_d curves obtained from the FE model and those derived using (Eq. 4.39) adopting as static scheme a uniformly loaded shear beam. The proposed formulation seems to be able to reproduce the FE behavior.

$$G_{eq} = k \frac{F_D L}{A \sum_{i=1}^{\lfloor m/2 \rfloor} \frac{2L}{\underline{B}sm} \cdot 10^{\frac{(V_{i-1} - F_i) \cdot \omega \cdot \xi \cdot L}{nm} \frac{s}{2\underline{A}} - 1}} \qquad \textit{(Eq. 4.39)}$$

4.5 Conclusions

The results of the parametric analyses showed that the floorboard disposition is a governing parameter in determining the in-plane response of a timber floor-diaphragm. Single span boards behaved mainly as rigid bodies where all the deformation was concentrated into the nails which exhibited almost no deformation in the direction orthogonal to the load direction. On the contrary when longer and staggered floorboards were present, the nail deformation in the direction parallel to the load direction and the flexural deformation of the boards became significant. In all cases the shear deformability of the timber elements appeared to be negligible. Not surprisingly, the diaphragm stiffness proved to be directly related to the nail pattern and spacing. The importance of the flooring configuration is generally not acknowledged in literature. It must be said that the FE model adopted in this work was not able to detect any “interlocking effect” due to direct contact since no interaction between boards was allowed. In addition friction phenomena were not taken into consideration.

The study of the deformed shape showed that the behavior of a timber floor loaded by a load distribution reproducing the inertial load, can be schematized through a shear beam even if the lateral joists are prevented from rotating. However it was not possible to define a unique tendency in terms of “ideal deformed shape”. That is to say, according to the diaphragm characteristics the deformed shape was better depicted by a shear beam under uniformly distributed load or by a shear beam under parabolic load alternatively. When the diaphragms were loaded orthogonally to the joist direction, the shape was determined by the joist thickness. Floors with relatively thin joists were (like those which are common in Northern Europe, North America and New Zealand) were better represented by a uniformly loaded shear beam. Diaphragm with thicker joists (like those typical of the Mediterranean Countries), were scarcely affected by the restoring

moment couples generated by the nails and behaved like beams working in parallel showing a deformed shape similar to that of shear beam under parabolic load.

It was observed that single straight sheathed diaphragms present different responses according to the load direction. However a nonlinear response was registered in both directions even for not particularly severe seismic accelerations (with the exception of diaphragms with very thick joists).

An analytical formulation able to take into account the nonlinear behavior of the nails and the inertial load distribution was proposed. Good agreement was observed between the displacement values evaluated with the analytical formula and those provided by the FE model in case of single span flooring. Modification factors were also introduced to consider staggered floorboard dispositions. The analytical shear stiffness appeared to reproduce with sufficient accuracy the equivalent shear stiffness derived from the numerical model. Further study is however suggested, with special attention to different aspect ratios. In addition, the proposed approach should be extended to the direction orthogonal to the joists, particularly if thin joists are considered.

4.6 References

Baldessari, C., Piazza, M., Tomasi, R., (2009). *The refurbishment of existing timber floors: characterization of the in-plane behaviour.* ISBN: 978-0-415-55804-4. Protection of Historical Buildings. PROHITECH 09, London: Taylor & Francis, 255-260.

Brignola A., Podestà S., Pampanin S., (2008), *In-plane stiffness of wooden floor*, 2008 NZSEE Conference Proceedings

Brignola A., Pampanin S., Podestà S., (2012), *Experimental Evaluation of the In-plane stiffness of Timber Diaphragms*, Earthquake Spectra: November 2012, Vol. 28, No. 4, pp. 1687-1709.

CNR-DT 201/2005, (2005), *Studi Preliminari finalizzati alla redazione di: Istruzione per Interventi di Consolidamento Statico di Strutture Lignee mediante l'utilizzo di Compositi Fibrorinforzati*, Consiglio Nazionale delle Ricerche, In italian

CSI [Computers and Structures Inc.], (2004), *CSI Analysis Reference Manual For SAP2000*®, ETABS®, and SAFE®. CSI, Berkeley

FEMA 356, (2000), *Prestandard and Commentary for the Seismic Rehabilitation of Buildings,* American Society of Civil Engineers and Federal Emergency Management Agency, Reston, VA

Kuenzi E. W., (1955), *Theoretical Design of a Nailed or Bolted Joint under Lateral Load*, Report No. D1951, U.S. Dept. of Agriculture, Forest Production Laboratory, Madison, Wisconsin

McLain T. E., (1975), *Curvilinear Load-Slip Relations in Laterally-Loaded Nailed Joints*, Ph.D. thesis, Colorado State University, Fort Collins, Colorado

NZS 3603:1993, (1996), *Timber Structures Standard*, Standards Council, Wellington, New Zealand

NZSEE, (2006), *Assessment and improvement of the structural performance of buildings in earthquakes: prioritisation, initial evaluation, detailed assessment, improvement measures: recommendations of a NZSEE study group on earthquake risk buildings*, New Zealand Society for Earthquake Engineering, Wellington, New Zealand.

Pellicane P.J., Stone J.L., Vanderbilt M.D., (1995), *Generalized model for lateral load slip of nailed joints*, Journal of materials in civil engineering, V. 30, 1995

Peralta D. F., Bracci J. M., Hueste M. B. D., (200), *Seismic Performance of Rehabilitated Wood Diaphragm*, Texas A&M University, Department of Civil Engineering, College Station, Texas 77843-3136

Piazza, M., Baldessari, C., Tomasi, R., Acler, E. (2008). *Behaviour of refurbished timber floors characterized by different in-plane stiffness*. Structural Analysis of Historical Constructions, Bath, U.K., Dina D'Ayala, E. Fodde (Eds.).

Wilkinson T.L., (1971), Theoretical lateral resistance of nailed joints, Journal of the structural division proceedings of the American Society of Civil Engineers, N. 5, 1971

Wilson A., (2012), *Seismic Assessment of Timber Floor Diaphragms in Unreinforced Masonry Buildings*, University of Auckland, PhD Thesis, Auckland, New Zealand

5 EXPERIMENTAL CAMPAIGN ON THE IN-PLANE PROPERTIES OF TIMBER DIAPHRAGMS

5.1 Introduction

In the literature, several works pertaining to in-plane full-scale tests on timber diaphragms (reinforced and unreinforced) are available. Among them the most recent are those of Baldessari et al. [Baldessari et al (2009)], Brignola [Brignola (2009)], Corradi et al. [Corradi et al. (2006)], Dolan et al. [Dolan et al. (2003)], Filiatrault et al. [Filiatrault et al.(2002)], Gattesco and Macorini [Gattesco and Macorini (2008)], Peralta et al. [Peralta et al. (2004)], Valluzzi et al. [Valluzzi et al. (2010)] and Wilson et al. [Wilson et al. (2013)]. All these studies are based on tests carried out on new specimens specifically built for research purposes. Consequently there is an evident lack of data regarding the properties of existing timber floors. In addition, such works do not address (apart from Wilson et al.) the diaphragm behavior under loads acting in the direction orthogonal to the joists.

In this chapter the outcomes of a field testing campaign on the in-plane properties of old timber diaphragms are presented. The tests were carried out during an exchange-period at the University of Auckland (New Zealand). Both mechanical and dynamic properties of timber floors were investigated thanks to cyclic quasi-static tests and dynamic snap-back tests.

5.2 Campaign preparation

5.2.1 The Building

The building chosen for the testing campaign is a two-story brick masonry building located in Whanganui (New Zealand) which dates back to 1913 (Fig. 5.1). The walls' thickness is 350 mm (three leaves) at the ground floor and 220 mm (two leaves) at the first floor. The floor has a 9.7 m span and is supported at the center by a double timber beam lying on cast iron columns.

Fig. 5.1 Tested Building: a) front view; b) lateral view.

5.2.2 Floor sections

Two specimens, whose length was 5.6 m and 4.7 m were obtained from an available 17 m floor length (joists were orientated in the 9.6 m direction). Due to the advanced state of decay of the floor close to the North-West corner of the building, it was not possible to get more than two specimens. The difference in the specimen length is also related to the desire to test floors with different aspect ratios. It is plain that for a floor which is 9.7 m wide, a length variation of less than 1 m does not produce an extreme modification of the aspect ratio (20%, from 1.73 to 2.06). On the other hand smaller ratios would have required an excessively large external load, while a much slender specimen would have shown a beam-like behavior with an influence of the out-of plane properties of the joists being much greater than that one appreciable in a “real floor”.

The specimens, that from now on will be called A (9.6 m x 5.6 m) and *B* (9.6 m x 4.7 m), were made of 50 mm x 300mm NZ native timber rimu joists with an average spacing of 450 mm, covered by a layer of 130 mm x 22 mm NZ native timber matai floorboards.

Cross bracings were also present in the direction orthogonal to the joists, with a spacing of about 1.5 m (Fig. 5.2).

Fig. 5.2 Cross bracings.

5.2.3 Specimen manufacturing

Acknowledged that there was not much point in testing the in plane-properties of a floor that was unable to bear the vertical exercise load, some of the floorboards which were rotten were replaced with boards carefully extracted from a part of the building unsuitable for testing. The replacement boards were fixed to the joists using salvaged nails. The whole “refurbishment” intervention was carried out paying attention to reduce to the minimum the effects on the other parts of the specimens. On the bottom surface of the joists a ceiling was attached. The ceiling was made of 85 mm x13 mm NZ native timber kauri boards sheathed with metal sheets 0.3 mm thick.

Fig. 5.3 Ceiling boards and metal sheathing.

With the purpose of isolating the specimens from the supporting beam, each joist was lifted with an hydraulic jack so as to create the room for a saw blade to be inserted and cut the nails connecting the joist to the beam (Fig. 5.4a). Subsequently, to minimize the effects of friction phenomena, a couple of greased, low-friction sheets (polystone, 100 m x 300 m) were put under every joist (Fig. 5.4b).

Fig. 5.4 Isolation of the specimens: a) nail cut; b) insertion of the low-friction sheets.

5.2.4 The new anchoring system

Since the original anchoring system was deficient, new 16mm epoxy-grouted anchors were installed before starting the testing procedure (Fig. 5.5). The thickness of the timber blocking elements was 50 mm, while the washers measured 80 mm x 80 mm x 5 mm. Since all the diaphragm tests were in the direction orthogonal to joists, no fastener was applied to connect the blocking element to the adjacent joists.

The design of the new anchors was based on the diaphragm shear load transfer V_d determined in accordance with [NZSEE (2011)] assuming that the building was placed in Wellington, New Zealand (highly seismic area):

$$V_d = C_1 C_3 C_d(T_i) W_d = 255 kN \quad \textit{(Eq. 5.1)}$$

where C_1 = 1, C_3 = 1, $C(T_i)$ = 0.44 (very soft soil), W_d =585 kN. This value of shear load transfer corresponds to a shear unit load of 7.*5 kN/m*. The period of the whole diaphragm was calculated as proposed by [Wilson (2012)] with the coefficient α_w introduced by [Knox (2012)] to take into account the stiffness of the out-of-plane walls:

$$T_i = 0.7\sqrt{\frac{W_d L}{G_d B}}\alpha_w = 0.65\ sec \quad \textit{(Eq. 5.2)}$$

where α_w = 0.675, G_d = 175 kN/m [NZSEE (2011)], B = 17 m and L = 9.6 m.

The stiffness (K_y = 2.3 kN/mm) and the resistance (F_y = 15 kN) of the new anchors were obtained from a series of cyclic tests carried out on the walls of the same building. The setup adopted for these shear tests is reported in Fig. 5.7a. The external load applied by the hydraulic jack was measured by a 100 kN load cell, while a 50 kN load cell measured the axial load in the rod applied by the nut. Two linear inductive transducers (LVDTs) were also employed to read the blocking and the rod displacement. In order to keep the rod center aligned with the jack, two steel L-shaped brackets were used.

In Fig. 5.6 are shown the results of these tests in terms of envelope curves. The abbreviation *HT* means that the nut was hand-tight (0.8 kN) while *T* means that it was tighten up to 10 kN. The label *FL* stresses the presence of two low-friction sheets between the timber blocking and the wall.

Once determined the anchor performance and the diaphragm shear load transfer, it was possible to identify the maximum spacing *i* allowed for the new anchors:

$$i = \frac{2BF_y}{V_d} \sim 2.0\ m \quad \textit{(Eq. 5.3)}$$

The actual positioning was affected by the real possibility of inserting the anchor rod. The spacing value herein suggested has therefore to be considered as an average value on the specimen.

Fig. 5.5 Installation of the new anchors.

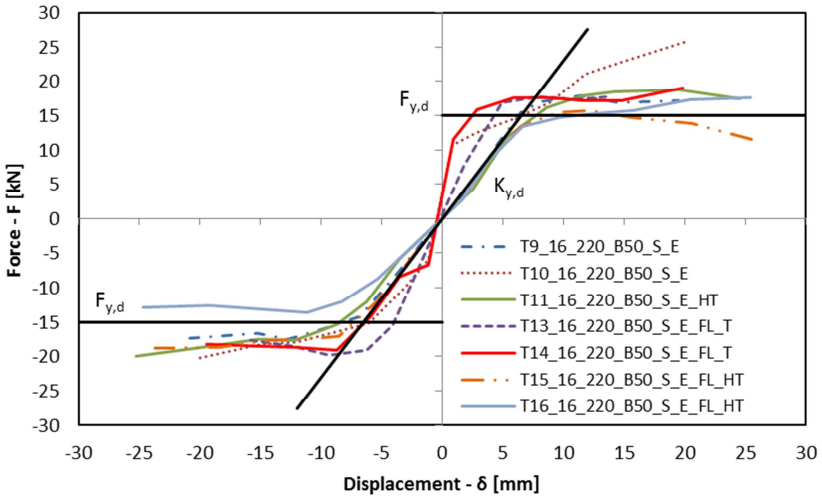

Fig. 5.6 Anchor test results (rod diameter 16 mm, embedment depth 220 mm, blocking thickness 50 mm).

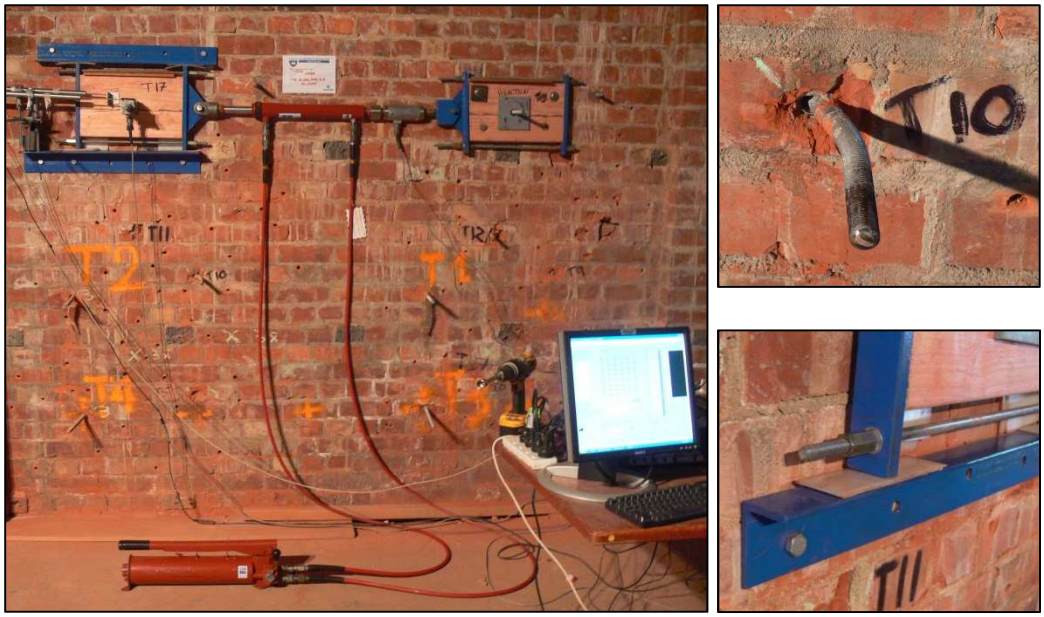

Fig. 5.7 Shear tests of the anchors: a) test setup; b) observed failure mode; c) low-friction sheets.

5.3 Test setup

5.3.1 Loading system

According to [FEMA 356], in order to identify the seismic response of a flexible diaphragm, the load distribution should reproduce the *"likely distribution of horizontal inertia forces"* given by the following expression:

$$f_d = \frac{1.5F_D}{L}\left[1-\left(\frac{2x}{L}-1\right)^2\right] \qquad \textit{(Eq. 5.4)}$$

where F_D is the total inertial load, L is the distance between the lateral support points of the diaphragm and x is the distance from the diaphragm's end. Taking into account a 4-point load application and dividing the floor into 4 parts of identical length, it is possible to approximate the inertial distribution by substituting it with a uniform distribution for each part, whose resultant is equal in module to that one of the inertial load which falls in its tributary length (Fig. 5.8). As a result $F_A \approx F_D/6$ and $F_B \approx F_D/3$.

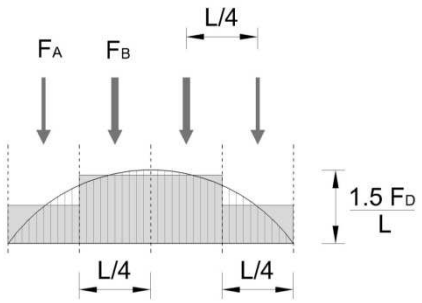

Fig. 5.8 Load distribution

Therefore, so as to apply the desired load pattern, a loading system made of pulleys and wire ropes was developed (Fig. 5.9). Provided that the equation $2\sin(\gamma)=\sin(\beta)$ is satisfied, the wire inclinations can be varied to one's liking without provoking any changes in the ratios between the applied forces. That means that the setup can be adapted to different specimens. Obviously, the bigger the angles the lower the tension into the wires and the lower the forces orthogonal to the loading direction introduced by the two outer loading plates. The main advantages of this setup are that it is "lightweight", "thin" and easy to relocate from one specimen to the next, with no need to move the reaction points. In addition, since the steel frame that keeps the pulleys in the right position, can be put at any distance from the load points (e.g. outside the tested specimen) the setup does not affect the diaphragm response in case of dynamic tests. On the other hand, in order to perform a cyclic test two setups are required (Fig. 5.12). It has to be noted that when a ceiling is present, a vertical eccentricity between the loading surface and the "center of in-plane stiffness" has to be taken into consideration[3].

The external force was applied by two hydraulic, single acting hollow cylinders positioned on both sides of the specimen (Fig. 5.10a). During the snap back tests the load was istantaneously released thanks to a snap shackle borrowed from the "sailing world" (Fig. 5.10b).

[3] By comparing the top to the bottom instrument (SP2/SP5), no out-of plane joist rotation was detected, probably due to the presence of the cross-bracing elements.

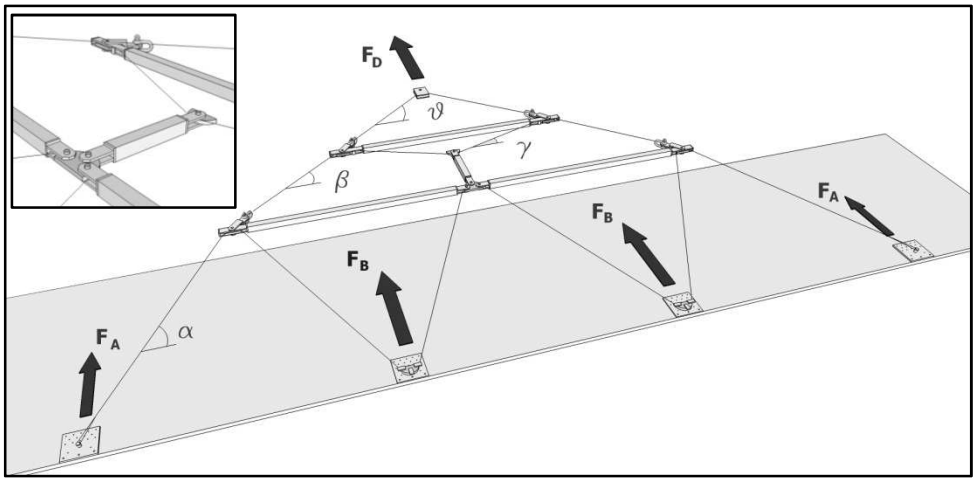

Fig. 5.9 Loading setup scheme

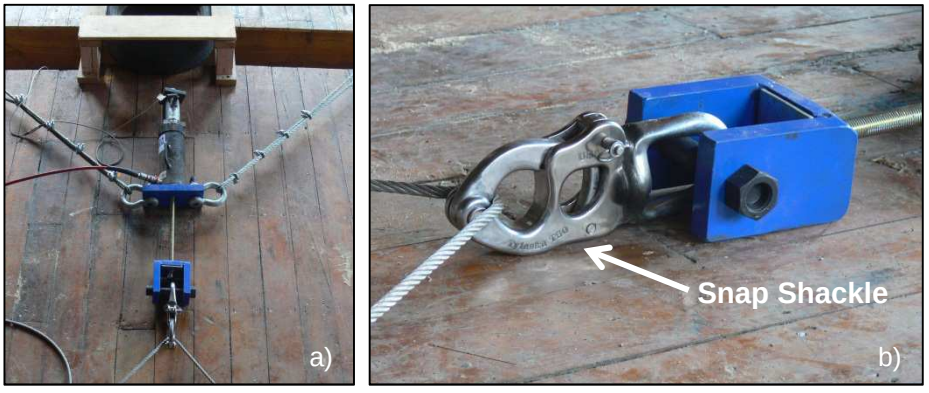

Fig. 5.10 Details: a) actuator; b) snap shackle.

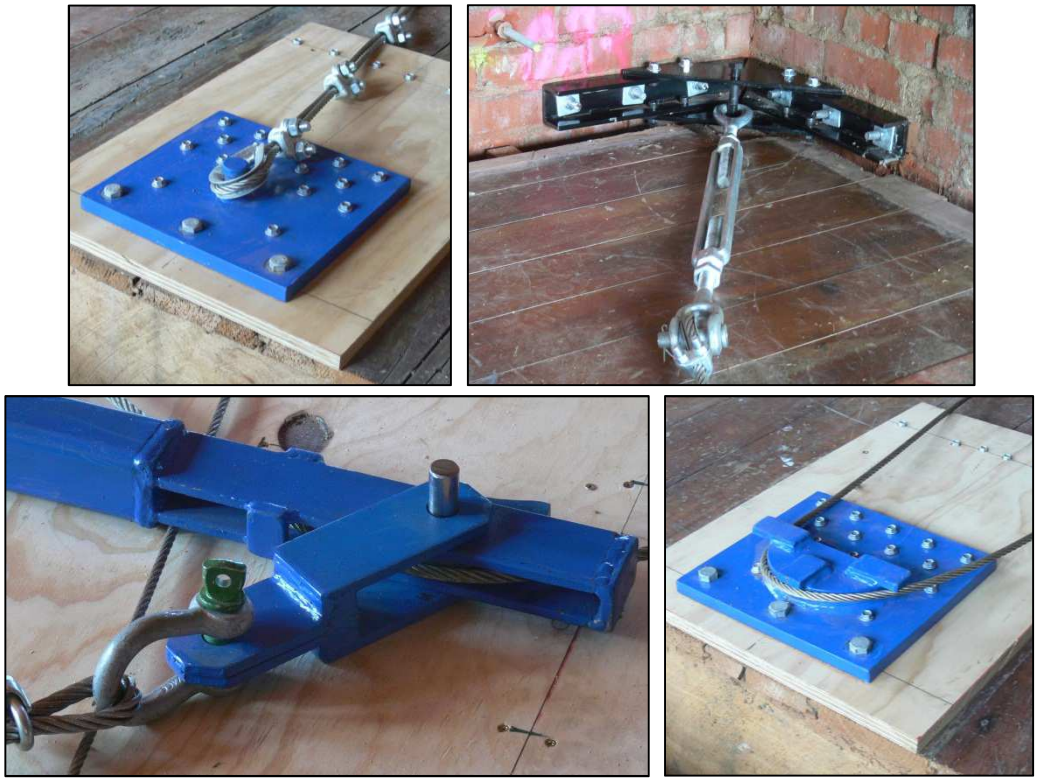

Fig. 5.11 Details: a) external loading plate; b) wall connection; c) frame pulley d) central loading plate;

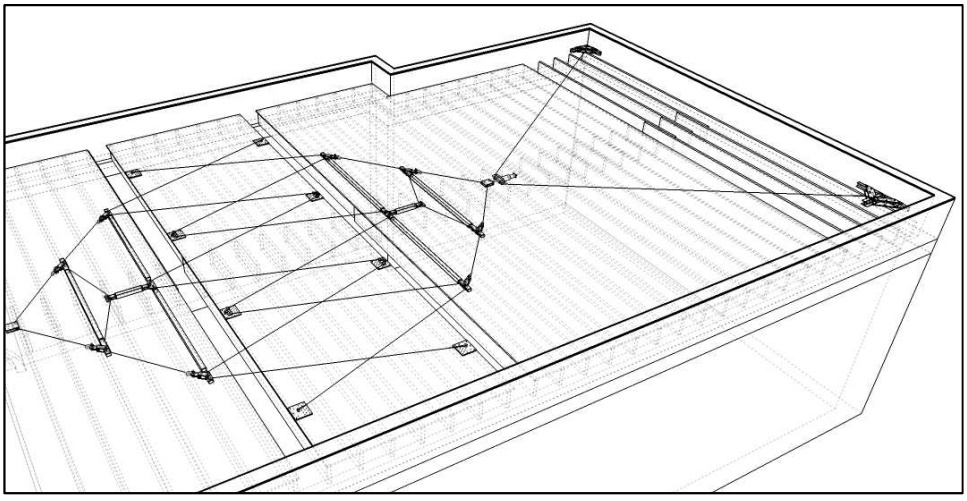

Fig. 5.12 Schematic view of the loading system

5.3.2 Measuring devices

The magnitude of the external load was measured by two 300 kN load cells while the displacements were recorded through the use of 5 string potentiometers, 2 LVDTs and 5 portal gages disposed as shown in (Fig. 5.13). The position of instruments SP1 and SP3 was due to the need of defining which ideal behavior was closest to the real one in terms of deformed shape. Therefore, considered where the ideal shapes (shear beam with uniform or parabolic load) differ the most, SP1 and SP3 were installed at a distance *d* from the diaphragm end equal to:

$$d = \frac{L}{2}\left(1 - \frac{1}{\sqrt{2}}\right) \qquad \textit{(Eq. 5.5)}$$

Five accelerometers were also employed to determine the dynamic properties of the specimens in the snap back tests.

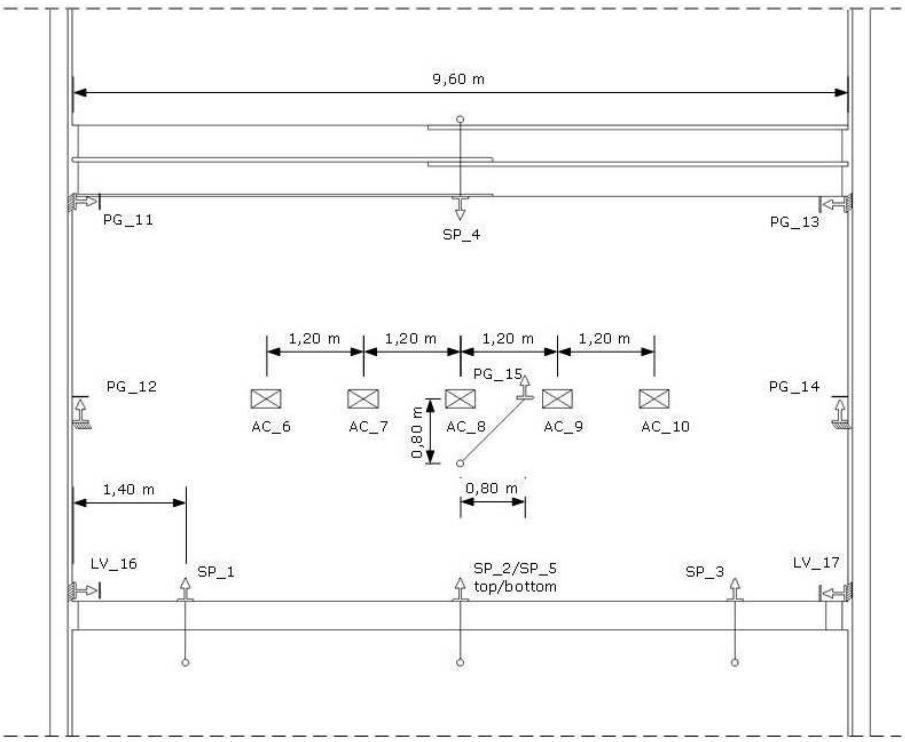

Fig. 5.13 Measuring Instruments

5.4 Mechanical properties of the materials

The mechanical properties of the materials constituting the tested floor, were determined throughout a series of additional tests (Fig. 5.14, Fig. 5.15).

5.4.1 Metal components

Nail and screw properties were obtained in accordance with ASTM F1575 (Tab. 5.1), while for metal sheathing ASTM E646 was adopted (Tab. 5.2). As one might imagine old nails resulted in quite scattered data, according to their different state of conservation. The very same consideration can also be addressed to the metal sheathing samples.

	New Nails	Screws (gauge 6)	Screws (gauge 8)	Old Nails (flooring)	Old Nails (ceiling)
Diameter φ [mm]	2.85	2.18	3.00	≈ 2.93	≈ 2.30
Bending Strength fm [MPa]	741	1785	1400	717	485
Tensile Strength ft [MPa]	693	1438	1289	759	733
n° of samples	8	10	8	12	11
Coefficient of Variation CoV	0.04	0.05	0.02	0.21	0.17

Tab. 5.1 Fastener properties

	Metal Sheathing
Thickness [mm]	≈ 0.31
Tensile Strength ft [MPa]	335
n° of samples	15
Coefficient of Variation CoV	0.37

Tab. 5.2 Sheathing properties

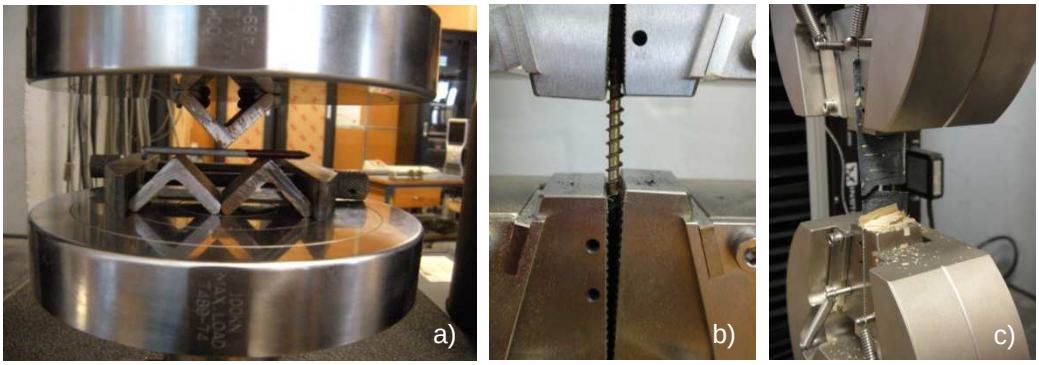

Fig. 5.14 Material testing: a) nail 3-point bending; b) screw tension test; c) metal sheathing tension test

5.4.2 Wood elements

Timber elements properties were obtained through 3/4 point bending tests consistent with [EN 408] (Fig. 5.15). A significant presence of bora was observed in the boards, especially in those forming the flooring. However, not all the diaphragm areas were equally affected by the insects, leading to large scatter of the test results (Tab. 5.3).

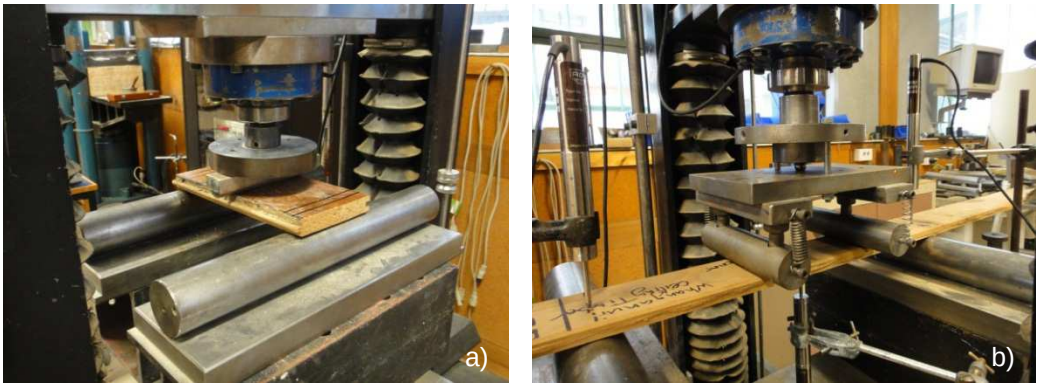

Fig. 5.15 Material testing: a) Floor boards; b) Ceiling boards

	Floor boards		Ceiling boards		Joists	
	f_m [MPa]	E [MPa]	f_m [MPa]	E [MPa]	f_m [MPa]	E [MPa]
Mean Value	59	5705	48	13289	47	8920
Coefficient of Variation CoV	0.38	0.28	0.36	0.25	0.23	0.17
Average Moisture Content	12%		11%			
n° of samples	7		8		6	
Average density ρ [kg/m^3]	575		568		519	

Tab. 5.3 Timber element properties. (f_m = bending strength)

5.5 Snap back tests

Considered the nonlinearity of the floor response, it was necessary to determine the period of each diaphragm (as built and retrofitted) at different target displacements. An initial period was assessed through snap back tests carried out at a displacement close to what was supposed to be the nominal yield displacement, while an "ultimate" period was detected by imposing a displacement consistent with the critical displacement causing the out-of-plane failure of the walls, which is approximatively equal to 70% of the wall thickness [Derakhshan (2011)]. In particular, the initial period corresponds to a midspan displacement of about 2.5 mm for the specimen reinforced with the plywood overlay and of about 10 mm for the other tests. This type of snap back tests (that will be called "small" from now on) was also employed to check the decay of diaphragm properties induced by the repetion of different tests. Consequently a small snap back test was performed before and after each cyclic test or "big" snap back test. It was decided not to rely on impact tests (with an instrumented hammer) or snap back tests at very small displacements, in order to minimize the influence of friction phenomena which might vary during the testing phase.

5.6 Cyclic tests

The loading protocol adopted for the cyclic tests was consistent with that suggested by the [EN 12512]. The tests were stopped once the displacement reached 150 mm or alternatively when the external load exeeded the thresold of 80 kN (for safety reasons). It should be noted that in some cases it was not possible to reach the target displacement of 150 mm owing to significant slacks in the system, despite the actuators at disposal had a 200 mm stroke and turnbuckles were positioned at the rope ends. This

was due to a combination of various factors such as rope relaxation, residual displacements from one half cycle and the following and slips in the wire rope grips used to connect the wires to different positions avoiding cuts.

All the tests were labelled with a progressive number followed by a letter representing the specimen.

Fig. 5.16 Twin loading frame setups

The results of the cyclic tests are given in Fig. 5.21 where the total force Vs. midspan displacement curves are represented. The backbone (envelope) curves were obtained by connecting the first cycle peak points for each displacement amplitude by means of straight lines [ASTM E2126].

5.6.1 Specimen A

5.6.1.1 Original condition

As far as specimen A is concerned, the first cyclic test (5_A) was carried out in the original condition, with both the ceiling and the metal sheathing still in place.

5.6.1.2 As – built condition

After that, since the basic diaphragm configuration in old URM buildings is that one with just the joists and the floorboards, the ceiling and the metal sheathing were removed (8_A). The significant decrease in stiffness, highlights the importance of not neglecting the ceiling stiffness when assessing existing floors.

5.6.1.3 New nail retrofit

Then, the specimen was renailed with two 2.85 mm x 75 mm nails for each board-to-joist intersection with a spacing of about 100 mm (18_A). The stiffening effect of the renailing solution is more noticeable at large displacements where the slope of the envelope curve of test 18_A, diverges from that one of test 8_A (Fig. 5.21f). This cost-effective strengthening solution was chosen following the results obtained from a series of cyclic tests, pertaining the floorboard to joist connection, carried out at the University of Auckland (Fig. 5.17). These tests represent the preliminary phase of a wider campaign still under progress. The envelope curves reported in Fig. 5.18 regards various type of fasteners (salvaged 65 mm rectangular iron nails, gauge 5 x 65 mm screws, 2.95 mm x 60 mm nails and 3.15 mm x 65 mm nails), inserted in salvaged rimu joists and boards. Each curve refers to a specimen as in Fig. 5.17a, made of two twin sub-specimens composed of a board connected to a joist through two fasteners. It appears that using 3.15 mm nails allows to achieve greater resistance and bigger ductility values with respect to those provided by screws of similar dimension. For all the tests, a double shear failure was registered. Given the failure mode, the lower ductility showed by the screw solution has to be related to the hardening process that the screws are subjected to.

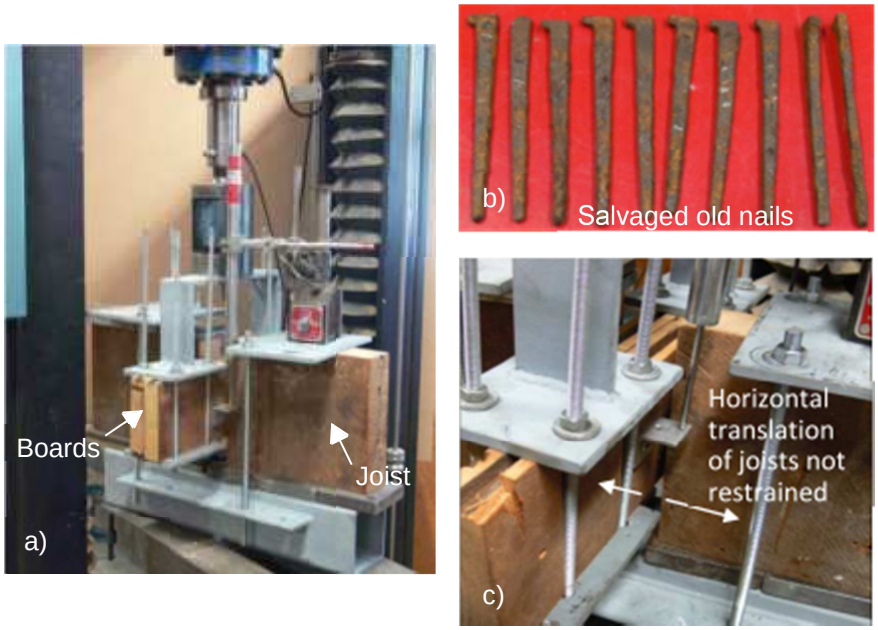

Fig. 5.17 Board-Joist connection preliminary testing campaign: details

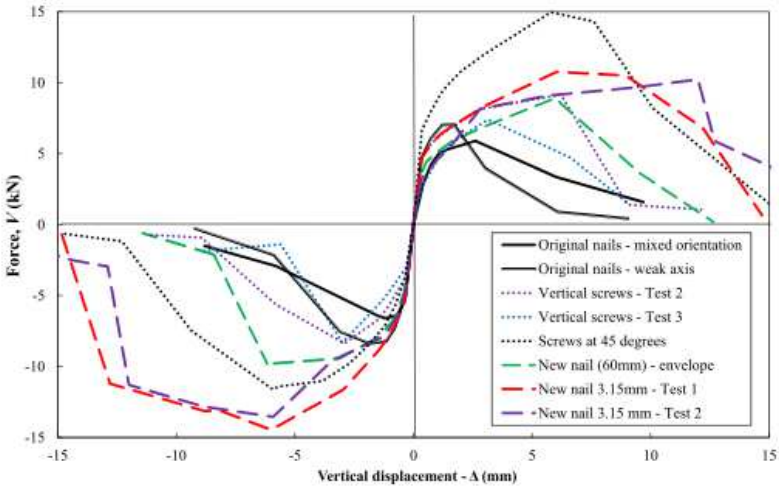

Fig. 5.18 Board-Joist connection preliminary testing campaign: envelope curves

5.6.2 Specimen B

5.6.2.1 As – built condition

In order to characterize the in-plane properties of the basic configuration in a way that wasn't affected by any decay due to previous testing, specimen B was tested directly without the ceiling and the sheathing (26_B).

5.6.2.2 Plywood panel overlay retrofit

Afterwards, the specimen was retrofitted with a layer of structural grade plywood panels placed on top of the existing floorboards (35_B). The panels measured 9 mm x 1200 mm x 2400 mm (AS/NZS 2269:2008) and were fixed to the flooring by means of gage 6 (30 mm long) screws inserted with a spacing of 150 mm on the edge of the panel and following a 300 mm by 300 mm mesh in the "field region". On the perimeter of the specimen, gage 8 (60 mm long) screws were used at 100 mm centers so as to create a chord-like effect and to effectively transfer the shear forces to the lateral walls. The panel disposition (Fig. 5.19, Fig. 5.20) was chosen to provide interlocking in both directions and thus increase the diaphragm stiffness "homogeneously". In addition, considered that gage 6 screws are not long enough to reach the joists, interlocking helps transfer the internal forces, thanks to direct contact between panels and no real solution of continuity. As a result, the on-site installation procedure is facilitated by the reduced need of cutting the panels because it is unnecessary to match the screw lines to the joist axes, whose spacing might not be constant.

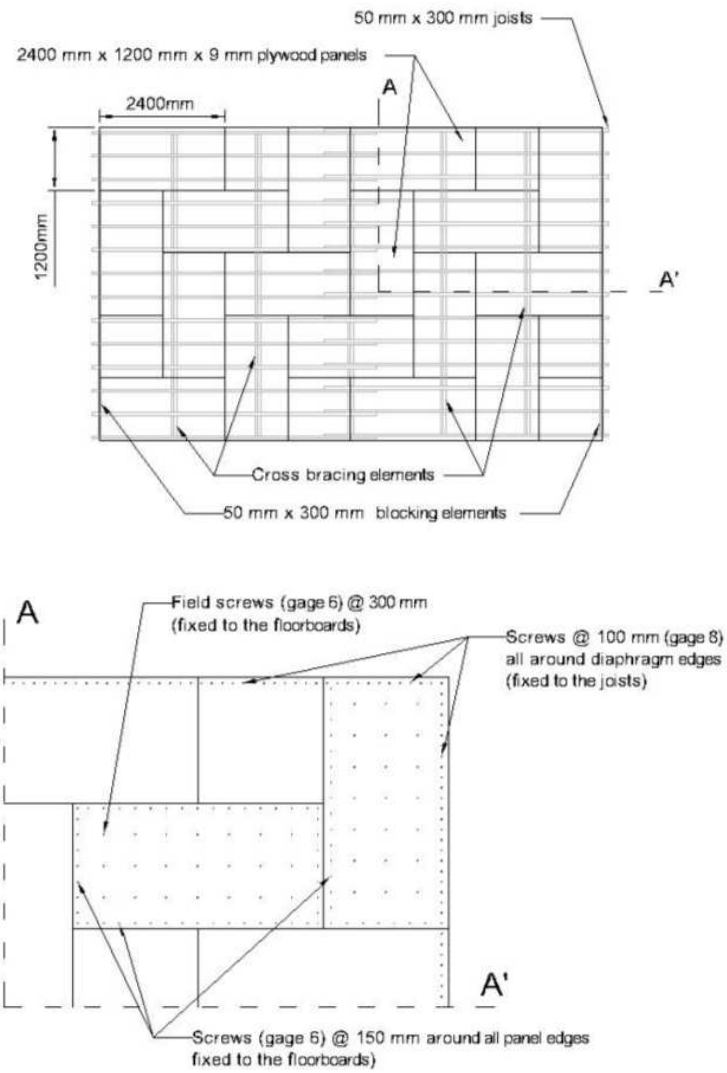

Fig. 5.19 Diaphragm B retrofit details

It must be noted that the diaphragms remained serviceable throughout the whole testing campaign and that no damages were registered, apart from some 45° "wrinklings" observed in the metal sheathing for test *5_A*.

5.6.3 Specimen C

The maximum midspan displacement attained in *35_B* was nearly 25 mm (corresponding to a drift d_r equal to 0.5%, $d_r = 2\delta/L$). So, in order to describe the

behavior at larger displacements of the diaphragm retrofitted with plywood panels, it was decided to cut specimen B and create a new smaller one (C) whose depth was 2.8 m. This cut was done in a way that reduced the panel interlocking so as to have a better chance of reaching larger deflections and to determine the retrofit effectiveness in the worst case scenario (by creating at the specimen midspan a solution of continuity parallel to the force direction). Fig. 5.22 shows the force Vs. midspan deflection curve of the monotonic test (43_C) carried out on specimen C. Slight buckling phenomena were registered on the panels at the compression side of the specimen, while a clear separation was observed between the panels at the center of the tension side (Fig. 5.23).This beam-like behavior was probably accentuated by the increased aspect ratio. It must be highlighted that this happened at unit shear load levels $v > 17$ *kN/m* which is more than twice the design value.

Fig. 5.20 Specimen B: plywood panel disposition

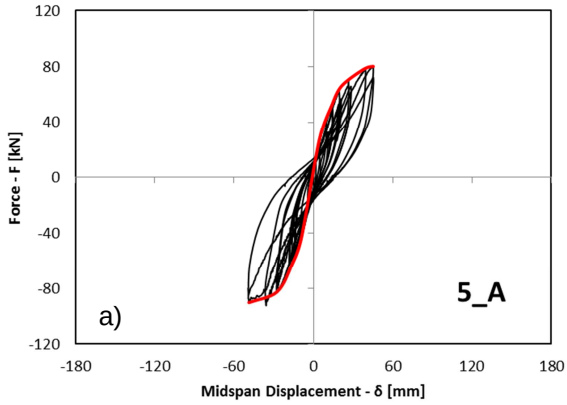
120
80
40
0
-40
-80
-120
Force - F [kN]
a)
5_A
-180
-120
-60
0
60
120
180
Midspan Displacement - δ [mm]

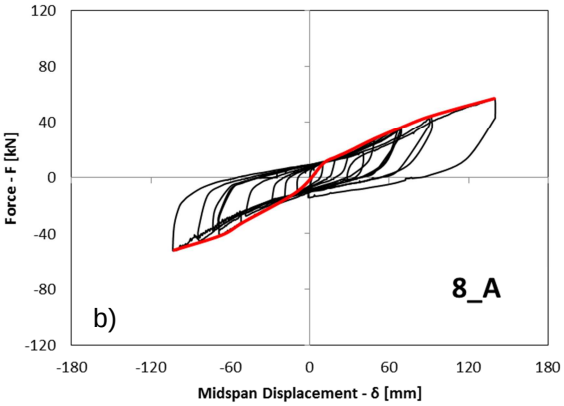
120
80
40
0
-40
-80
-120
Force - F [kN]
b)
8_A
-180
-120
-60
0
60
120
180
Midspan Displacement - δ [mm]

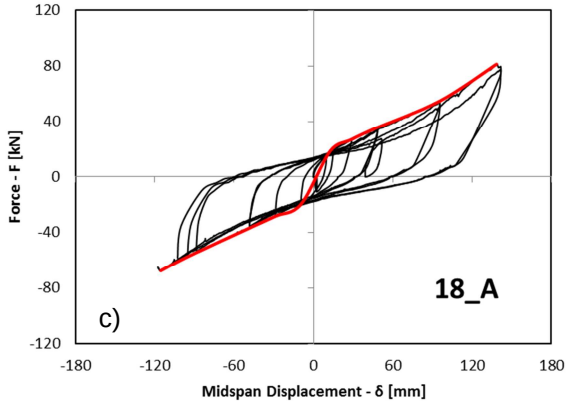
120
80
40
0
-40
-80
-120
Force - F [kN]
c)
18_A
-180
-120
-60
0
60
120
180
Midspan Displacement - δ [mm]

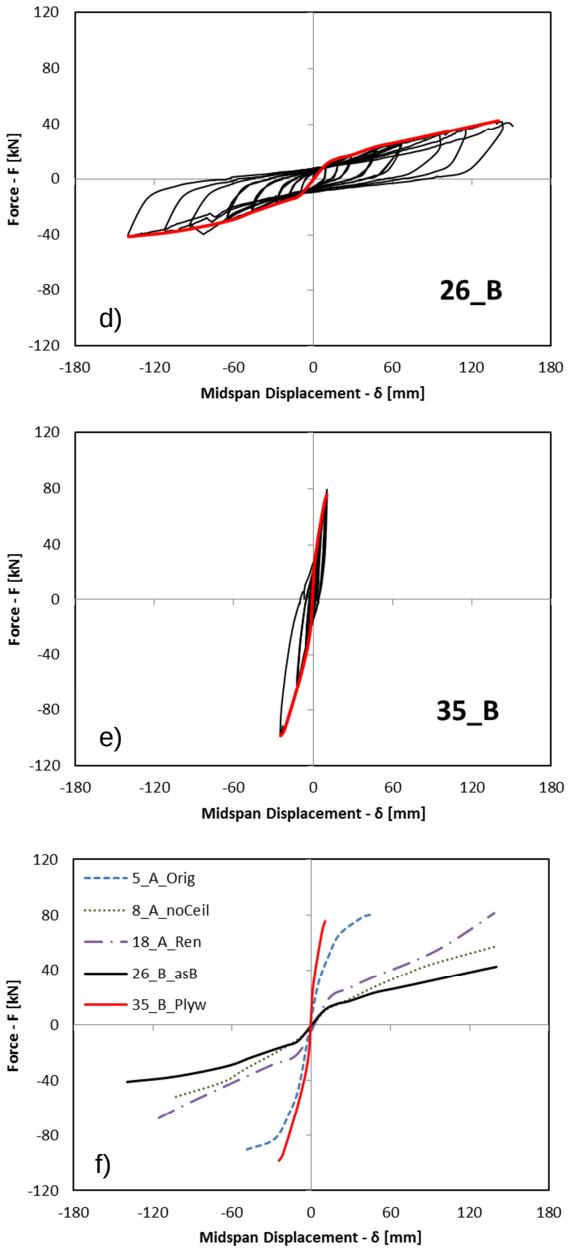

Fig. 5.21 Cyclic tests: a) specimen A – original condition (with ceiling and metal sheathing); b) specimen A – as-built; c) specimen A – re-nailed; d) specimen B – as-built; e) specimen B – reinforced with a plywood panel overlay; f) backbone curves

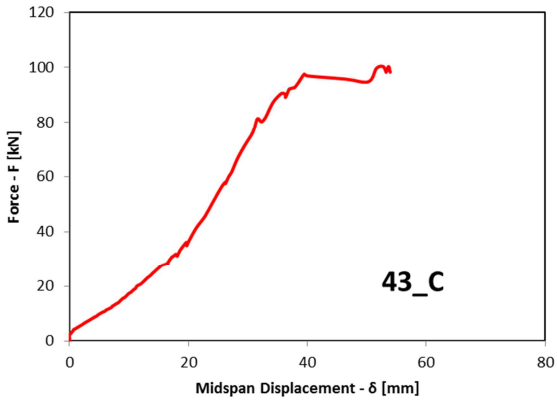

Fig. 5.22 Monotonic test (plywood overlay strengthening solution)

Fig. 5.23 Test 43_C a) panel gap widening b) plywood buckling

5.7 Data processing

5.7.1 Backbone curve Idealization

The majority of the international standards, like [FEMA 356, IBC 2006] describes the behavior of wood diaphragms through their properties at yield. On the other hand, in case of a distinct nonlinear behavior (e.g. *5_A*, *35_B*), the determination of the yield point can be affected by ambiguities [Munoz et al. (2008), Piazza et al. (2011)].

Hence, to depict the nonlinear behavior of the diaphragms, the second-order curve suggested by [ABK (1982)] was employed:

$$V(\delta) = \frac{F_u \cdot \delta}{F_u / k_i + |\delta|} \qquad \textit{(Eq. 5.6)}$$

where k_i is the initial stiffness, $F_u = \nu_u B, \nu_u$ is the unit shear strength and $V(\delta)$ is the shear resultant at the diaphragm end. The values derived for the different diaphragms are reported in Tab. 5.4, while the comparison between the experimental curves and the ideal ones is given in Fig. 5.24.

Diaphragm type	Unit shear [kN/m]	Initial Stiffness [kN/mm]	Correlation factor
5_A	9.86	3.99	0.9990
8_A	9.88	0.43	0.9997
18_A	13.35	0.55	0.9984
26_B	6.22	0.46	0.9998
35_B	14.09	6.51	0.9964

Tab. 5.4 Parameters adopted in the idealization process

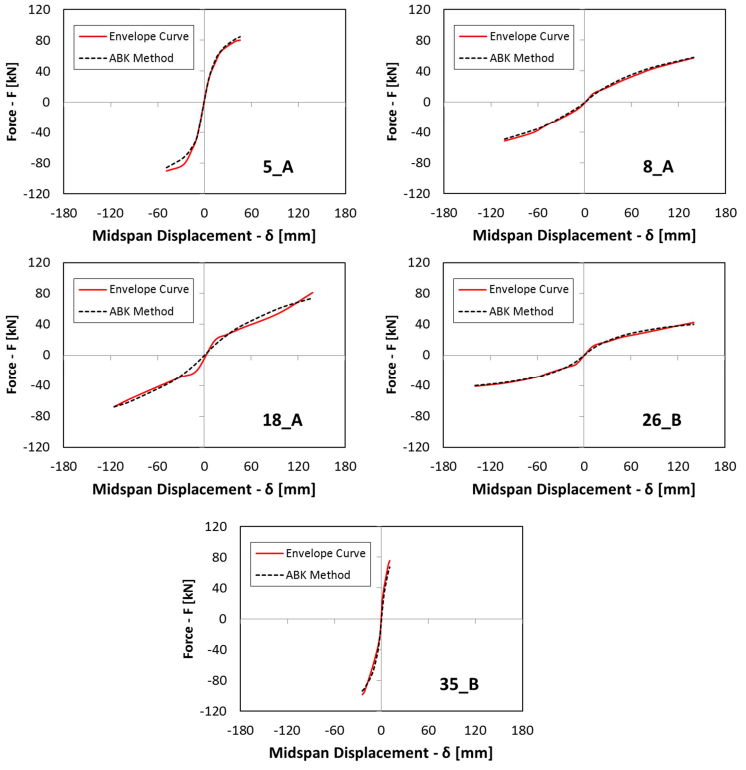

Fig. 5.24 ABK idealisation procedure

It might appear that tests *18_A* and *26_B* (partly even test *8_A*) showed a clear "bilinear behavior" and consequently it would have been more appropriate to schematize their behavior with a bilinear curve as suggested in [EN 12512] (Fig. 5.25, Tab. 5.5). The main drawback of this reasoning is that the first branch of the envelope curve is highly dependent on the amplitude of the first set of cycles. That is to say, if the first set is not small enough it may happen that the envelope has an initial slope smaller than it should, because of the line connecting the origin with the first peak point. Since the loading was provided by hand pumps it was not possible to manage very small cycle amplitudes. As a matter of fact, at low force levels, even extremely little movements of the pump lever was enough to produce relatively significant displacements of the piston. Observing the initial slopes of the monotonic tests carried out to load the diaphragm for the snap back tests, it seems that after an initial very short phase (about 1 mm) highly influenced by friction phenomena (with an almost vertical slope) the curve adjusted itself on the same slope of the line connecting the first peak points of the first and the second set of cycles. Therefore, the yield points given in Tab. 5.5 have to be taken into consideration "*cum grano salis*".

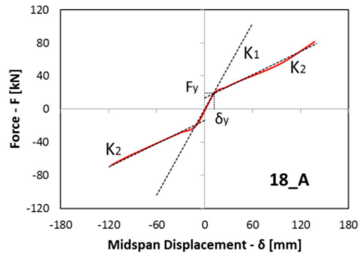

Fig. 5.25 Bilinearisation of the backbone curve

	K1	K2	δy	Fy
	[kN/mm]	[kN/mm]	[mm]	[kN]
8_A	1.02	0.39	13.72	14.00
18_A	1.73	0.47	10.76	18.60
26_B	1.14	0.24	11.85	13.50

Tab. 5.5 Yield points and stiffnesses obtained through the bilinearization process

As far as test 43_C is concerned, an equivalent elastic-plastic (EEEP) curve was adopted, acknowledging the presence of a plateau (first branch slope *k1 = 2.3* kN/mm, plateau at *96 kN*).

5.7.2 Determination of the equivalent stiffness

The in-plane behavior of timber floors is commonly characterized by an equivalent shear modulus G_d. The determination of this modulus is based on the ideal scheme assumed to describe the deformed shape of the diaphragm. From the analysis of the experimental deformed shape it can be observed that despite the applied load being reproduced as a parabolic load, the floor deflection is better described through a shear beam subjected to a uniform load. In Fig. 5.26 is given, as an example, the comparison between the experimental deformation of specimen B (at different step of the midspan displacement) and the ideal shape of a shear beam under diverse load pattern. Therefore the equivalent stiffness was obtained with the following formulae:

$$G_d = \frac{1}{8}\frac{F_d L}{\delta B} \qquad \textit{(Eq. 5.7)}$$

where δ is the midspan displacement, B is the specimen depth, F_d is the total load and L is the specimen span. Fig. 5.27 shows the equivalent secant stiffness obtained for each diaphragm configuration (unretrofitted/retrofitted) at different target displacements. Regarding the “as built” condition, it can be noticed a slight difference in the initial stiffness between specimen *A* (test *8_A*) and *B* (test *26_B*), due to the tests carried out on specimen *A* with the ceiling and the sheathing still attached. The new nails made the stiffness increase of around 30% at both small and large displacements. Thanks to the plywood overlay, G_d values 6 times bigger than those observed in the as built condition were obtained.

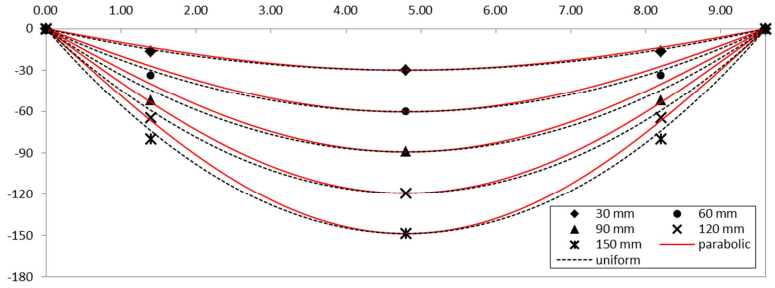

Fig. 5.26 Experimental Vs. Ideal deformation (test 26_B)

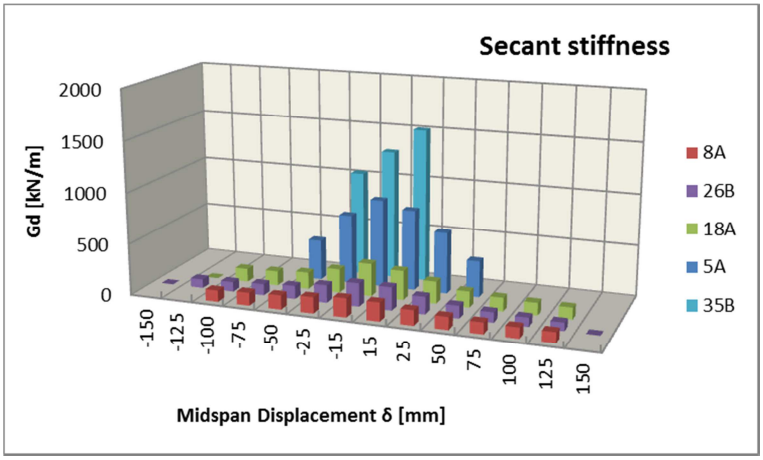

Fig. 5.27 Equivalent shear stiffness comparison

Mid. Displ. [mm]	Drift [%]	5_A	8_A	18_A	26_B	35_B	43_C
15	0.3	821	165	212	190	1343	986
25	0.5	609	154	199	169	961	986
50	1.0	371	133	172	126		986
75	1.6		116	152	108		549
100	2.1		104	136	91		411
125	2.6		93	123	79		329
150	3.1		85	112	70		274

Tab. 5.6 Equivalent shear stiffness [kN/m]

With the purpose of comparing the experimental data to the values contained in the Standards, yield displacements were calculated in accordance with [FEMA 356, ASCE/SEI 41-06]. Subsequently, for those target displacements, experimental secant stiffness was determined relying on (Eq. 5.7) and on (Eq. 5.6). The results are showed in Tab. 5.7. It seems that adopting the G_d value suggested by [FEMA 356, ASCE/SEI 41-06] for single straight sheathing, leads to overestimate the stiffness of old timber

floors (at least in the direction orthogonal to the joists). NZSEE (2011) on the other hand, recognizing the orthotropic behavior of this type of diaphragms, provides values very close to the experimental ones (somewhat on the safe side, provided the considerable bora affecting the floorboards). With reference to the wood panel overlay solution, the shear stiffness obtained in the testing campaign was consistent with that one given by the FEMA/ASCE provisions despite the use of relatively thin plywood panels and short screws.

		Single Straight Sheathing	Wood Panel Overlays on Straight Sheathing (Blocked, Unchorded)
FEMA 356, ASCE/SEI 41-06		350	1225
NZSEE (2011)	Good	175 150 (with joist connection)	-
	Fair	150 125 (with joist connection)	-
	Poor	110 95 (with joist connection)	-
Experimental	8_A	155	-
	26_B	171	-
	18_A	200	-
	35_B	-	1238
	43_C	-	986

Tab. 5.7 G_d values [kN/m]

As far as diaphragm shear capacity is concerned, it was preferred not to define any shear strength value since no force loss or plateau was detected in the backbone curves (apart from test *43_C*). However it is interesting to see what is the shear capacity of the different diaphragm typology for a drift level compatible with the activation of the out of-plane mechanisms (i.e. $\delta = 150\ mm$, $d_r = 3.1\%$). Employing the idealization curve previously proposed, it was discovered that the as-built floors can support a unit shear load of *4.8 kN/m*, which is quite lower than the design load assumed for the anchor system. The “re-nailing” strengthening technique proved to be a sufficiently valid intervention, since it permits to reach a shear capacity of *7 kN/m* which is very close to the strength requested in an extremely severe seismic condition. On the other hand, if one considers the strength contribution of the ceiling and the sheathing, it is possible to satisfy the seismic demand within a drift of 1%. Specimen 43_C showed a clear plateau

at a unit shear resistance corresponding to *v = 17.1 kN/m*. The maximum resistance was reached at a drift equal to 0.9%. However no ductility factor can be defined, since no failure was registered.

5.7.3 Period determination

The fundamental periods of the specimens at various stages were determined by means of a toolbox based on Matlab code and developed at the University of Auckland [Beskhyroun (2011)]. Various identification techniques (both frequency-domain based and time-domain based) were taken into consideration so as to obtain a more robust solution to the problem. In particular five methods were adopted: peak picking (PP) [Bendat and Piersol (1993)]; frequency domain decomposition (FDD) [Brincker et al. (2000)] ; enhanced frequency domain decomposition (EFDD) [Brincker et al. (2000); Jacobsen et al. (2007)]; eigen realisation algorithm (ERA) [Juang and Pappa (1985)] combined with the natural excitation technique (NeXT) [James et al. (1993)]; stochastic subspace identification (SSI) [Overschee and Moor (1996)].

Modal assurance criteria (MAC) values were also determined for each test. The minimum MAC value observed in the whole campaign was 0.8, which is an excellent indicator of the good reliability of the results. In addition, a rough check of the diaphragm periods was conducted analyzing the videos of the tests recorded by a high frame rate camera.

Tab. 5.8 depicts the fundamental frequencies determined with the above-mentioned techniques, as well as the average periods and the initial conditions in terms of total load and midspan displacement (global deflection) at the time of release.

Test 7_A and 29_B represent the repetition of tests 6_A and 27_B respectively. No appreciable variation in fundamental period or stiffness was detected. On the other hand if one compares the small snap back tests carried out before and after the cyclic test on the retrofitted floor sections (17_A to 21_A and 33_B to 38_B), a certain strength loss can be observed despite no period difference. This might be related to the role played by friction, which is more important at small displacement levels.

The period value determined for test 10_A was quite higher than what was supposed to be, given the load and the displacement at the moment of the snap back. Unfortunately it was not possible to perform the backup identification since the video of the test was corrupted.

Test n°	PP	FDD	EFDD	ERA	SSI	T [s]	Load [kN]	Displ. [mm]	Specimen Condition
2_A	11.52	11.52	11.52	11.00	-	0.09	21.00	2.40	Original (ceiling + sheathing)
3_A	14.06	14.01	14.01	13.59	13.72	0.07	14.50	1.90	“
4_A	8.50	8.35	8.35	7.40	8.16	0.12	40.50	10.00	“
6_A	4.00	4.05	4.05	-	4.04	0.25	77.03	61.82	“
7_A	4.10	4.15	4.15	3.63	4.12	0.25	76.21	60.68	“
10_A	2.15	2.15	2.15	1.74	2.29	0.48	11.00	10.87	As built (no ceiling and sheathing)
11_A	2.64	2.67	2.67	2.50	2.99	0.37	64.78	131.12	“
13_A	7.18	7.14	7.14	5.97	6.84	0.15	6.57	10.16	“
15_A	2.49	2.53	2.53	2.42	2.29	0.41	63.87	152.55	“
17_A	7.32	7.32	7.32	7.70	9.94	0.13	16.00	9.64	Retrofitted (new extra nails)
19_A	3.00	3.04	3.04	2.60	2.87	0.34	65.22	120.97	“
21_A	7.18	7.18	7.18	6.90	6.89	0.14	10.21	9.78	“
23_A	3.08	3.08	3.08	2.80	2.86	0.34	54.38	101.57	“
25_B	6.15	6.19	6.19	5.91	6.39	0.16	11.73	10.27	As built (no ceiling and sheathing)
27_B	2.20	2.23	2.23	2.18	2.22	0.45	38.83	157.15	“
29_B	2.27	2.31	2.31	2.20	1.98	0.45	35.20	152.89	“
31_B	6.96	6.99	6.99	7.31	7.09	0.14	-	11.23	“
33_B	13.55	13.55	13.55	12.65	13.51	0.07	23.17	2.30	Retrofitted (plywood panels)
36_B	10.25	10.22	10.22	9.16	9.82	0.10	42.02	10.09	“
38_B	12.82	12.85	12.85	10.90	12.77	0.08	14.25	2.57	“
39_B	31.86	31.82	31.82	28.27	31.55	0.03	27.92	2.20	“
41_C	11.43	11.46	11.46	10.42	13.09	0.09	10.05	2.61	Retrofitted (plywood panels)
44_C	6.15	6.08	6.08	5.58	6.06	0.17	35.83	15.69	“

Tab. 5.8 Snap back tests: period determination

In order to estimate the diaphragm period, [ASCE/SEI 41-06] suggests the use of the following formulae:

$$T_1 = \sqrt{3.07\Delta_d} \qquad \textit{(Eq. 5.8)}$$

where Δ_d is the midspan deflection generated by a lateral load of *1.0 g*. (Eq. 5.8) can be rewritten as:

$$T_1 = \sqrt{\frac{3.07}{4}\frac{W_d L}{G_d B}} = 0.88\sqrt{\frac{W_d L}{G_d B}} \qquad \textit{(Eq. 5.9)}$$

This formulae, as shown by [Wilson, (2012)], derives from the application of the Rayleigh's quotient [Chopra (2007)] to a fixed-ended flexural beam. Considering the experimental deformed shape of the diaphragms, the Rayleigh's quotient should be recalculated relying on the shape function determined for a shear beam under a uniformly distributed load pattern. Consequently (Eq. 5.9) becomes:

$$T_1 = 0.63\sqrt{\frac{W_d L}{G_d B}} \qquad \textit{(Eq. 5.10)}$$

(Eq. 5.10) provides natural periods 30% shorter than (Eq. 5.9). To find out which of the two approaches better approximates the wood diaphragm natural period, a comparison with the experimental data is offered in Tab. 5.9. So as to make the theoretic values comparable with the experimental ones, a parameter θ was introduced. It takes into account that for each given snap back displacement, the actuator load (F_d) should represent the seismic mass multiplied by a *1.0 g* acceleration ($F_d = W_d$). At the release moment, in fact, the floor behavior can be described (it is obviously an approximation) through a shear beam whose stiffness is equal to the equivalent secant stiffness calculated at that displacement level and whose mass is equal to F_d/g. The problem is that during the dynamic tests the actual weight was just the floor dead load ($p = 0.35$ *kN/m*^{2})[4]. Therefore the θ factor was determined as follows:

[4] The reasons behind the decision of not to add any extra-mass to the floor sections were various. Firstly there was the safety issue related to possible flying objects. Secondly, not knowing *a priori* the diaphragm stiffness it might have occurred that it was not possible to reach the "snap displacement" implied by the selected floor seismic mass.

$$\theta = \left[1 - \left(\frac{F_d - pBL}{F_d}\right)\right]^{0.5} \qquad \textit{(Eq. 5.11)}$$

Hence (Eq. 5.9) becomes:

$$T_1 = 0.88\sqrt{\frac{W_d L}{G_d B}}\theta \qquad \textit{(Eq. 5.12)}$$

Similarly (Eq. 5.10) becomes:

$$T_1 = 0.63\sqrt{\frac{W_d L}{G_d B}}\theta \qquad \textit{(Eq. 5.13)}$$

A general tendency to overestimate the diaphragm periods (with a mean error of almost 40%) is noticeable when using (Eq. 5.12). Such mean error can be reduced to nearly 8% by employing (Eq. 5.13).

Experimental data			(Eq. 1.13)		(Eq. 1.12)	
Test n°	T [s]	θ	T [s]	Err. [%]	T [s]	Err. [%]
T4_A	0.12	0.68	0.12	1%	0.17	38%
T6_A	0.25	0.49	0.22	12%	0.30	23%
T7_A	0.25	0.50	0.22	12%	0.30	22%
T11_A	0.37	0.54	0.35	6%	0.48	30%
T15_A	0.41	0.54	0.38	7%	0.53	29%
T19_A	0.34	0.54	0.33	3%	0.46	35%
T23_A	0.34	0.59	0.33	1%	0.46	38%
T27_B	0.45	0.64	0.49	9%	0.68	51%
T29_B	0.45	0.67	0.51	13%	0.71	57%
T36_B	0.10	0.61	0.12	19%	0.17	65%
T44_C	0.17	0.51	0.16	3%	0.22	34%

Tab. 5.9 Estimated period values compared to experimentally derived ones

No α_w coefficient was adopted, since the tests involved just timber floor sections not influenced by the out-of-plane stiffness of the orthogonal walls.

It should be underlined that (Eq. 5.10) must be considered just as a tool to make an educated guess of timber diaphragm period, in order to define the shear load transferred to the resistant walls. Some strong assumptions are, in fact, behind that formulae. First of all, the diaphragms are addressed as linear elastic systems since all the nonlinearities are concentrated in the variation of G_d. Secondly, there is the hypothesis of constant stiffness along the diaphragm span (SP1 and SP3 showed displacements bigger than those expected by assuming a constant equivalent shear modulus). In addition, the experimental data contained the effects of the anchor deformations which are not explicitly considered in the formulae. The reason why these effects are not accounted, can be roughly explained by considering the floor stiffness (direct stiffness measured at the midspan) as a spring in series with the spring representing the anchor system stiffness. Since the anchor system stiffness (K_A) is much higher than floor stiffness (K_F), the resultant stiffness can be taken as:

$$K_T = 1 \Big/ \left(\frac{1}{K_F} + \frac{1}{K_A} \right) \qquad \textit{(Eq. 5.14)}$$

$$K_A \gg K_F \;\rightarrow\; \frac{1}{K_A} \approx 0, \qquad K_T \approx K_F \qquad \textit{(Eq. 5.15)}$$

Therefore, to keep the formulae as simple as possible it was assumed that the anchors' behavior does not affect the floor fundamental frequency (however during the period determination process, diaphragm shear stiffness was calculated relying on the "global" midspan displacements, not depurated from the lateral deformation). (Eq. 5.10) does not also contain any reference to damping or friction phenomena.

It must be noted that the theoretical period values contained in Tab. 5.9 were calculated using the experimental G_d values. To understand which level of "error" might be encountered when adopting constant stiffness values, as suggested by standards, a case-study diaphragm (9.6 m x 17 m) was chosen. The natural periods calculated for different possible levels of seismic weight (the mass contribution pertaining to the out-of-plane walls was neglected), are reported in Tab. 5.10 (as built condition) and Tab. 5.11 (new plywood panel overlay on the existing flooring). The first seismic weight level (*1.1 kN/m^2*) is representative of a residential building and corresponds to a total load of *180 kN*. It can be noted that for the as built condition, both standards suggest a higher

stiffness than that one derived from the experimental curves[5], leading therefore to shorter period values. The difference was *58.4%* for ASCE and *30.3%* for NZSEE. On the other hand when the retrofit is applied, the increase in stiffness is such that the deflection generated by this relatively small mass is quite lower than the yield displacement associated with the G_d values offered by the ASCE standard. Hence the difference between the period calculated with the experimentally derived stiffness and that one obtained using the ASCE stiffness was about 30%. By contrast, for seismic weights related to higher occupancy levels (*2.0 kN/m²* and *3.0 kN/m²*) such difference seems less significant, with "ASCE-derived" periods slightly shorter than that ones linked to the experimental stiffness.

	Existing single square sheathing		
	Experim.	NZSEE	ASCE
Seismic Weight [kN/m^2]	1.1	1.1	1.1
Wd [kN]	180	180	180
V(δ) [kN]	30 (T8_A) 25 (T26_B)	-	-
Gd [kN/m]	86 (T8_A) 35 (T26_B) 61 mean	125 (95)*	350
(Eq. 1.10) T [s]	0.81	0.57 (0.65)*	0.47
Var. %		30.3 (20.1)*	58.4

* Values determined in case of a "poor" condition rating

Tab. 5.10 Natural period calculated relying on experimental G_d values compared with those obtained using the stiffness values suggested by different standards

[5] In Tab. 5.10 and Tab. 5.11 the corresponding *V(δ)* values which are required to derive the G_d stiffness from the experimental curves, are also given.

Plywood Panel Overlay on existing single square sheathing

	Experim.	ASCE	Experim.	ASCE	Experim	ASCE
Seismic Weight [kN/m2]	1.1	1.1	2.0	2.0	3.0	3.0
Wd [kN]	180	180	326	326	490	490
V(δ) [kN]	25 (T35_B)	-	45 (T35_B)	-	40 (T43_C)	-
Gd [kN/m]	2079 (T35_B)	1250	1059 (T35_B)	1250	986 (T43_C)	1250
(Eq. 1.10) T [s]	0.14	0.18	0.26	0.24	0.33	0.30
Var. %		29.0		7.9		11.2

Tab. 5.11 Natural period calculated relying on experimental G_d values compared with those obtained using the stiffness values suggested by different standards

5.7.4 Energy dissipation

In accordance with [Chopra (2007)] the hysteresis damping properties of the specimens were measured by the equivalent viscous damping ratio ξ, which represents the ratio between the dissipated energy in one half cycle and the available potential energy multiplied by 2π [EN 12512].

5A	I°	II°	III°	IV°	V°	VI°	VII°	VIII°	IX°	X°	XI°
F_{max}^{+} [kN]	52.44	48.03	50.35	62.94	52.93	47.66	70.85	65.85	61.60	78.35	80.24
d_{Fmax}^{+} [mm]	14.49	14.23	14.42	19.54	19.04	17.96	26.66	28.45	28.22	39.06	45.04
F_{max}^{-} [kN]	57.29	56.89	56.20	61.82	62.96	61.04	82.19	79.77	76.96	92.47	89.87
d_{Fmax}^{-} [mm]	14.16	14.21	13.95	16.19	18.10	18.12	27.67	26.80	27.32	35.72	48.66
ξ %	14.30	13.24	14.03	13.54	12.77	12.24	12.68	11.56	11.03	11.98	13.46

8A	I°	II°	III°	IV°	V°	VI°	VII°	VIII°	IX°
F_{max}^{+} *[kN]*	10.21	14.53	18.76	27.86	35.88	34.93	34.99	44.39	42.56
d_{Fmax}^{+} *[mm]*	9.76	18.92	29.00	48.72	68.30	68.49	65.69	91.47	90.37
F_{max}^{-} *[kN]*	9.76	14.23	18.19	27.41	41.31	37.32	38.12	45.49	52.33
d_{Fmax}^{-} *[mm]*	9.54	18.70	28.50	48.37	66.58	67.90	73.10	83.40	103.16
ξ %	33.69	28.17	23.60	18.83	17.30	16.11	16.05	16.27	15.01

18A		I°	II°	III°	IV°	V°	VI°	VII°
F_{max}^{+}	*[kN]*	15.08	26.58	35.10	34.20	54.41	53.74	81.20
d_{Fmax}^{+}	*[mm]*	9.87	28.34	47.87	48.16	95.42	94.92	139.12
F_{max}^{-}	*[kN]*	19.17	27.76	35.74	35.18	53.86	56.70	59.01
d_{Fmax}^{-}	*[mm]*	8.35	28.74	48.22	47.87	87.14	93.71	101.86
ξ	*%*	31.09	26.23	24.08	22.37	20.25	17.38	15.94

26B		I°	II°	III°	IV°	V°	VI°	VII°	VIII°	IX°	X°	XI°	XII°	XIII°	XIV°
F_{max}^{+}	*[kN]*	9.51	9.71	14.85	14.17	17.08	17.30	23.41	21.74	21.57	26.93	25.88	33.09	36.66	42.42
d_{Fmax}^{+}	*[mm]*	9.58	9.24	18.84	18.69	28.17	28.71	47.66	47.14	47.27	65.95	65.88	95.02	113.45	140.06
F_{max}^{-}	*[kN]*	10.77	10.41	14.60	14.00	17.44	16.79	23.37	22.72	22.30	30.01	27.75	39.18	37.22	41.03
d_{Fmax}^{-}	*[mm]*	9.08	9.04	18.20	18.02	27.58	27.01	45.64	46.17	46.26	64.77	64.29	83.04	111.64	138.87
ξ	*%*	28.53	27.07	30.94	21.94	30.96	38.63	18.36	17.43	17.55	32.30	16.33	16.92	16.62	16.37

35B		I°	II°	III°	IV°	V°	VI°	VII°	VIII°	IX°	X°	XI°	XII°	XIII°
F_{max}^{+}	*[kN]*	22.33	22.28	22.85	36.29	35.76	35.57	45.83	45.45	46.45	67.91	72.42	73.02	79.05
d_{Fmax}^{+}	*[mm]*	0.93	0.85	0.88	2.55	2.43	2.41	4.26	4.11	4.14	8.11	9.74	9.50	10.52
F_{max}^{-}	*[kN]*	17.75	17.36	17.04	31.19	29.94	29.93	40.20	40.80	39.99	62.71	63.77	62.65	98.64
d_{Fmax}^{-}	*[mm]*	1.68	1.63	1.56	3.60	3.48	3.54	5.56	5.71	5.65	11.79	11.81	12.00	24.55
ξ	*%*	27.31	28.80	27.55	20.52	19.86	19.17	19.90	17.32	17.14	11.38	15.58	13.77	14.51

Tab. 5.12 Equivalent viscous damping ratio

All the tested diaphragms (apart from specimen 5_A) showed high dissipating capabilities with initial values of ξ close to 30%. However, a value of 15% is deemed as acceptable when determining earthquake response spectra.

It is important to stress that no significant strength loss was detected between following cycles with the same amplitude, in accordance with what deduced by the snap back tests which showed no substantial period variations due to test repetition.

This seems to prove that the choice of testing the same specimen in different conditions did not invalidate the consistency of the results. In other words the stiffness values given in Tab. 5.6 are useful not only in determining a “trend of improvement” (in order to evaluate the effectiveness of a strengthening technique) or the effect of a post-earthquake intervention (on decayed floors) but can also be adopted as representative values of those conditions.

Therefore, the reduced stiffness offered by test 43_C in comparison with test 35_B should not be attributed to a mechanical property decay, linked to the load history, but to the effect of the lack of interlocking caused by the particular “specimen manufacturing” as previously explained.

5.7.5 Boundary condition assessment

Regarding the performance of the new anchoring system, not all the specimen were suitable for a clear check, because of the boundary conditions. Some pilasters were in fact present on both sides of the specimens and it was not possible to determine whether the joist pockets were tight or if the joists were allowed to slightly move. As far as specimen *A* is concerned, it seems that on one side (monitored through PG_14) the presence of two pilasters limited the “sliding” in one direction (*test 5_A*, Fig. 5.28). The restraining action decreased with the execution of the other tests, probably due to mortar crushing (no debris was observed though). This induces to think that on the other side, the pockets were big enough to allow a 3/5 mm of displacement, since no sudden change in the slope of the envelope curve was detected. Specimen C was cut so that one side (PG_14 side) was in a zone free from pilasters. In this way it was possible to check the real shear force borne by the anchors during the tests. In Fig. 5.29, the average shear displacement Vs. the shear load of one anchor for test *43_C* is given. It is also reported the ideal curve deducted from the anchor tests (Fig. 5.6). It can be noted that the strength showed by the rods was significantly higher than the one observed in the anchor tests while the stiffness was quite lower. It should be added that on that side of the floor, a particularly low “side stiffness” was registered even for specimen B (especially test 26_B). This meant displacements > *10 mm* (*v < 5 kN/m*) which were very unlikely to be compatible with any alleged gap in the pockets. The reason might so be found in local degradation of the mechanical properties of masonry.

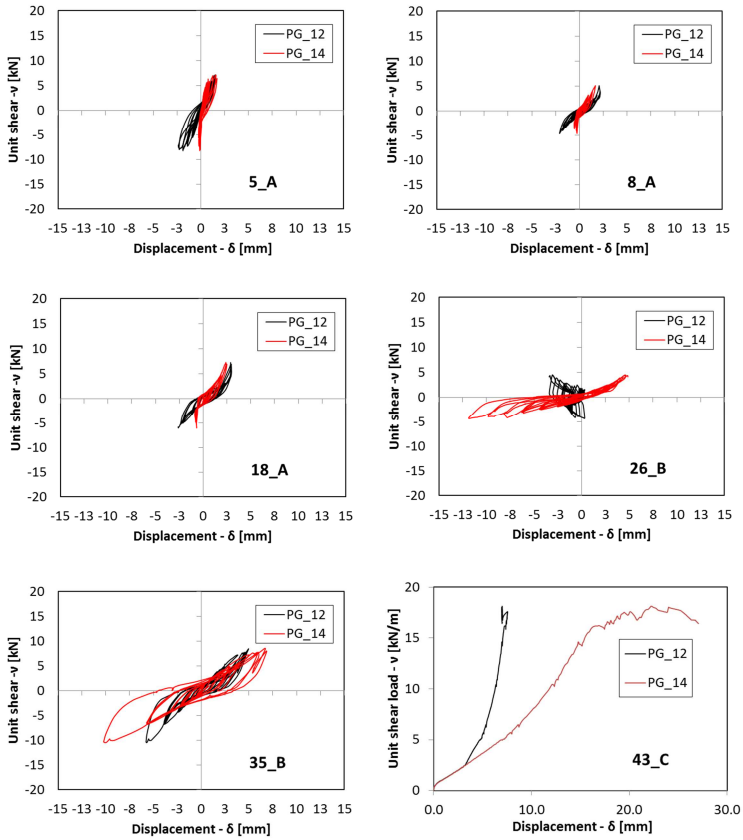

Fig. 5.28 Displacement at the diaphragm ends Vs. Unit shear action.

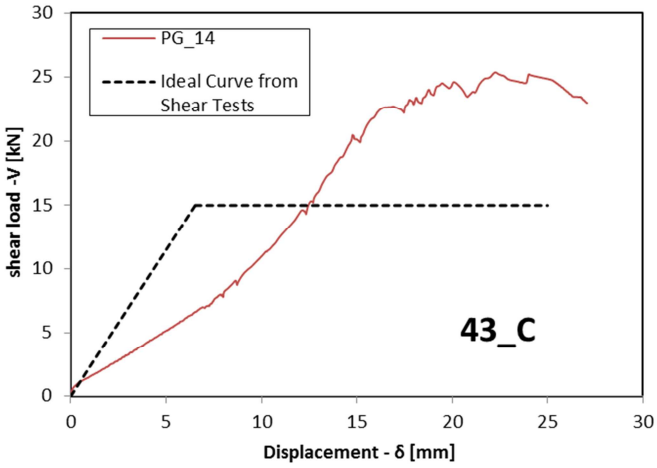

Fig. 5.29

5.8 Conclusions

The test results showed that the critical aspect in assessing the in-plane response of old timber floor diaphragms is the choice of the target point. Most of the international standards in fact, provide equivalent shear stiffness and unit shear strength at yield as the basic instrument to define the in-plane behavior of timber floors in URM buildings. The problem is that for as-built diaphragms, the development of the full strength capacity requires displacements much bigger than those permitted by the out-of plane stability of walls orthogonal to the seismic action (no damage was detected in the tested floor sections). Hence, considering the nonlinearity of the response, it is necessary to determine the stiffness at a deformation level compatible with the seismic load rather than rely on a bilinear schematization characterized by an initial stiffness, a yield strength and a ductility factor. Therefore, for both displacement controlled and force controlled acceptance criteria it is necessary to define the appropriate target point. The same consideration can be made for diaphragms strengthened with new nails. Different is the case of floors retrofitted with a plywood overlay which showed a yield point at a drift level of less than 1%, that enables a univocal determination of the diaphragm capacity.

However, by comparing the experimental results to the standards at a displacement level compatible with the yield point provided by the standards themselves, it appears that NZSEE suggests G_d values for single straight sheathed diaphragm very close to those registered experimentally, while FEMA and ASCE tend to overestimate the diaphragm stiffness. The reason might be related to the fact that all the tests were performed in the direction orthogonal to the joists. The orthotropic behavior of single straight sheathed diaphragms, in fact, is an aspect contemplated only by NZSEE which also considers the flooring condition. On the other hand, once the plywood layer is applied, the diaphragm response is governed by the plywood itself (much stiffer than the original flooring) whose behavior is not affected by the loading direction, thanks to the particular panel disposition adopted. Consequently the stiffness value offered by FEMA and ASCE is similar to that one registered experimentally.

From the test results it appears that to assess the natural period of a timber diaphragm, the best option is to adopt a formulation based on the static scheme of a shear beam under uniformly distributed load. Other approaches, linked to other schemes (e.g. flexural fixed beam), tend to overestimate the fundamental frequency of wooden floors, which is a fact that might not be on the safe side when determining the shear load

transfer. Particular attention should also be paid to the choice of the G_d value which has to be related to the seismic mass.

As regards the strengthening solutions, the “re-nailing” method proved to be a valid option. In fact, with a very low cost-effectiveness ratio, it permitted to obtain a plus 30% in stiffness which guaranteed to the tested floor section the capability of transferring shear loads corresponding to severe seismic events within acceptable drift levels. An extremely stiff response was achieved through the installment of a plywood panel overlay on the existing floorboards. Such behavior was maximized by the peculiar panel disposition which also allowed a very fast assembly procedure.

Acknowledging the significant mechanical property variability in old timber floors, more *in-situ* tests (in direction both parallel and orthogonal to the joists) are required to better characterize the in-plane response of wood diaphragms under every circumstance. The test setup designed for this experimental campaign showed to be non-invasive, easy to install (no need of lifting system) and versatile (adaptable to different-sized specimens).

5.9 References

Agbabian & Associates, S.B. Barnes & Associates, and Kariotis & Associates, (1982), *(ABK) A Joint Venture; Methodology for mitigation of seismic hazards in existing unreinforced masonry buildings: Interpretation of diaphragm tests*, Rep. No. ABK-TR-05 (draft), El Segundo, California

AS/NZS 2269:2008, (2008), *Structural Plywood*, Australian/New Zealand Standard

ASCE-SEI 41/06, (2007) *Seismic rehabilitation of existing buildings*, American Society of Civil Engineers, Reston, Va.

ASTM E2126, (2010), *Cyclic (reversed) load test for shear resistance of vertical elements of the lateral force resisting systems for buildings*, ASTM E2126-10, ASTM International

ASTM F1575, (2008), *Standard Test Method for Determining Bending Yield Moment of Nails,* ASTM F1575-03, ASTM International

ASTM E646, (2007), Standard Test Method for Tensile Strain-Hardening Exponents (n -Values) of Metallic Sheet Materials, ASTM E646-07, ASTM International

Baldessari C., Piazza M., Tomasi R., (2009), *The refurbishment of timber floors: characterization of the in-plane behavior,* PROHITECH International Conference, Taylor & Francis, Rome, Italy, pp. 255-260

Bendat J. S., Piersol A. G., (1993), *Engineering applications of correlation and spectral analysis*, Wiley

Beskhyroun S., (2011), *Graphical Interface Toolbox for Modal Analysis*, Proceedings of the Ninth Pacific Conference on Earthquake Engineering: Building an Earthquake-Resilient Society 14-16 April 2011, Auckland, New Zealand

Brignola A., (2009), *Evaluation of the in-plane stiffness of timber floors for the performance-based retrofit of URM buildings*, PhD Thesis, Department of Civil, Environmental and Architectural Engineering, University of Genoa, Italy

Brincker R., Zhang L., Andersen P., (2000), *Modal identification from ambient responses using frequency domain decomposition*, Proceedings from the 18th International Modal Analysis Conference (IMAC), San Antonio, Texas, USA

Chopra A. K., (2007), *Dynamics of Structures: Theory and Applications to Earthquake Engineering*, Prentice Hall, Upper Saddle River, NJ, 3rd edition

Corradi M., Speranzini E., Borri A., Vignoli A., (2006), *In-plane shear reinforcement of wood beam floors with FRP*, Composites: Part B 37 (2006), pp. 310–319

Derakhshan H., (2011), *Seismic Assessment of Out-of-Plane Loaded Unreinforced Masonry Walls*, PhD Thesis, Department of Civil and Environmental Engineering, University of Auckland, New Zealand

Dolan J. D., Carradine D. M., Bott J. W., Easterling W. S., (2003), *Design Methodology of Diaphragms*, the CUREE-Caltech Woodframe Project, CUREE Publication No. W-27

EN 12512, (2001) *Timber structures - Test methods - Cyclic testing of joints made with mechanical fasteners*, European Standard

EN 408:2010+A1, (2012), *Timber structures – Structural timber and glued laminated timber – Determination of some physical and mechanical properties*, European Standard

FEMA 356, (2000), *Prestandard and Commentary for the Seismic Rehabilitation of Buildings,* American Society of Civil Engineers and Federal Emergency Management Agency, Reston, VA

Filiatrault A., Fischer D., Folz B., Uang C. M., (2002), *Experimental parametric study on the in-plane stiffness of wood diaphragms*, Canadian Journal of Civil Engineering, NRC Research Press, Vol. 29, pp. 554-566

Gattesco N., Macorini L., (2008), *High reversibility technique for in-plane stiffening of wooden floors*, Structural Analysis of Historic Construction, SAHC, © 2008 Taylor & Francis Group, London, ISBN 978-0-415-46872-5

IBC, (2006), *International Building Code*, International Code Council, ISBN:1580012507, 01/03/2006

Jacobsen N. J., Andersen P., Brincker R., (2007), *Using EFDD as a robust technique to deterministic excitation in operational modal analysis*, Proceedings from the 2nd International Operational Modal Analysis Conference (IOMAC), Copenhagen, Denmark

James G. H., Carne T. G., Lauffer J. P., (1993), *The natural excitation technique for modal parameter extraction from operating wind turbines*, Report No. SAND92-1666, UC-261, Sandia National Laboratories

Juang J. N., Pappa R. S., (1985), *An eigensystem realization algorithm for modal parameter identification*, Journal of Guidance, Control and Dynamics, 8(5), pp. 620-627

Knox C. L., (2012), *Assessment of Perforated Unreinforced Masonry Walls Responding In-Plane*, University of Auckland, PhD Thesis, Auckland, New Zealand

Munoz W., Mohammad M., Salenikovich A., Quenneville P., (2008), *Determination of yield point and ductility of timber assemblies: in search for a harmonised approach*, Presented at 2008 Annual Conference of the Canadian Society for Civil Engineers, Quebec, Canada

NZSEE, (2011), *Assessment and Improvement of Unreinforced Masonry Buildings for Earthquake Resistance*, New Zealand Society for Earthquake Engineering, Wellington, New Zealand

Overschee P. V., Moor B. L. R. D., (1996), *Subspace identification for linear systems: theory, implementation, applications*, Kluwer Academic Publishers, Boston

Peralta D. F., Bracci J. M., Hueste M. B. D., (2004) *Seismic Behavior of Wood Diaphragms in Pre-1950s Unreinforced Masonry Buildings*, Journal of Structural Engineering, ASCE, Vol. 30, No. 12, ISSN 0733-9445/2004/12-2040-2050

Piazza M., Polastri A., Tomasi R., (2011), *Ductility of timber joints under static and cyclic loads*, Proceedings of the ICE - Structures and Buildings (April 2011), 164 (2), pp. 79-90

Standards New Zealand (SNZ), (2004a), *NZS 1170.5:2004 Structural Design Actions Part 5: Earthquake actions*, Standards New Zealand, Wellington, New Zealand

Valluzzi M. R., Garbin E., Dalla Benedetta M., Modena C., (2010), *In-plane strengthening of timber floors for the seismic improvement of masonry buildings*, World Conference on Timber Engineering, WCTE, Riva del Garda, Italy

Wilson A., (2012), *Seismic Assessment of Timber Floor Diaphragms in Unreinforced Masonry Buildings*, University of Auckland, PhD Thesis, Auckland, New Zealand

Wilson A., Quenneville P. J. H., Ingham J. M., (2013), *In-plane orthotropic behavior of timber floor diaphragms in unreinforced masonry buildings*, Journal of Structural Engineering, doi:10.1061/(ASCE)ST.1943-541X.0000819

PART 2

6 EXPERIMENTAL TESTS ON TIMBER-TO-TIMBER STRENGTHENING METHODS FOR IMPROVING THE OUT-OF-PLANE BEHAVIOR OF EXISTING WOOD DIAPHRAGMS

6.1 Introduction

A fundamental aspect that need to be keenly considered when retrofitting unreinforced masonry buildings is the evaluation of timber floor stiffness, both in-plane and out-of-plane. It is well-known that the in-plane stiffness of floors influences the structural performance of a building subjected to lateral loads. The stiffer the diaphragms, the deeper the walls work altogether in the resisting system, forming an envelope building. Besides, it is not uncommon that in order to meet standard requirements also the out-of-plane behaviours needs the designers' attention. Timber-to-timber composite structures are a solution which grants the possibility of fulfilling these tasks and satisfying the reversibility issues raised by heritage administration agencies. For example, a possible technique [C.M. 617 (2009)] is that of putting a thick wooden plank directly onto the existing joist and tying them together by means of mechanical (dry) fasteners. The purpose of this chapter is to evaluate the effectiveness of this type of interventions and possibly determine the best configuration and fastener (screw) typology.

6.2 Experimental data

Experimental data have been obtained from a series of tests carried out at the Laboratory of the Department of Mechanical and Structural Engineering (DIMS) of the University of Trento. Every specimen consists of a *150×200 mm*^{2} GL24h glulam beam, with a *500×80 mm*^{2} thick board superposed. Between the beam and the plank there is a layer of *180×30 mm*^{2} floorboards (spruce). Four different timber-to-timber strengthening techniques all by means of screws have been taken into account (Tab. 6.1, Fig. 6.2). The screw spacing (fixed for all the fastener configurations) is connected to the flexural strength of the beam in configuration *4*. In Fig. 6.1 is reported the test setup. The choice of the beam span (*l = 7500 mm*) is due to the decision of reproducing an existing floor previously tested by the authors [Crosatti et al. (2009)] and to the need of reducing the influence of shear deformability to the minimum. Indeed, if this influence is expressed through the ratio between the shear (w_s) and flexural (w_f) component of the midspan deflection, than it is obtained:

$$\frac{w_s}{w_f} = \frac{32}{41}\chi\frac{E}{G}\left(\frac{h}{l}\right)^2 \qquad \textit{(Eq. 6.1)}$$

Where χ is the shear factor, F is the total load, E is the elastic modulus, G is the shear modulus and h is the height of the cross-sectional area.

Screw Type	Length [mm]	Nominal Diameter [mm]	Thread	Dispo-sition
SFS WT-T-8,2x300	300	8.2	Double Thread	X at 45°
SFS WT-T-8,2x300	300	8.2	Double Thread	45°
VGZ9320	320	9.0	All- Thread	X at 45°
HBS10200	200	10.0	Single Thread	90°

Tab. 6.1 Connector typology and disposition

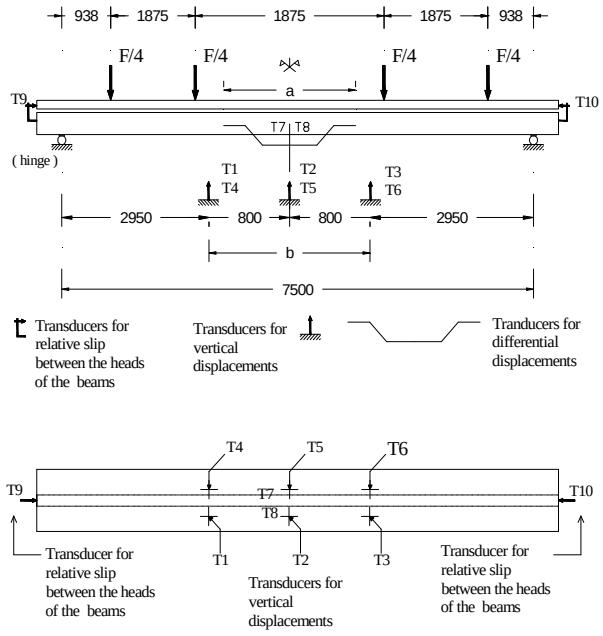

Fig. 6.1 Test setup

So as to simulate a uniformly distributed load pattern, the external load has been applied on four points. Before carrying out the collapse tests, a series of elastic bending

tests has been performed in order to determine the MOE of the considered elements [EN 408]. Slips and displacements have been measured by linear inductive transducers (LVDT), while the actuator's force has been detected with a *300 kN* load cell.

Bearing in mind the loading scheme, it is clear that there is no shear in the central part of the element. Therefore the local value of MOE has been determined relying on the theory of elasticity:

$$E_{loc} = \frac{1}{64}\frac{\Delta F}{\Delta w} l'^2 \qquad \textit{(Eq. 6.2)}$$

Where ΔF is the variation in the actuator load, Δw is the variation in the differential deflection (measured at the midspan), $l'/2$ is the distance between the midspan and the point chosen for the differential deflection evaluation. Every beam and plank has been tested three times. Both direct measurements (employing *T1, T2, T3, T4, T5* and *T6* instruments) and "indirect" ones (using data from the instruments *T7*, *T8* at yokes). In the first case $l'=b$, in the second one $l'=a$ (Fig. 6.1). In Tab. 6.2 the mean values of the local MOE for the tested elements are reported (in the linearization process of the load Vs. displacement curves, a minimum coefficient of determination R^2 equal to *0.9984* has been observed). Averaging the values shown in Tab. 6.2 one can obtain a mean value E_{mean} equal to *11536 MPa* for planks and to *12730 MPa* for beams, in spite of a value of *11600 MPa* suggested by [EN 1194:1999].

	Plank	Beam
	E_{loc}	E_{loc}
	[MPa]	[MPa]
Floor 1	11333	13120
Floor 2	11144	10276
Floor 3	11996	13523
Floor 4	11671	14001

Tab. 6.2 Experimental mean values of local MOE

After determining the Young's modulus for every single element, the composite beams without mechanical connections have been tested. In this way it has been possible to check to what extent the beam and the plank work together as parallel elements or are affected by other phenomena such as friction. In Tab. 6.3, a comparison between the

experimental values $EJ_{0,s}$ (derived through the theory of elasticity applied to the no shear tract) and the theoretic ones $EJ_{0,t}$ obtained by simply adding the beam flexural stiffness (with $E = E_{loc}$) to that of the plank (the two elements are considered to work in parallel).

While for specimens number 1,3 and 4 a good correspondence between theoretical and experimental data has been observed, that does not apply for floor No. 2, which has shown an error greater than 7% (it is to remember that the beam of this specimen differs from the others in MOE value of about 20%, Tab. 6.2). Before venturing any reasons that explain this discrepancy, it seems appropriate to report in Tab. 6.4 the results that one would have obtained not considering the data from yokes. In this case the aforementioned error goes down to 2.7%.Considering that for elastic tests (small loads), the differential deflection magnitude is an order lower than the direct deflection measurements (therefore much more sensitive to errors) it has been preferred not to take into account, during data processing, displacement values obtained from yokes.

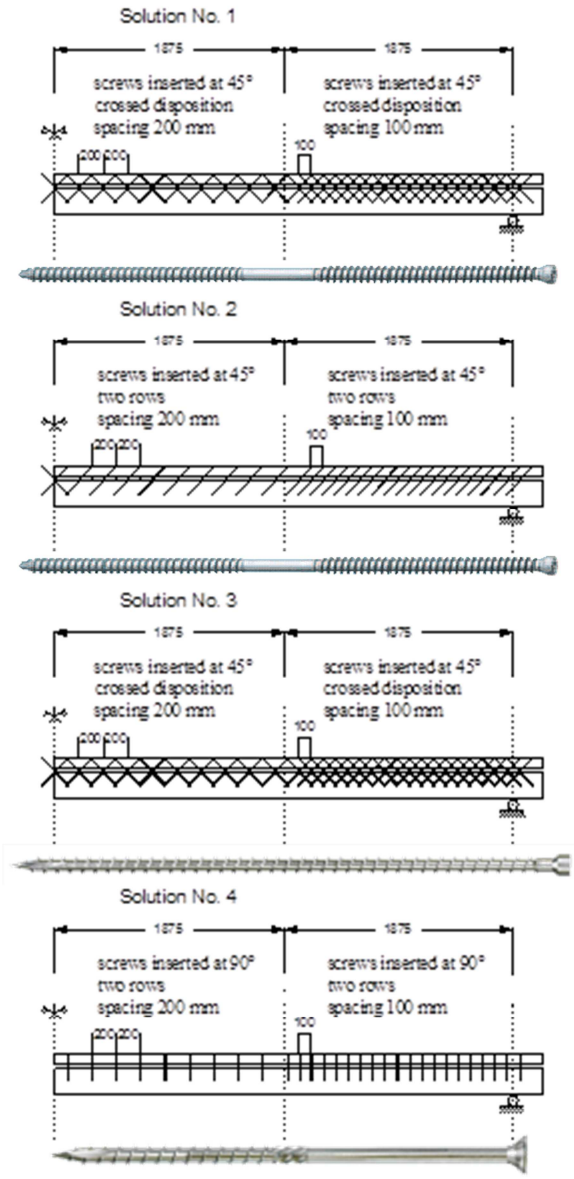

Fig. 6.2 Analysed strengthening solutions

So as to determine the reinforced floor stiffness, elastic tests have been conducted on the composite beams once the connectors were applied. Subsequently all the specimens have been tested to failure (Fig. 6.5). From Fig. 6.6 Failure tests it is possible to observe how the first three strengthening typologies yield the same effects in terms of stiffness although with different values of collapse load (specimen No. *2* reaches an

ultimate load significantly higher than No. 1 and No. *3*). On the other hand, floor No. *4* (single threaded screws orthogonal to the shear plane) after an initial behaviour comparable to that of the other specimens, has shown a noticeable decrease in stiffness that has led to a collapse load of *72 kN*. A failure mode similar to that reported in Fig. 6.5 has been detected for every reinforced floor.

Fig. 6.3 Bend tests on single elements

Fig. 6.4 Floor 2 - composite beam with no connections

Fig. 6.5 Floor 1 – collapse mode

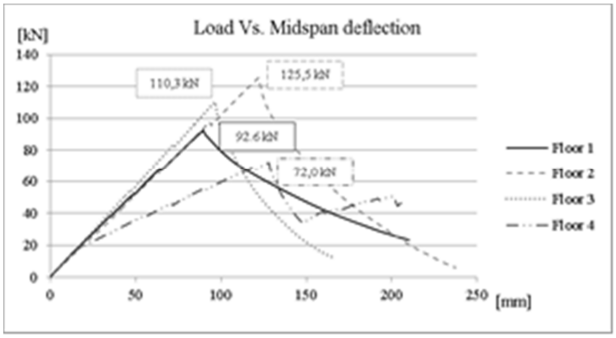

Fig. 6.6 Failure tests

Composite beam without connection

	$EJ_{0,s}$ [Mpa]	$EJ_{0,t}$ [Mpa]	Err. [%]
Floor 1	1.568E+12	1.554E+12	0.9%
Floor 2	1.363E+12	1.265E+12	7.2%
Floor 3	1.636E+12	1.608E+12	1.7%
Floor 4	1.698E+12	1.649E+12	2.9%

Tab. 6.3 Flexural stiffness of the composite system without connections (comparison between theoretic and experimental values)

	Plank	Beam	Composite connection	beam	without
	Eloc [MPa]	Eloc [MPa]	EJ0,s [MPa]	EJ0,t [MPa]	Err. [%]
Floor 1	11104	13094	1.562E+12	1.546E+12	1.0%
Floor 2	10814	10265	1.291E+12	1.257E+12	2.7%
Floor 3	11719	13225	1.548E+12	1.573E+12	1.6%
Floor 4	11336	13614	1.610E+12	1.603E+12	0.4%

Tab. 6.4

6.3 Data processing

It has already been stressed how the collapse load of the tested strengthening solutions is quite unlike. However it seems that, with reference to normal use conditions, the influence of different reinforcements is not so pronounced. Let us suppose a beam spacing of *0.5 m* and a service load of *4 kN/m²* (corresponding to an actuator load of *15 kN*). In Fig. 6.7 the midspan deflection curve has been reported for each specimen before (-·-) and after (---) the screw insertion (R^2_{min}*=0.9991*). It has been also reported the midspan deflection curve in case of an ideal connection (—) which prevents any slip between the beam and the plank. It is possible to observe how the reinforced floors behave very similarly to the ideal composite beam. Furthermore there are no appreciable differences in stiffness between specimens No. *1, 3* and *4*. The lower stiffness shown by floor No. *2* is due to the lower MOE registered for beam No. *2*. As a matter of fact if one determines the connection efficiency, it is clear how all the solutions behave likewise (Tab. 6.5). In order to obtain a more direct measure of the efficiency, referring to the midspan deflection instead of the global values of flexural stiffness, has been preferred. The value of the connection efficiency has been determined as follow:

$$\eta_w = \frac{w_{real} - w_0}{w_\infty - w_0} \qquad \textit{(Eq. 6.3)}$$

where w_{real} is the measured deflection of the reinforced composite beam, w_0 is the measured deflection without connection and w_∞ is the theoretic deflection of the composite beam with an ideal connection. Since the floorboards lay to the compressed

part of the composite floor, their axial stiffness has been considered into the determination of w_∞. Floorboard flexural stiffness has on the other hand been neglected.

	η_w [%]
Floor 1	94,6 %
Floor 2	96,3 %
Floor 3	95,1 %
Floor 4	95,5 %

Tab. 6.5 Connection efficiency under service loading

Employing the model exposed by [Tomasi et al., (2010)], the stiffness K_c of a screw couple has been calculated for every strengthening solution (Tab. 6.6).

The comparison between experimental and theoretic values of midspan deflection for a 15 kN actuator load is given in Tab. 6.6. The theoretical calculation, relies on the theory developed by Newmark et al. in 1951 for a concentrated load and makes use of the superposition principle. Differently from the [EN 1995-1-1] which considers the fastener stiffness k_c as constant along the beam axis (assuming an equivalent spacing s_{eq}, $k_c = K_c/s_{eq}$), in the proposed numerical model, the real screw spacing has been taken into account. In particular, the basic equations are:

$$N_1^{II} - \frac{k_c^I}{k_c} - k_c N_1 \left[\frac{EJ_\infty}{EA_0 EJ_0} \right] = k_c \frac{M}{EJ_0} a \qquad \textit{(Eq. 6.4)}$$

$$w^{IV} - \frac{k_c^I}{k_c} w^{III} - k_c \left[\frac{EJ_\infty}{EA_0 EJ_0} \right] w^{II} = -\frac{1}{EJ_0} M^{II} + \frac{1}{EJ_0} \frac{k_c^I}{k_c} M^I + k_c \left[\frac{EJ_\infty}{EA_0 EJ_0} \right] M \qquad \textit{(Eq. 6.5)}$$

where N_1 is the axial force in the upper element of the composite beam, w is the beam deflection, k_c is the distributed stiffness of fasteners (defined by means of a Fourier transform), a is the distance between the centreline of the two elements, M is the bending moment, EJ_0 is the flexural stiffness of the composite beam with no mechanical connections, EJ_∞ is the flexural stiffness of the ideal composite beam, $EA_0 = (\sum 1/EA_i)^{-1}$, EA_i is the axial stiffness of the i-th element, $X^{I..i}$ is the i-th derivative of the X quantity.

From the results presented in Tab. 6.6 there seems to be a good agreement between numerical and experimental data for specimen No. 1, 2 and 3. The floor reinforced with

single threaded screws instead, has shown a far “better” behaviour than the expected. That is to say, so as to match the experimental deflection a k_c value of *21420 N/mm* should have been used (not consistent with the connector typology). A possible reason might be found in the frictional forces caused by the pressure that the screws generate. During assembly, the fastener is screwed in until its head starts to penetrate into the plank. For this reason, each screw can exert a compressive load equal to the pull-through resistance (as a maximum) $F_{ax,Rk}$ [EN 1995-1-1]:

$$F_{ax,Rk} = f_{head} \cdot d_h^2 \cdot \left(\frac{\rho_k}{350} \right)^{0.8} = 4.01kN \qquad \textit{(Eq. 6.6)}$$

where f_{head} = *10.5 MPa* [ETA-11/0030], d_h = *18.5 mm*, ρ_k = *402 kg/m*^{3}. With a static friction coefficient timber-to-timber μ= *0.25* a friction force of *1 kN* is obtained.

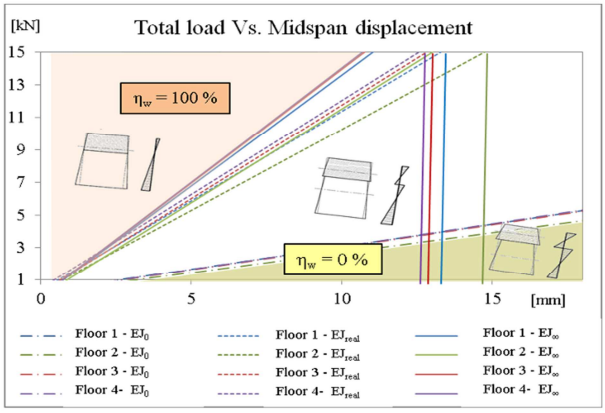

Fig. 6.7 Effectiveness of the proposed solutions

	Screw Type	k_c [N/mm]	$w_{exper.}$ [mm]	$w_{theor.}$ [mm]	Err. [%]
Floor 1	SFS WT-T 8.2x300	30102	13.29	12.34	7.1
Floor 2	SFS WT-T 8.2x300	36493	14.74	14.10	4.4
Floor 3	VGZ9320	33028	12.82	11.94	6.9
Floor 4	HBS10200	5383	12.56	16.47	31.1

Tab. 6.6 Experimental midspan displacement Vs. Expected theoretic deflection (15 kN load)

Fig. 6.8 provides the shear force acting at the contact surface when a fictitious screw stiffness is used, in order to make the numerical midspan deflection mirror the experimental one (k_c = *21420 N/mm*). It is also reported the friction developing along the beam, due to the pressure produced by the fasteners. It can be seen how, in the central part of the composite beam, the acting shear is lower than the friction. Consequently the numerical midspan deflection has been recalculated considering the k_c value presented in Tab. 6.6 (in accordance with the formulation proposed by EN 1995-1-1) and locking the slip between the two inner loads. As a result the error decreases to about *9%* (Tab. 6.7).

	Screw Type	k_c [N/mm]	$w_{exper.}$ [mm]	w_{theor} [mm]	Err. [%]
Floor 4	HBS10200	5383	12,56	13,64	8,6

Tab. 6.7 Theoretical midspan displacement of Floor 4 (central slip locked)

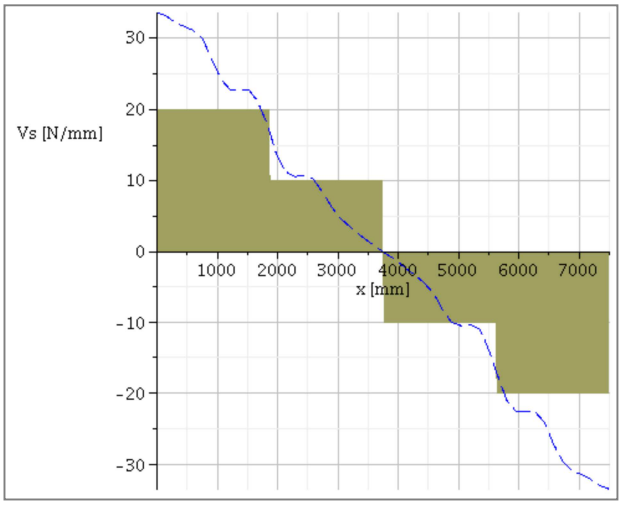

Fig. 6.8 *Shear acting at the contact surface (blue line) Vs. Friction along the beam axis.*

As outlined in Tab. 6.8, if the midspan deflection is determined through the EN 1995-1-1 approach, slightly lower values (non-conservative side) compared to those in Tab. 6.6 are obtained (except for Floor 4).

	γ_1	$EJ_{eff.}$ [MPa]	$w_{exper.}$ [mm]	$w_{theor,EC5}$ [mm]	Err. [%]
Floor 1	0.87	6.777 E+12	13.29	12.16	8.5
Floor 2	0.90	5.949 E+12	14.74	13.85	6.0
Floor 3	0.88	7.007 E+12	12.82	11.76	8.3
Floor 4	0.53	4.914 E+12	12.56	16.77	33.4

Tab. 6.8 Theoretic midspan deflection according to the European Standard (mechanical properties experimentally determined)

On the other hand if one focuses on the tract between *19 kN* and *30 kN* (corresponding to *5 kN/m²* and *8 kN/m²* respectively) it can be registered how the efficiency of floors 1, 2 and 3 remains unchanged while specimen No.4 efficiency goes down to *58.8 %*. In this situation, from the confrontation between the variation in the experimental deflection $\Delta w_{exper.}=20.789$ *mm* and the variation in the predicted deflection (provided the overcoming of friction) $\Delta w_{theor.}=12.078$ *mm*, the numerical model appears to overestimate the real stiffness of the composite beam, generating an error in the deflection prediction of more than 40%. To reproduce exactly the experimental behaviour, a k_c value of *1330 N/mm* should have been employed.

Tab. 6.9 shows the comparison between the experimental and the predicted values (obtained following the EN 1995-1-1 approach) of the collapse load. It is also reported (Tab. 6.10) the stress level on the tension side of the beam at the moment of collapse.

	$F_{U,exper.}$ [kN]	$F_{U,theor}$ [kN]	Err. [%]
Floor 1	92.6	74.3	19.8
Floor 2	125.5	78.2	37.7
Floor 3	110.3	75.1	31.9
Floor 4	72.0	62.6	13.1

Tab. 6.9 Ultimate load comparison (experimental Vs. theoretical)

	σ_r	$f_{m,k}$
	[MPa]	[MPa]
Floor 1	29.91	24.00
Floor 2	38.50	24.00
Floor 3	35.24	24.00
Floor 4	27.62	24.00

Tab. 6.10 Beam stress on the tension side at the collapse point

The results of a series of parametric analyses are given in Fig. 6.9 (the geometrical and mechanical properties of the composite beams are the same obtained for specimen No. 4). It can be seen that the more *increases (decreases)* the *equivalent spacing (fastener stiffness)*, the more scattered are the data for different spacing patterns. It should be noted that following the approach embodied in [EN 1995-1-1 (2004)], just one solution can be found for all the A-to-E configurations (where $s_{max} \leq 4s_{min}$). However the midspan deflection values determined with this approximate solution are not significantly different from the displacements computed with a more detailed model.

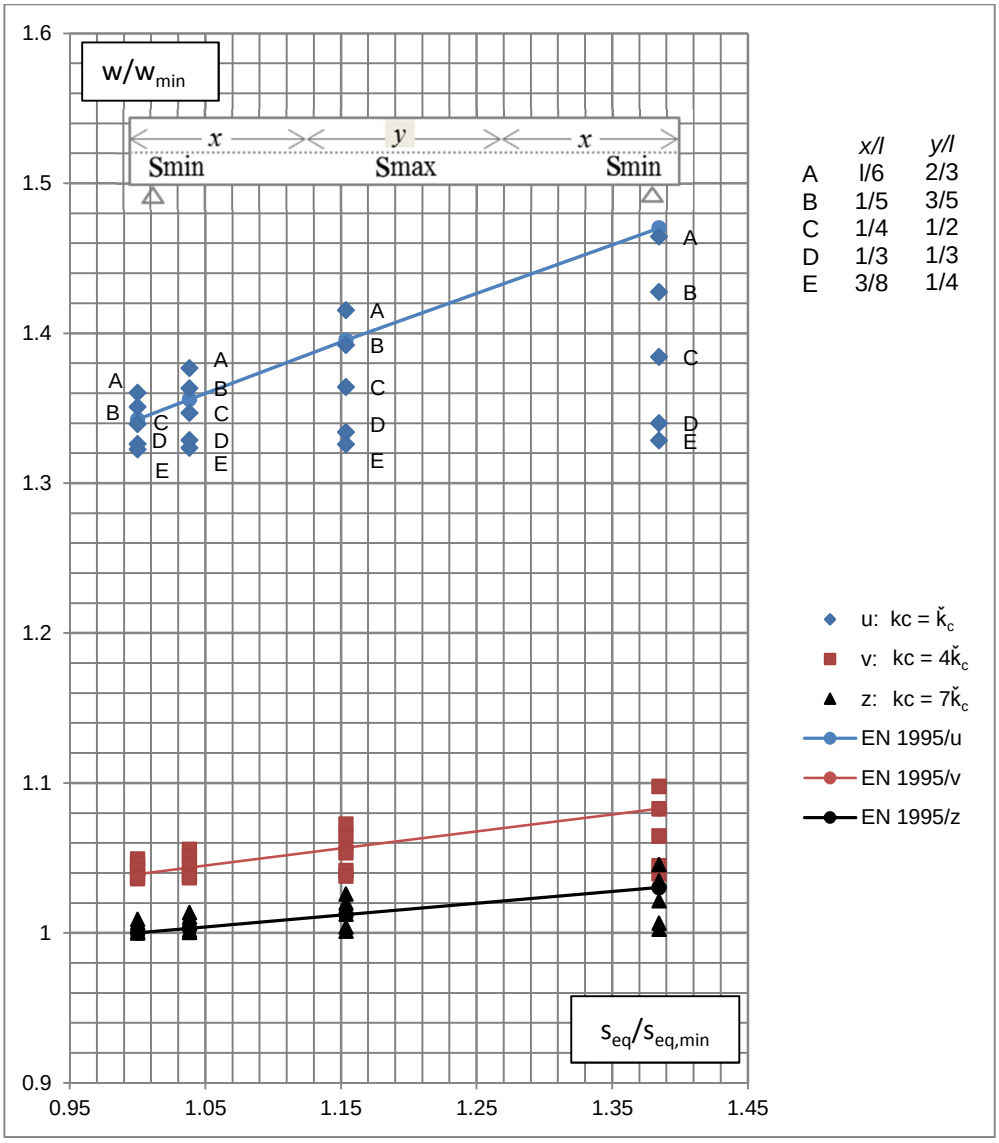

Fig. 6.9 *Parametric analyses ($\check{k}_c$ = 5000 N/mm, $s_{eq,min}$ =110 mm, uniformly loaded beam)*

6.4 Conclusions

Regarding the specimen *1*, *2* and *3*, no significant differences have been observed in the behaviour in normal use, even if a certain trend is noticeable. As a matter of fact it was expected that the 45°, not crossed disposition showed an efficiency higher than the other two configuration owing to internal stress-components which are generated by the "screw pressure". In particular the "compression" produced by the double-threaded screws, considered the inclination of the connectors themselves, yields horizontal components of distributed forces acting at the contact surface between the beam and the plank, in the opposite direction to the acting shear.

Applying the stiffness calculation method proposed by [Tomasi et al.] to the approach embodied in the [EN 1995-1-1] it is possible to estimate the midspan displacement with sufficient accuracy. It would seem that (with reference to the adopted geometry) it is not necessary to employ finer models able to take into account the variation in the connection stiffness along the beam principal axis.

As far as specimen number *4* is concerned, the experimental behavior under loads close to those in normal use, appears to be deeply influenced by friction phenomena whose being and magnitude are not guaranteed in any case. However, during the phase immediately after the intervention, the real behavior of the composite beam could actually be quite stiffer than that one expected from the theoretic model.

6.5 References

C.M. 617: 02-02-2009, (2009),. *Istruzioni per l'applicazione delle «Nuove norme tecniche per le costruzioni» di cui al decreto ministeriale 14 gennaio 2008*

Crosatti A., Piazza M., Tomasi R., Angeli A., (2009), *Refurbishment of traditional timber floor with inclined screw connectors,* Proceeding of the International Conference on Protection of Historical Buildings, Prohitech 09, Roma, 21-24 June 2009, CRC Press, Taylor&Francis, Vol 1.: 273-279

DIN 1052:2004-08, (2008) *Entwurf, Berechnung und Bemessung von Holzbauverken – Allgemaine Bemessungsregeln und Bemessungsregeln fur den Hochbau*

EN 1194:1999, (2009), *Timber structures - Glued laminated timber - Strength classes and determination of characteristics values*

EN 1995-1-1, 2004, (2004), Eurocode 5: *Design of timber structures - Part 1-1: General – Common rules and rules for buildings*

EN 408:2003, (2003), *Timber structures. Structural timber and glued laminated timber. Determination of some physical and mechanical properties*

Gliniorz, K., Mosalam, K. M., Natterer, J., (2002), *Modeling of layered timber beams and ribbed shell frameworks. Composites: Part B 33, 367-381*

Kreuzinger, H., *Flächentragwerke Platten, Scheiben und Schalen Berechnungsmethoden und Beispiele*

Möhler, K., (1956), Über das Tragverhalten von Biegeträgern und Druckstäben mit zusammengesetzten Querschnitt und nachgiebigen Verbindungsmitteln. Habilitation. *Technical University of Karlsruhe*. 1956:I-II: 1-73

Newmark N.M., Siess C.P., Viest I.M., (1951), *Tests and Analyses of Composite Beams with Incomplete Interaction. Proceedings, Society for Experimental Stress Analysis, Vol. 9, No. 1, 75-92*

NiCoLe, (2001), *Norma tecnica per la progettazione, esecuzione e collaudo delle costruzioni di legno* – Consiglio Nazionale delle ricerche, commissione di studio e consultiva per le norme tecniche relative alle costruzioni, Roma

Piazza M., Tomasi R., Modena R., (2005), *Strutture in legno. Materiale, calcolo e progetto secondo le nuove normative europee,* Biblioteca Tecnica Hoepli

Scholz, A., (2004), *Eigenspannungszustände an Verbundquerschnitten infolge von Dehnungsunterschieden – Anwendung eines neueren Rechenverfahrens auf einen bewährten Lösungsansatz*. Bautechnik (81), Heft 3, 180-188

Stürzenbecher, R., Hofstetter, K., Eberhardsteiner, J., (2010), *Cross laminated timber: a multi-layer, shear compliant plate and its mechanical behavior. Proceedings of the World Conference on Timber Engineering*

Tomasi R., Crosatti A., Piazza M., (2010), *Theoretical and experimental analysis of timber-to-timber joints connected with inclined screws.* Construction and Building Materials, 24, 1560-1571

7 PROPOSAL OF A NEW METHOD FOR CAMBERING TIMBER COMPOSITE BEAMS BY MEANS OF SOLE SCREWS

7.1 Introduction

When rehabilitating historical masonry buildings it is certainly not rare to come to deal with sagged timber floors which cannot be buttressed due to heritage issues. A similar problem occurs when historical buildings are readapted to a new building usage which provides for an increase in floor loads. In this case the timber floors, originally designed to bear low loads, will inevitably show an excessive midspan deflection (serviceability limit state). Therefore the development of a procedure which enables to “lift” a beam by just superposing a “dry reinforcement element”, could prove of some interest.

If one considers a composite beam, as in Fig. 7.1a, where the fasteners forms a 90° angle with the beam axis, it can be seen that without any other external load all the compression forces due to the pressure generated by the screws are in equilibrium and therefore the beam remains undeformed. As soon as a load is applied Fig. 7.1b, the beam begins to sag and the two component elements exchange a system of forces similar to that in Fig. 7.1c. On the other hand, if the screws are positioned as in Fig. 7.1d, in order to reach the equilibrium, the two contact surfaces have to exchange a shear action (Fig. 7.1e) that is opposite to that in Fig. 7.1c and consequently the beam rises.

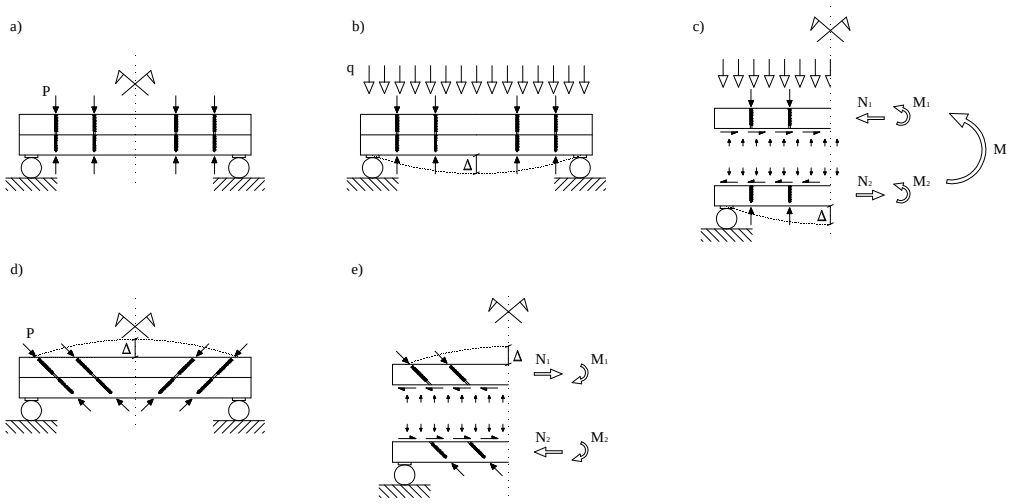

Fig. 7.1 Cambering principles for a composite beam

It must be highlighted that the proposed method permits to camber a timber beam without the need of any buttressing or application of external forces other than the screws.

7.2 The experimental tests

The aim of this chapter is to investigate the possibility of cambering a timber beam by simply putting another beam on top of it and inserting screws inclined at *45°* relative to the beam axis. So as to discover it, three tests have been carried out at the Laboratory of the Department of Mechanical and Structural Engineering (DIMS) of the University of Trento. Each specimen is composed by two *0,1 x 0,1 m^2* glulam beams *4 m* long, connected by double threaded screws (Fig. 7.2). The fastener spacing (*100 mm*), is related to the need of obtaining a clear camber (more than *10 mm*) through the connectors at disposal. It is utterly acknowledged that the flexural stiffness of a composite beam is directly related to the fasteners capability of hindering the two contact surfaces from slipping each other. Since the interface slip is maximum at the ends of the composite beam and minimum in the central part, cambering is expected to be more difficult when the screw assembly starts from the outer parts of the beam rather than when it starts from the inner part. Consequently tests No. 1 and 3 have been performed inserting the screws from the middle to the ends (Int-to-Ext) and test No. 2 has been carried out from the ends to the middle (Ext-to-Int). Before inserting any

mechanical connector, a series of elastic bending tests has been performed in order to determine the modulus of elasticity (MoE) of the considered elements (Tab. 7.1).

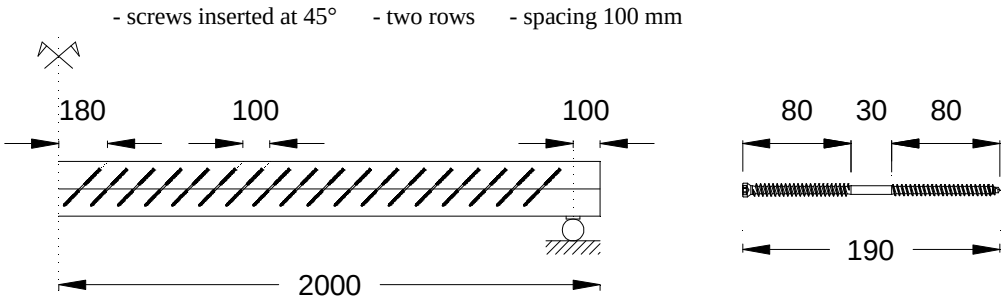

Fig. 7.2 Test setup (measures in [mm])

Composite Beam	C1		C2		C3	
Element	M1	M2	M3	M4	M5	M6
E [MPa]	7327	12024	11863	8712	11358	9245

Tab. 7.1 MoE of tested elements

	$w_{L/2}$ [mm]	Screwing pattern
C1	13.39	Int-to-Ext
C2	6.94	Ext-to-Int
C3	14.92	Int-to-Ext

Tab. 7.2 Experimental upward camber

Tab. 7.2 shows the results of the cambering procedure. As expected, test No. 2 (Ext-to-Int) exhibits a final value significantly lower than the other tests.

The camber amount (it has been observed an upward deflection of about one three-hundredth of the total beam length) could possibly be increased by reducing the screw spacing or by using fasteners able to generate a greater pressure. In doing so, keen attention should be paid to the magnitude of the internal stress state imposed by the cambering procedure. It is also quite evident that further testing is needed so as to fully understand the behavior of such a composite beam in the long-term period. For the time being, the three assembled specimens have been monitored for 48 hours, during which no camber loss has been detected.

Fig. 7.3 Composite beam C1 after fastener insertion (starting from the beam centre)

7.3 The numerical model

A numerical model has been developed through the finite element software SAP2000. In particular, as to reproduce the act of inserting the screws one after the other, the nonlinear staged-construction function has been employed [CSI (2004)]. The choice of not utilizing the structure symmetry is due to the impossibility, during “real” assembly, of inserting the fasteners on symmetric positions simultaneously. However in that case, a slightly lower value of the final camber would have been reached since at the application of the screw pressure, the connector stiffness is already in place (other solutions have been tested but have led to excessive values of upward camber). Both the fasteners and the wood elements have been modeled as linear elastic materials. The stiffness of the screw couple K_c has been determined in accordance with [Tomasi et al. (2010)] (K_c = *26303 N/mm*) and has been reproduced by means of two crossed rods (inclined at 45°) whose axial stiffness is equal to K_c itself. The screw pressure has been introduced as a system of two inclined forces acting at the screw nodes. In addition, inextensible rods have been used to keep locked the distance between the barycenter lines of the wood elements.

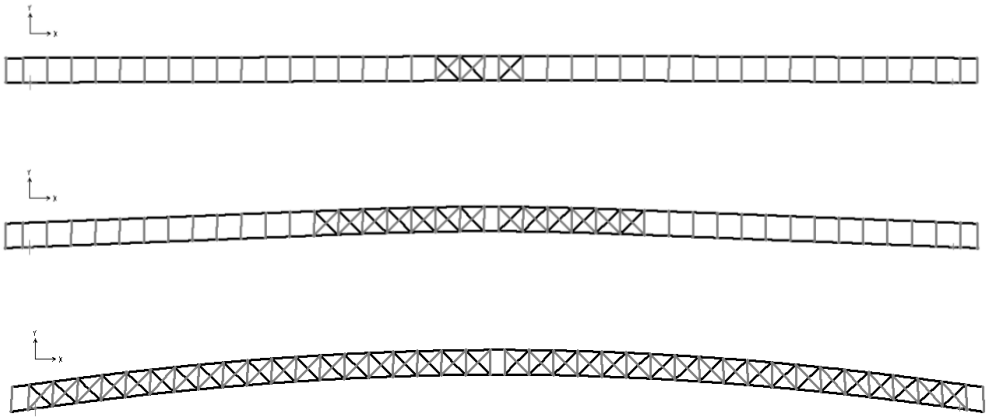

Fig. 7.4 The F.E. model (deformed shape scale factor = 10)

So as to determine what sort of pressure is to be assigned to the screw couple, some tests have been performed, relying on the setup shown in Fig. 7.5. Many parameters have been pried (e.g. screw angle with respect to the grain direction, initial pressure, head penetration length, threaded part length, connector typology, wood density, time-dependence) and further testing will be presented in the next chapter. A resultant pressure value of *4.4 kN* for the single screw has been deemed as acceptable.

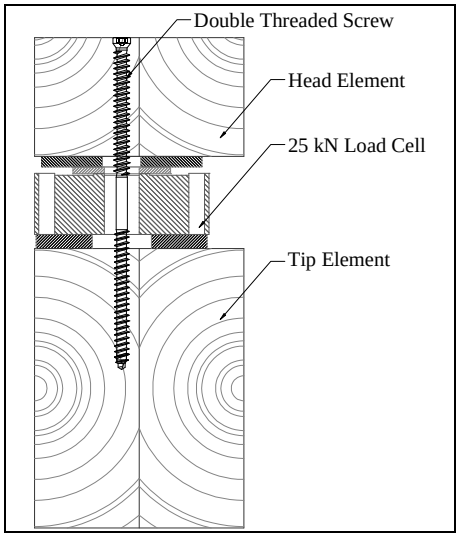

Fig. 7.5 Screw pressure test setup

The results obtained from the numerical model are given in Tab. 7.3. Regarding specimens C1 and C3, it could be seen that the numerical model reproduces the experimental behavior with sufficient precision for both the tested screwing patterns (Int-to-Ext and Ext-to-Int). An underestimation of the camber value has been observed for specimen C3.

	Experimental	Numerical	Err. %
C1	13.39	13.78	2.91
C2	6.94	7.40	6.63
C3	14.92	12.52	16.09

Tab. 7.3 Experimental data Vs. Numerical values [mm]

7.4 The analytical formula

In order to better understand the details of the analytical formulation proposed herein, a brief description of the theory developed by [Newmark et al.(1951)] concerning composite beams with incomplete interaction, is provided. This theory leans on the following assumptions:

1. The materials involved are linear elastic.
2. Small displacements and deformations.
3. Both elements have the same curvature (no interpenetrations).
4. Plane sections remain plane (Euler-Bernoulli).
5. Mechanical fasteners can be considered uniformly distributed along the compound beam axis.
6. Beam sections are constant along the longitudinal axis.

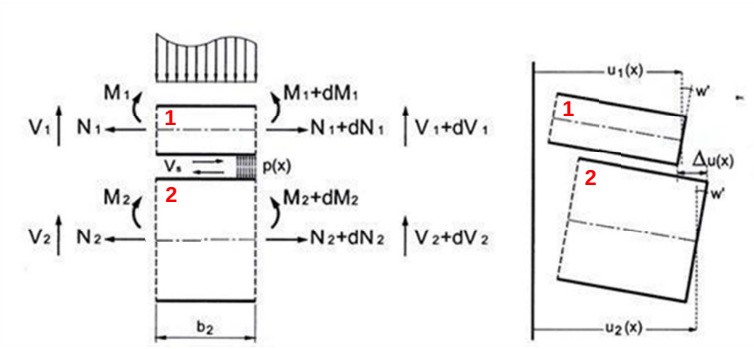

Fig. 7.6 Elements of a composite beam: internal forces [Ballerini]

The hereafter described symbols will be adopted.

- k_c is the distributed stiffness of fasteners;
- a is the distance between the centerline of the two elements;
- $\alpha = [(k_c\, EJ_\infty)/(\, EJ_0\, EA_0)]^{0.5}$;
- EJ_0 is the flexural stiffness of the composite beam with no mechanical connections;
- EJ_∞ is the flexural stiffness of the ideal composite beam;
- $EA_0 = (\sum 1/EA_j)^{-1}$;
- EA_j is the axial stiffness of the *j-th* element;

Considering the compound element in Fig. 7.6, the imposition of the equilibrium on the whole element produces:

$$N_1 + N_2 = 0 \qquad \textit{(Eq. 7.1)}$$

$$V_1 + V_2 = V(x) \qquad \textit{(Eq. 7.2)}$$

$$M_1 + M_2 - N_1 \cdot a = M(x) \qquad \textit{(Eq. 7.3)}$$

The imposition of the equilibrium condition on the compound element in Fig. 7.6, produces:

$$V'(x) = -q(x) \qquad \textit{(Eq. 7.4)}$$

$$M'(x) = V(x) \qquad \textit{(Eq. 7.5)}$$

$$M''(x) = -q(x) \qquad \textit{(Eq. 7.6)}$$

The equilibrium equations for element 1 are:

$$N'_1(x) = -V_s(x) \qquad \textit{(Eq. 7.7)}$$

$$V'_1(x) = -\big(q(x) - p(x)\big) \qquad \textit{(Eq. 7.8)}$$

$$M'_1(x) = V_1(x) - V_s(x)\frac{h_1}{2} \qquad \textit{(Eq. 7.9)}$$

For element 2 instead:

$$N'_2(x) = V_s(x) \qquad \textit{(Eq. 7.10)}$$

$$V'_2(x) = -p(x) \qquad \textit{(Eq. 7.11)}$$

$$M'_2(x) = V_2(x) - V_s(x)\frac{h_2}{2} \qquad \textit{(Eq. 7.12)}$$

From the hypothesis number 3:

$$w_1'' = w_2'' = w'' \qquad \textit{(Eq. 7.13)}$$

The slip at the interface surface can be expressed as:

$$\Delta u(x) = u_2(x) - u_1(x) + w'(x)\frac{h_1}{2} + w'(x)\frac{h_2}{2} = u_2(x) - u_1(x) + w'(x)a \qquad \textit{(Eq. 7.14)}$$

Since all the materials are linear elastic:

$$w''_1(x) = -\frac{M_1(x)}{E_1 J_1} \qquad \textit{(Eq. 7.15)}$$

$$w''_2(x) = -\frac{M_2(x)}{E_2 J_2} \qquad \textit{(Eq. 7.16)}$$

$$V_s(x) = k_c \Delta u(x) \qquad \textit{(Eq. 7.17)}$$

From the rotational equilibrium of the whole element:

$$M_1 + M_2 = M(x) + N_1 a \qquad \textit{(Eq. 7.18)}$$

By employing the congruence equation (Eq. 7.13) and the constitutive law, it can be obtained:

$$M_2(x) = \frac{M_1(x)}{E_1 J_1} E_2 J_2 \qquad \textit{(Eq. 7.19)}$$

Then, substituting (Eq. 7.19) in (Eq. 7.18) yields:

$$M_1\left(\frac{E_1 J_1 + E_2 J_2}{E_1 J_1}\right) = M(x) + N_1 \cdot a \Rightarrow \; M_1(x) = \frac{E_1 J_1}{E J_0}\left(M(x) + N_1(x)a\right) \qquad \textit{(Eq. 7.20)}$$

Similarly for M_2:

$$M_2(x) = \frac{E_2 J_2}{E J_0}\left(M(x) + N_1(x)a\right) \qquad \textit{(Eq. 7.21)}$$

Provided (Eq. 7.14) and (Eq. 7.17), the derivative of (Eq. 7.7) becomes

$$N''_1(x) = -V_s'(x) = -k_c \Delta u'(x) = -k_c \left(u'_2(x) - u'_1(x) + w''(x)a \right) \qquad \textit{(Eq. 7.22)}$$

Taking into account that:

$$u'_2(x) = \varepsilon_2(x) = \frac{N_2(x)}{E_2 A_2} = -\frac{N_1(x)}{E_2 A_2} \qquad \textit{(Eq. 7.23)}$$

$$u'_1(x) = \varepsilon_1(x) = \frac{N_1(x)}{E_1 A_1} \qquad \textit{(Eq. 7.24)}$$

$$w''(x) = -\frac{M_1(x)}{E_1 J_1} = -\frac{M(x) + N_1(x)a}{EJ_0} \qquad \textit{(Eq. 7.25)}$$

(Eq. 7.22) can be rewritten as:

$$N''_1(x) = -k_c \left[-\frac{N_1(x)}{E_2 A_2} - \frac{N_1(x)}{E_1 A_1} - \frac{M(x) + N_1(x)a}{EJ_0} a \right] \qquad \textit{(Eq. 7.26)}$$

Which can be rearranged as:

$$N''_1(x) - k_c N_1(x) \left[\frac{1}{E_1 A_1} + \frac{1}{E_2 A_2} + \frac{a^2}{EJ_0} \right] = \frac{k_c a}{EJ_0} M(x) \qquad \textit{(Eq. 7.27)}$$

$$N''_1(x) - k N_1(x) \left[\frac{EJ_0 + EA_0 a^2}{EA_0 EJ_0} \right] = \frac{ka}{EJ_0} M(x) \qquad \textit{(Eq. 7.28)}$$

Finally, the following second order equation with constant coefficients is obtained:

$$N''_1(x) - \alpha^2 N_1(x) = \beta M(x) \qquad \textit{(Eq. 7.29)}$$

From the solution of (Eq. 7.29) it is possible to deduce all the other internal actions. As regards displacement components, the following fourth order equation with constant coefficients is determined starting from the expression of the beam curvature (Eq. 7.25):

$$w^{IV}(x) - \alpha^2 w''(x) = \alpha^2 \frac{M(x)}{EJ_\infty} + \frac{q(x)}{EJ_0} \qquad \textit{(Eq. 7.30)}$$

The biggest issue with (Eq. 7.29) and (Eq. 7.30) is that they are based on the assumption that k_c is constant. By contrast, the cambering procedure relies on a sequential insertion of the fasteners. Hence the connector stiffness should be time-dependent and vary along the beam axis. In other words, the composite structure is already working during the assembly due to the horizontal forces introduced by the screws themselves. In that phase there is a part of the beam which is loaded and stiffened by the screws while the remaining part is free. To solve the problem, it is assumed that two connector couples placed at the same distance from the midspan section but in an opposite position, are inserted simultaneously. Now it is possible to exploit the problem symmetry by considering the simply supported composite structure as a cantilever compound beam (Fig. 7.7). It must be noted that the following formulation is valid only for a Int-to-Ext assembly procedure (which yields higher cambering values) with a constant fastener spacing.

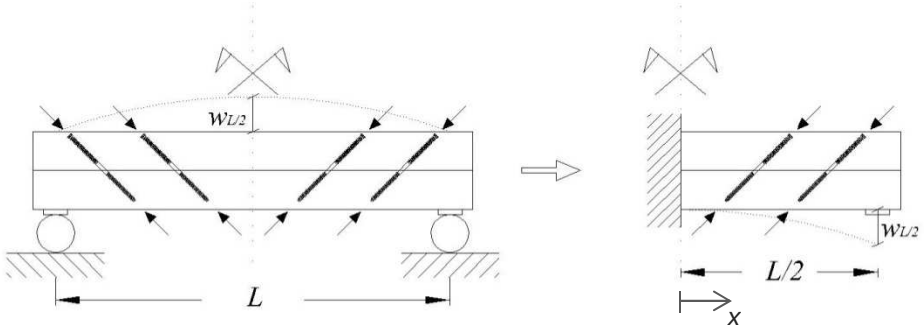

Fig. 7.7 Static scheme adopted for the analytical formulation

Since all the materials forming the compound beam are linear elastic it is possible to employ the linear superposition principle (Fig. 7.8). Thus, the issue of taking into account the staged assembly is solved by counting the effect of each connector couple separately. However, remains the fact that the connection stiffness cannot be considered uniformly distributed, because of the beam part where the screws are yet to be inserted. However let us put this aside for a moment. If one thought of cutting the composite cantilever beam right after the first screw couple ($x = s$, s = position of the first screw couple) exactly at the moment of its insertion, they would get a compound beam where the distributed connector stiffness can be deemed as constant. Therefore,

the second order differential equation presented hereafter could be obtained by following the same procedure as for (Eq. 7.29):

$$N_1''(x) - \alpha^2 N_1(x) = 0 \qquad \textit{(Eq. 7.31)}$$

With the boundary conditions:

$$N_1(0) = 0,\ N_1(s) = T \qquad \textit{(Eq. 7.32)}$$

where:

- N_1 is the axial force in the upper element of the composite structure (the beam length is equal to s);
- N_1'' is the second derivative of N_1;
- T is the horizontal component of the resultant pressure yielded by one couple of inclined screws;

The solution of (Eq. 7.32) is:

$$N_1(x) = \frac{T \sinh(\alpha x)}{\sinh(\alpha s)} \qquad \textit{(Eq. 7.33)}$$

At this point, acknowledging that $M(x)$ is null, (Eq. 7.25) becomes:

$$w''(x) = -\frac{N_1(x) \cdot a}{EJ_0} \qquad \textit{(Eq. 7.34)}$$

In accordance with the external constraints, the boundary conditions are:

$$w(0) = 0, w'(0) = 0 \qquad \textit{(Eq. 7.35)}$$

Consequently, in the cut beam, the displacements originated from the external pressure introduced by the screw couple are described by:

$$w(x) = \frac{Ta}{EJ_0 \alpha \sinh(\alpha s)} \cdot \left[x - \frac{\sinh(\alpha x)}{\alpha} \right] \qquad \textit{(Eq. 7.36)}$$

In order to determine the cambering value on the original beam soon after the assembly of the first screw couple, it is necessary to take into account the contribution offered by the rigid movement of the free part of the beam that was previously cut. As a result:

$$w_{L/2} = w(s) + w'(s) \cdot \left(\frac{L}{2} - s \right) \qquad \textit{(Eq. 7.37)}$$

(Eq. 7.37) represents the solution to the problem in case of a single screw couple (obviously it could be a single screw). Hence, as already mentioned, the linear superposition principle has to be exploited. So as to achieve this, as many fictitious beams as the total number of screw couples have to be created as shown for the first fastener couple. For the generic *i-th* beam:

$$N_{1,i}(x) = \frac{T \sinh(\alpha x)}{\sinh(\alpha si)} \qquad \textit{(Eq. 7.38)}$$

where:

- $N_{1,i}$ is the axial force in the upper element of the composite structure (the beam length is equal to *si*);
- *i* is the number of the screw couple (labeling starts from the internal side);
- *s* is the fastener spacing.

The *i-th* beam deflection becomes:

$$w_i(x) = \frac{Ta}{EJ_0 \alpha \sinh(\alpha si)} \cdot \left[x - \frac{\sinh(\alpha x)}{\alpha} \right] \qquad \textit{(Eq. 7.39)}$$

Therefore the contribution of the *i-th* screw couple to the beam camber is:

$$\Delta w_{i,L/2} = w_i(si) + w_i'(si) \cdot \left(\frac{L}{2} - si \right) \qquad \textit{(Eq. 7.40)}$$

Finally the evaluation of the beam camber is obtained:

$$w_{L/2} = \sum_{i=1}^{n} \Delta w_{i,L/2} = \sum_{i=1}^{n} \left\{ \frac{1}{2} \frac{Ta\left[\cosh(\alpha si)(2si - L) + L\right]}{\sinh(\alpha si) EJ_0 \alpha} \right\} - \frac{nTa}{\alpha^2 EJ_0} \qquad \text{(Eq. 7.41)}$$

where *n* is the total number (Fig. 7.9) of fastener couples.

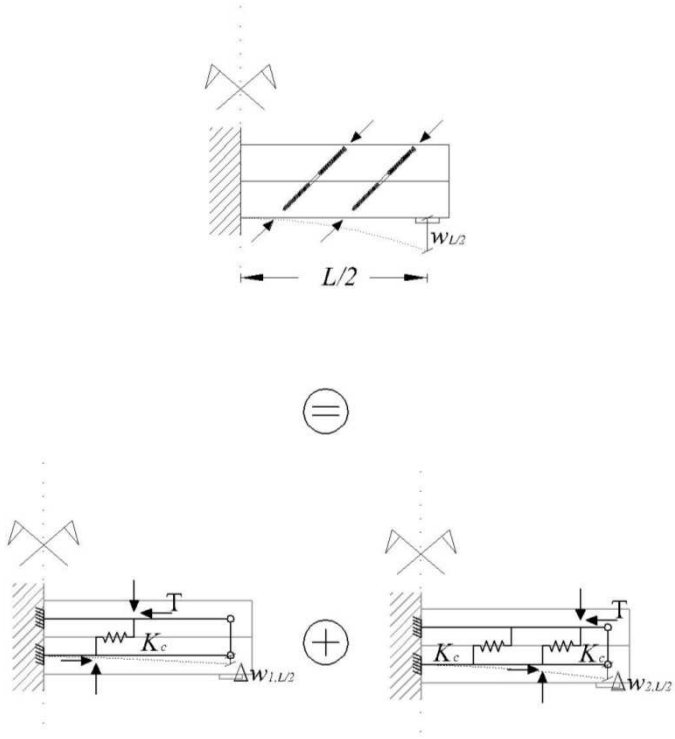

Fig. 7.8 Static scheme: linear superposition principle

	Experimental	Analytical	Err. %
C1	13.39	13.28	0.82
C2	6.94	-	-
C3	14.92	12.88	13.68

Tab. 7.4 Experimental data Vs. Analytical values [mm]

Tab. 7.4 provides a comparison between experimental data and analytical values obtained through eq.(Eq. 7.41). The proposed formula seems able to reproduce the

experimental camber of C1 specimen with quite good precision, while a certain error (*13%*) has been observed for C3 specimen. It should be noted that for composite beam C3 the numerical model gave a very similar prediction (*19%* err..).

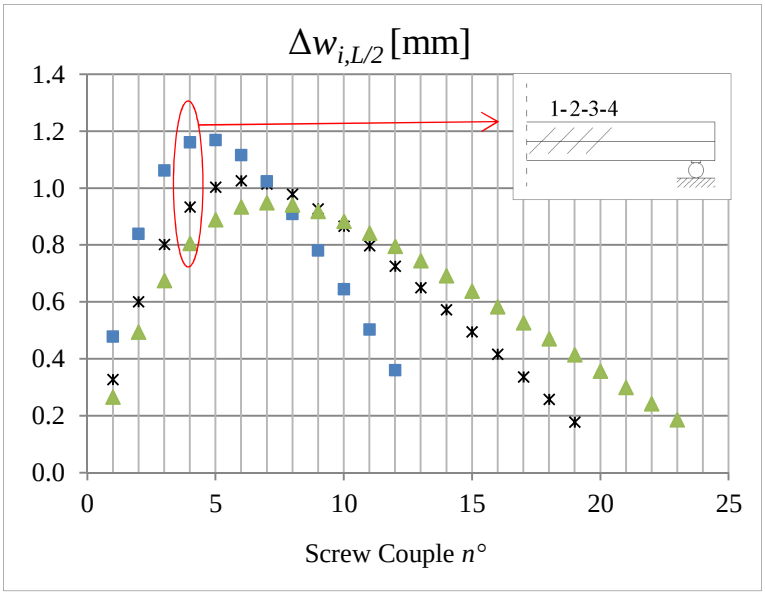

Fig. 7.9 Couple effectiveness to the upward camber

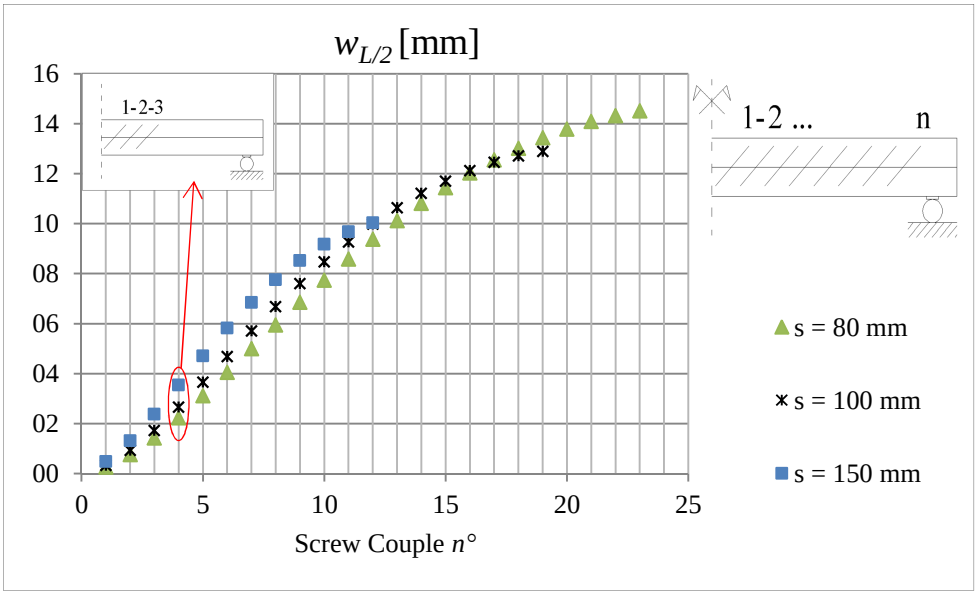

Fig. 7.10 Camber evolution

As outlined in Fig. 7.9, the effectiveness of an *i-th* screw couple depends on how many couples have already been inserted and on the fastener spacing. Although it has been observed that (Fig. 7.11) the greater the spacing the greater the effectiveness, if one focuses on the global result it is clear that increasing the spacing reduces the amount of screws and consequently the final camber (Fig. 7.10).

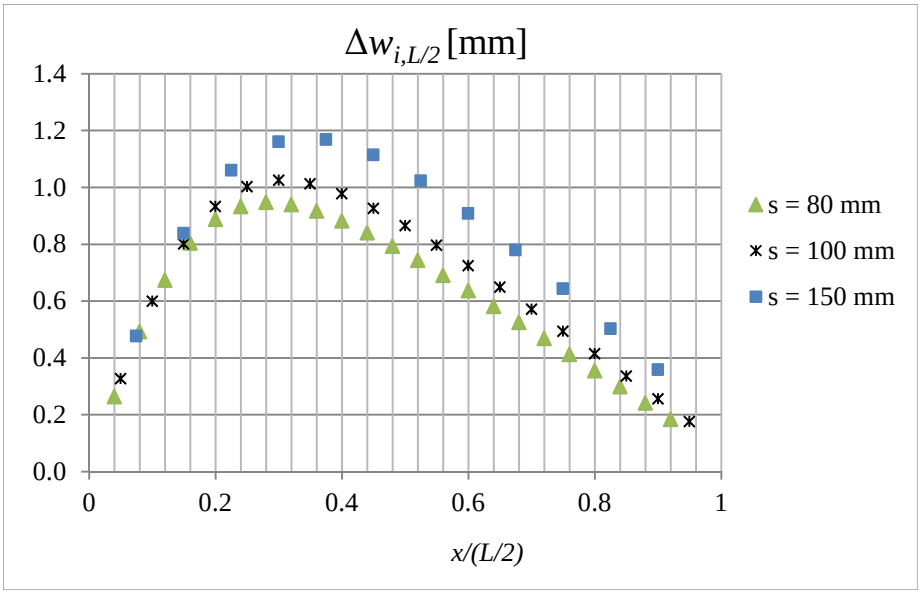

Fig. 7.11 Screw couple effectiveness Vs. Screw position along the beam

7.5 Conclusions

The exposed cambering procedure has proved to be effective and permits to obtain significant values of upward deflection. Obviously, the camber has to be consistent with what is connected to beam. In addition, it ought to be underlined that the experimental tests presented in the paper, have involved new timber beams with clearly defined boundary conditions. To assess the real effectiveness of this method (regarding the refurbishment of old floors), an experimental campaign on existing sagged beams, should therefore be undertaken. Particular attention will have to be paid to the internal forces that this procedure generates into an allegedly deteriorated beam.

Both the experimental tests and the numerical model have shown that the best way to obtain an upward deflection is to start the assembly from the center and proceed towards the ends of the beam.

The proposed analytical formula seems to be able to reproduce the experimental behavior and presents the benefit of being “easily manageable”. This is mainly due to the choice of considering a constant fastener spacing along the beam axis. Otherwise, it would have been necessary to introduce Fourier transforms (Chapter 6) that would have

prevented the analytical model from being handled without a specific software for symbolic calculation.

7.6 References

Ballerini M., *Composite beams with deformable connections*, Course handbook

CSI [Computers and Structures Inc.], (2004), *CSI Analysis Reference Manual For SAP2000*®, ETABS® and SAFE®, *CSI, Berkeley*

Newmark N.M., Siess C.P., Viest I.M., (1951), *Tests and Analyses of Composite Beams with Incomplete Interaction*, Proceedings, Society for Experimental Stress Analysis, Vol. 9, No. 1, 75-92

Tomasi R., Crosatti A., Piazza M., (2010), *Theoretical and experimental analysis of timber-to-timber joints connected with inclined screws*, Construction and Building Materials 24: 1560-1571

8 EXPERIMENTAL CAMPAIGN ON THE COMPRESSION PRESSURE DEVELOPED BY SCREW FASTENERS

8.1 Introduction

As reported in Chapter 6, the friction phenomena due to the pressure generated by screw fasteners, have a significant influence on the behavior of composite timber structures. Moreover, the effectiveness of the original cambering method proposed in Chapter *7*, relies completely on the possibility of introducing in the composite beam elements axial forces by means of inclined screws. In addition, a better knowledge of the pressure level that is applicable through screws, could prove quite useful for the small-scale production of glulam beams and cross lam panels by local carpentries. So as to address all these issues an extensive testing campaign (170 tests) was carried out at the Laboratory of the Department of Mechanical and Structural Engineering (DIMS) of the University of Trento. Many parameters and screw typologies were investigated.

8.2 Test setup

The basic setup adopted for the tests was fairly simple and is reported in (Fig. 8.1). The pressure level was registered by four *25 kN* load cells with a *20 mm* central hole which allowed the passage of the fasteners. The dimensions of the steel load-spreading rings were chosen so as not exceed the design compressive strength perpendicular to the grain [EN 1995]. The stress level on the head element surface, has been determined considering the equivalent T-stub in compression approach [EN 1993-1-8]. Timber elements were made out of C24 double laminated (duo-beams) spruce. The moisture content (ω_{mean} *= 12.5 %, CoV = 7 %*) and material density (ρ_{mean} *= 450 kg/m*^{3}*, CoV = 4 %*) were measured for each wood specimen right before its use. The specimen width and depth were *160 mm* and *220 mm* respectively, while the specimen height was dependent on screw length. For the double-thread screws in fact, there was the need of inserting both threads equally into the timber elements since the room occupied by the load cell was bigger than the smooth part of the screw shank (except for SFS-WT-T 8.2x330).

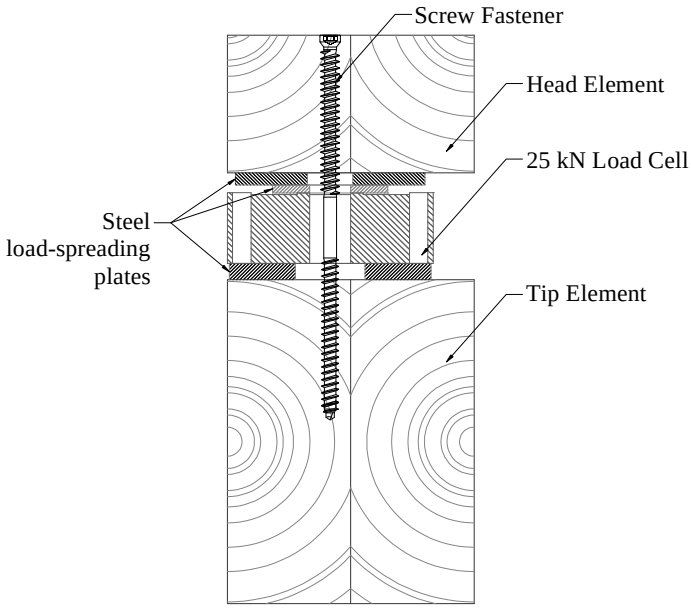

Fig. 8.1 Basic test setup

8.3 Preliminary tests

A first set of *20* tests were performed so as to determine which parameters had a real influence on the development of the screw pressure. The tests were conducted using double-thread self-tapping *8.2 mm x 190 mm* SFS-WT-T [Z-9.1-472] screws (Fig. 8.2), with the exception of 4 tests carried out using longer screws (*8.2 mm x 220 mm* and *8.2 mm x 300 mm* SFS-WT-T).

Fig. 8.2 SFS –WT-T screw

The preliminary-test matrix is given in Tab. 8.1 where 7 different test typologies are reported. For each typology a minimum of two repetitions were carried out. “Short term” (ST) means that the screw pressure was monitored at least for *30 min* while “long term” (LT) implies a test duration of more than *15 h*. Considered the specimen dimension, to facilitate the assembly it was necessary to apply a certain pre-load to the wood elements by means of two clamps, which were removed right after the screw insertion.

The standard pre-load adopted for the preliminary tests was *0.6 kN*. To investigate the influence of this parameter, type *2* tests were instead carried out with a pre-load of *2.4 kN*, which might also represent the effect produced by the presence of an adjacent screw. Type *3* tests were performed with the fastener positioned on the glueline between the two lamella forming the double laminated element. The effect produced by possible predrilling was investigated in type *4* tests, while type *5* tests were thought to study what happens when the fasteners are driven in the "radial" direction rather than in the "tangential" one. In test type *6* instead, the screws were inserted with a 45° angle to the grain direction, a configuration which is quite common for double thread screws.

Test type *7* saw the use of longer screws (*300 mm*) which permitted to have a first glimpse on the relation between the resultant pressure and the thread length[6]. The motivation behind this test type (thread length might seem an "obvious" parameter which therefore should have been left for the main campaign) was to confirm the design load adopted for the load-spreading plates.

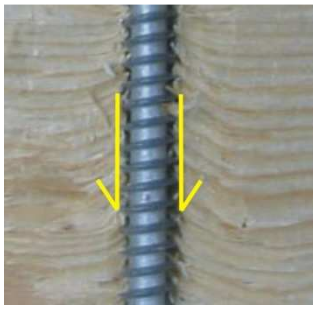

Fig. 8.3 Wood grain-fastener screw interaction

The capability of exerting a certain pressure is due to the screw on the threaded part of the fastener. Let us consider a single thread screw. Once the fastener head is in contact with the timber element, each screw spin "bends" the wood grain because any screw feed is hindered by the head contact (Fig. 8.3). This produces a compression stress between the two timber elements. Such compression load, whose spreading area depends on the wood stiffness, grows until the fastener head starts penetrating the timber (that is when the screw-driving usually stops). The number of spins required to fully develop that load, varies according to the timber modulus of elasticity (MoE). Consequently the resultant pressure is not affected by the load-spreading plate dimensions which yet determine the "spin number". Different is the case of a double

[6] The load-spreading plate thickness was *12 mm*.

thread screw where the number of spins is governed by the need of not having any thread crossing the interface between the two timber elements. Hence, given the "spin number", the bigger the load-spreading area the higher the resultant pressure. To deepen the understanding of this issue, test type 8 were carried out increasing the plate thickness from *6 mm* to *25 mm* (so that the stress distribution could be considered uniform on the whole specimen surface). For the sake of comparison, to have the same effective thread-length[7], *8.2 mm x 220 mm* SFS-WT-T were used. It is evident that very thick plates mean quite a wide load spreading that might not be consistent with the real condition where two timber elements are in contact. On the other hand, this "diffusion length" is difficult to estimate since it depends on the resultant pressure magnitude which is the object of the testing campaign.

Test label	Duration	Duo-Lam orientation	Inclination to the grain direction	Pre-drilled hole diameter [mm]	Position	Clamp Load [kN]
1a	LT	Vertical	90°	-	Mid-Lamellae	0.6
1b	ST	Vertical	90°	-	Mid-Lamellae	0.6
1c	ST	Vertical	90°	-	Mid-Lamellae	0.6
2a	ST	Vertical	90°	-	Mid-Lamellae	2.4
2b	ST	Vertical	90°	-	Mid-Lamellae	2.4
2c	LT	Vertical	90°	-	Mid-Lamellae	2.4
3a	ST	Vertical	90°	-	Glue line	0.6
3b	ST	Vertical	90°	-	Glue line	0.6
4a	ST	Vertical	90°	5	Mid-Lamellae	0.6
4b	ST	Vertical	90°	5	Mid-Lamellae	0.6
5a	ST	Horizontal	90°	-	Mid-Lamellae	0.6
5b	ST	Horizontal	90°	-	Mid-Lamellae	0.6
5c	LT	Horizontal	90°	-	Mid-Lamellae	0.6
6a	LT	Vertical	45°	-	Mid-Lamellae	0.6
6b	ST	Vertical	45°	-	Mid-Lamellae	0.6

[7] Considered that the load-cell height plus the plate thickness is bigger than the smooth part of the fastener shank, "effective thread length" stands for "thread length really inserted into the timber element".

6c	ST	Vertical	45°	-	Mid-Lamellae	0.6
7a	ST	Vertical	90°	-	Mid-Lamellae	0.6
7b	LT	Vertical	90°	-	Mid-Lamellae	0.6
8c	ST	Vertical	90°	-	Mid-Lamellae	0.6
8d	LT	Vertical	90°	-	Mid-Lamellae	0.6

Tab. 8.1 Preliminary-test matrix

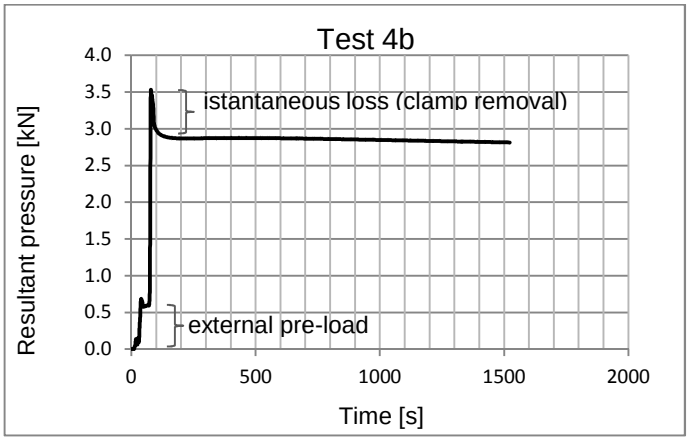

Fig. 8.4 Typical Resultant pressure Vs. Time curve

Fig. 8.4 reports a typical resultant pressure Vs. time curve. It can be noted a first step corresponding to the load applied by the two clamps. An instantaneous pressure loss due also to the clamp removal is noticeable. Such loss was nearly the same amplitude as the pre-load.

The comparison between the test results obtained from the preliminary testing phase is given in Fig. 8.5. It appeared that the presence of a pre-drilled hole did not influence the resultant pressure as well as the “radial screw driving”. A slightly bigger change (a variation of about 10% with respect to test type 1) was observed for test type 3 and test type 6. It must be noted that test type 6 were affected by a high scattering (*CoV = 0.16*) and therefore required further investigation. Test type 7, as expected, provided a much higher resultant pressure than the reference type 1, while test type 8 permitted to reach an extra *1 kN*. Same pressure level was achieved simulating the presence of an adjacent fastener, by imposing a 2.4 kN external load through the clamps (type 2). As previously asserted, from Fig. 8.6 it can be seen that even in case of a higher external

load, the pressure loss measured at clamp release moment (with respect to the maximum pressure point) was about the same value as the clamp pre-load.

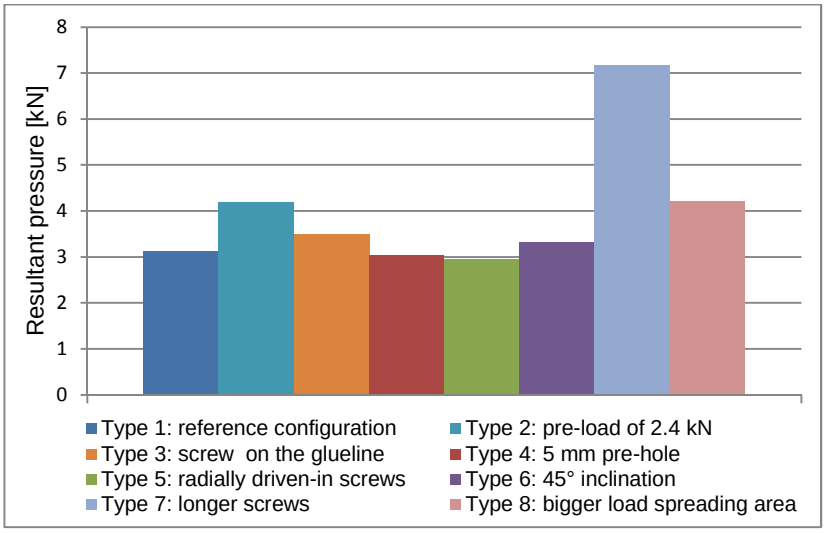

Fig. 8.5 Preliminary-test result comparison (10 min after the clamp removal)

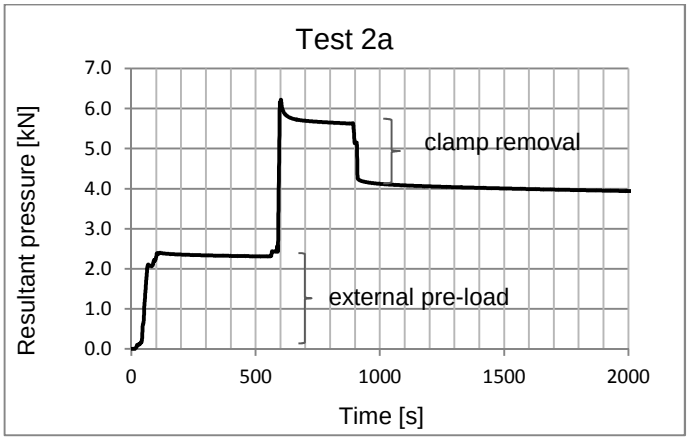

Fig. 8.6 Resultant pressure Vs. Time

Regarding the *LT* tests, the resultant-pressure variation, measured in the *15* hours following the clamp removal, is given in Tab. 8.2. Obviously, the number of tests

involved does not allow to make any general statement. It is interesting to note that test *1a* showed a bigger loss than test *2c* where, despite the same spreading plates, a bigger compression pressure was achieved due to a higher clamp load. By contrast, test 8b which provided the same pressure magnitude as test *2c*, behaved as it was supposed to, showing a lower pressure loss because of the employment of thicker plates.

Test	$\Delta P_{15\,h}$ [%]
1a	39.9
2c	30.2
5c	23.0
6a	19.7
7b	28.2
8b	15.1

Tab. 8.2 Pressure loss 15 h after the clamp removal

8.4 Main experimental campaign

In the main set of tests, which consisted of *150* tests, *5* different connector typologies were taken into account. Both double-thread and single-thread screws were considered (Fig. 8.7). Each fastener typology was tested with different diameters and thread lengths. The effect of a *45°* inclination to the grain direction was also investigated. A minimum of two *ST* tests plus one *LT* test was performed for every combination of investigated parameters. All the tests were conducted with an external load of *0.8 kN* to avoid any specimen spinning due the torque applied by the drill during the assembly. To roughly approximate a realistic load diffusion, two spreading plates thicknesses were chosen according to the thread length: *6 mm* plates were used for fastener with a thread length smaller or equal to *75 mm*, while for longer threads *12 mm* plates were adopted.

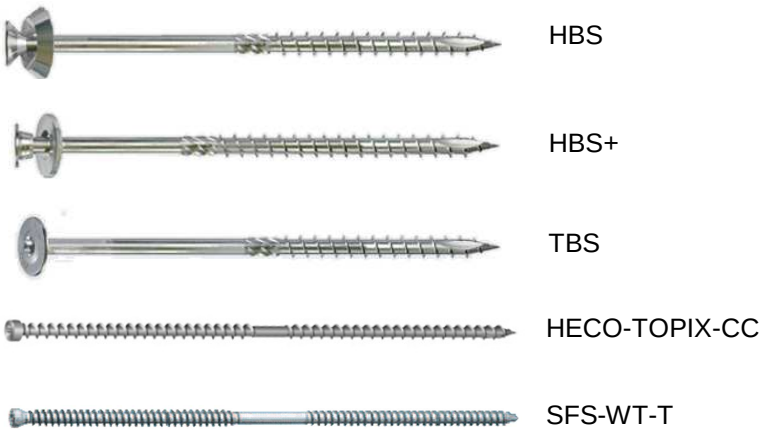

Fig. 8.7 Tested connector typologies

HBS			HBS Plus			TBS		
d [mm]	L [mm]	Effective thread length [mm]	d [mm]	L [mm]	Effective thread length [mm]	d [mm]	L [mm]	Effective thread length [mm]
6	120	47	6	120	47	6	120	47
	260	75		260	75		200	75
8	260	80	8	260	80	8	260	100
	300	100		300	100		300	100
10	260	80						
	300	100						

SFS-WT-T			HECO-Topix-CC		
d [mm]	L [mm]	Effective thread length [mm]	d [mm]	L [mm]	Effective thread length [mm]
6.5	190	68.5	6.5	190	68.5
	220	83.5		215	81.0
8.2	220	83.5	8.5	215	81.0
	330	135		350	148

Tab. 8.3 Tested connector size

Tests were also conducted on chestnut specimens (ω_{mean} *= 27.0 %,CoV = 26 %,* ρ_{mean} *= 814 kg/m, CoV = 1 %*). It must be said that the torsional force necessary to drive the screws into the chestnut specimen, was such to determine several snaps of the

fasteners, which determined the impossibility of testing some of the fastener configurations.

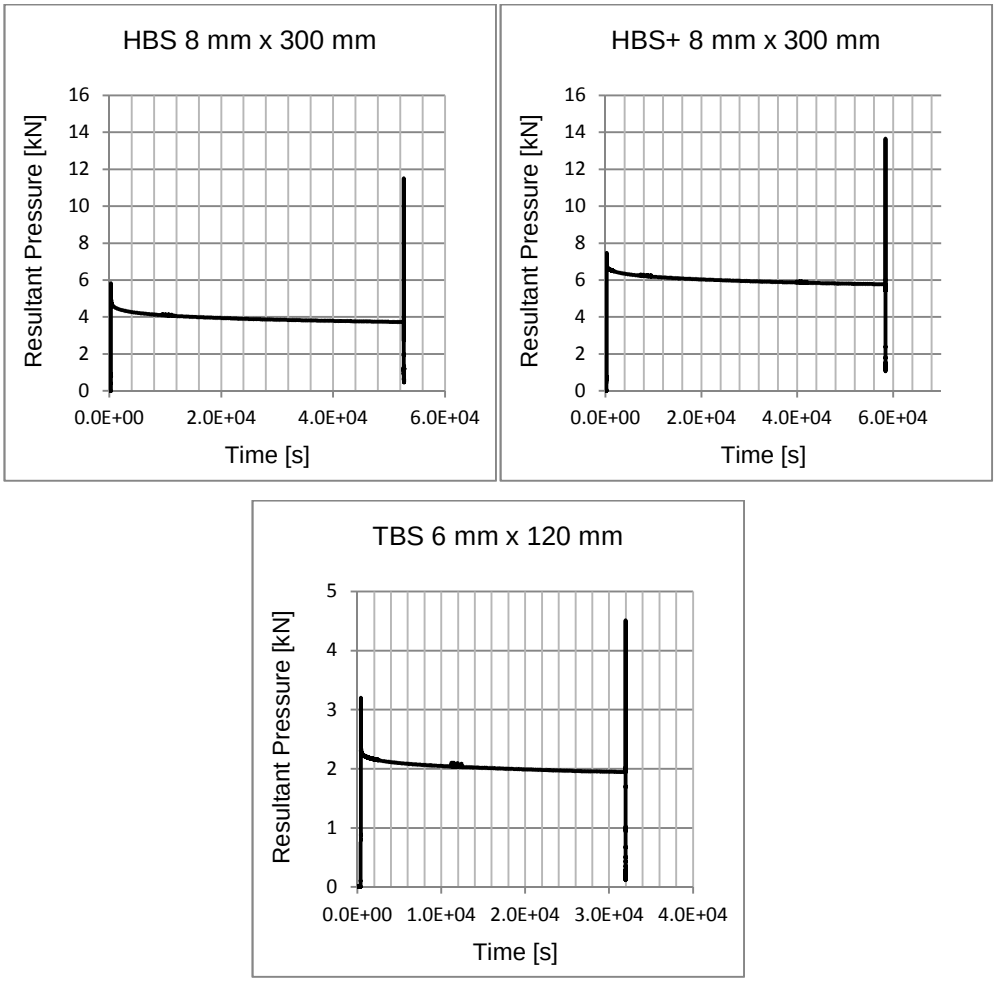

Fig. 8.8 Single thread screws with washer: effect of an excessively prolonged driving-in procedure

As previously mentioned, the screw driving usually terminates when the fastener head starts penetrating the timber element. In case of washer usage (or screws with an enlarged head, like *TBS*'s), particular attention should be paid to avoid an excessive screwing, since failure occurs with no notice. Allowing a certain "head embedment" (about *5 mm*) makes it possible to reach much higher pressure values. Fig. 8.8 reports the resultant pressure Vs. time curves of three tests where extra screwing was applied

after *15 h* (so as not to waste any test). An instantaneous compression-increase was observed, up to resultant pressure values close to the nominal withdrawal capacity of the fastener. Then, suddenly the grain rupture made the screw spin and the pressure go down to almost zero.

8.5 Test result comparison

From the test results presented in Fig. 8.9 it seems that double thread screws permit to obtain compression levels much higher than those reached with single thread screws, even in case of washer presence. The pressure generated by single thread screws was in fact limited by the fastener head pull-through capacity. As a result, the compression level observed in the tests corresponds to the head pull-through capacity determined following the provisions contained in the product standard [ETA 11/0030]. The employment of washers, on the other hand, allowed to reach a compression load of about *60*% of the pull-through capacity of the washers. The *HBS+* screws, with their head specifically designed to limit the timber penetration, yielded a mean compression level *50 %* higher than that one generated by the "standard" *HBS*. An extra *30 %* was achieved by employing *TBS* fasteners which have a larger head.

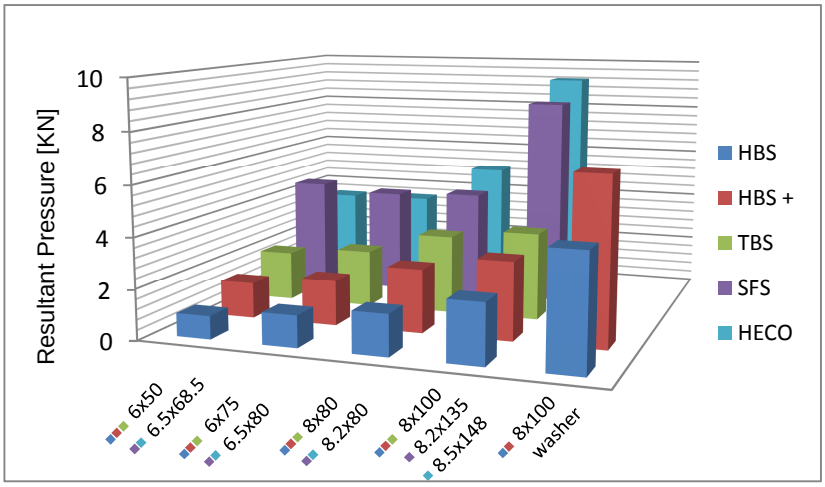

Fig. 8.9 Resultant pressure for different fastener typologies and sizes (diameter x thread length[8]), 30 min after the clamp removal

[8] For double thread screws, thread length corresponds to the length of one thread.

As regards the effect of the grain direction, it appears that the fastener inclination is not a key parameter in determining both the pressure level (Fig. 8.10) and the time-dependent behavior[9] (Fig. 8.13, Fig. 8.14). The only exception was observed for the *HBS 10x300* screws. In that case the pressure level rose of nearly *80 %* going from a fastener inclination of 90° to a 45° one.

[9] Obviously this consideration might not be valid for screw-to-grain angles smaller than 45°.

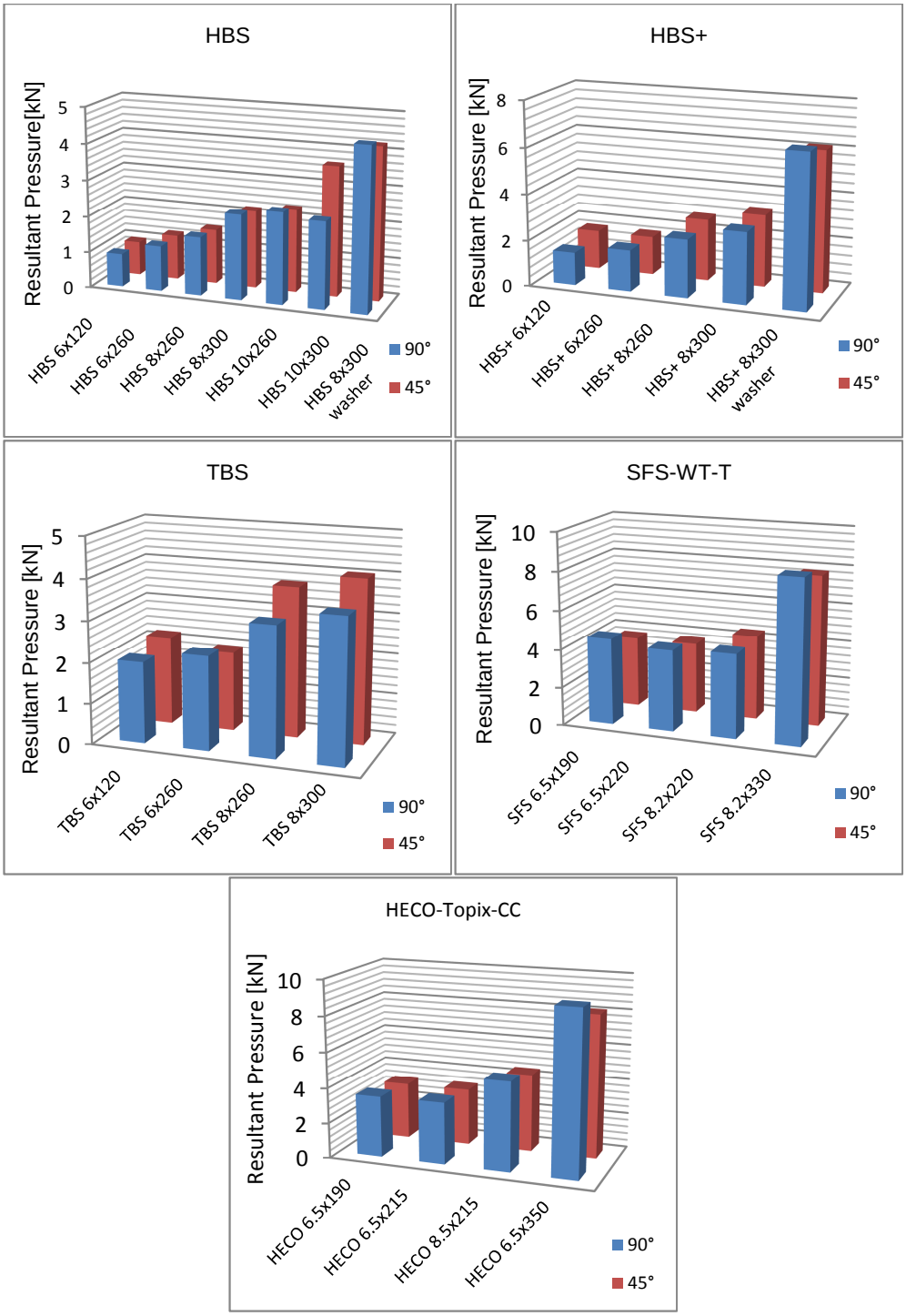

Fig. 8.10 Comparison between tests with screws at 45° and tests with screws at 90°

Fig. 8.11 gives the results obtained from the tests carried out on the chestnut timber elements. An average increase of nearly *60 %* of the compression generated by single thread screws was observed. A probable reason might be found analyzing the pull-through capacity formula [ETA 11/0030] which contains the following member:

$$\left(\frac{\rho_k}{350}\right)^{0.8} \qquad \textit{(Eq. 7.42)}$$

Consequently, providing that the head pull-through capacity is the limiting factor, it can be noted how a wood density *80 %* bigger (as it was observed for the chestnut), would yield a pressure increase of *60 %*. Double-thread screw pressure, appeared instead not to be positively influenced by the augmented wood density. This result seems to be in contrast with the hypothesis regarding the effect of a MoE variation on double-thread screw pressure which was previously expressed. As a matter of fact the higher density offered by the chestnut is accompanied by a higher MoE as well, which did not result in a bigger compression level. The cause might be related to the different microstructure that characterizes hardwoods.

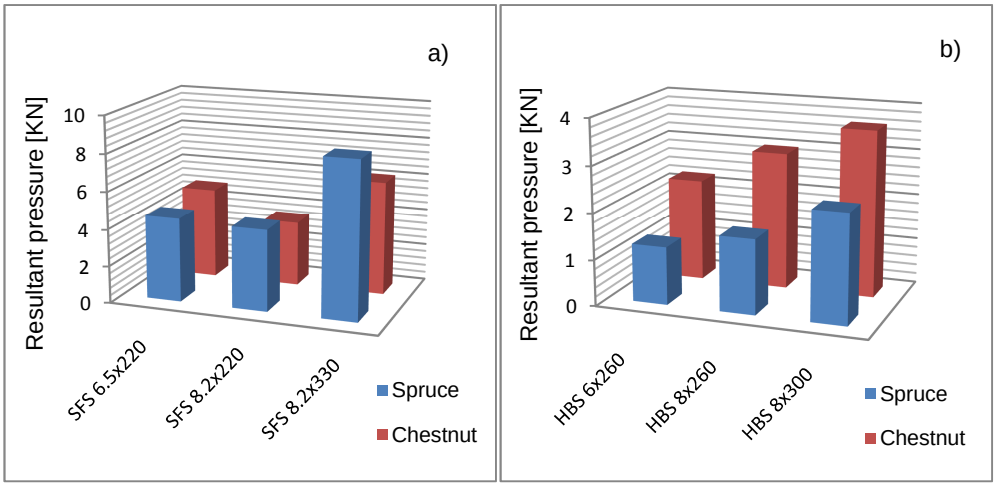

Fig. 8.11 Effect of wood species:a) Double-Thread screws; b) Single-Thread screws

The pressure loss measured *30 min* after the clamp removal is reported in Fig. 8.12, for each fastener typology. It can be seen that the loss was affected by the screw size: the bigger the screw (diameter or thread length) the smaller the reduction. Double thread screws showed the lowest decrease, with *SFS-WT-T* which presented even a gain. Such peculiar behavior can be appreciated in Fig. 8.14 where the specimen pressure loss is plotted against time for the first half an hour after the clamp removal. *TBS* screws

that offered the highest compression values among the single thread screws, were also those affected by the highest loss. This trend is clearly noticeable just in the first hour after the fastener insertion. At *15 h* from the clamp removal, the single thread screws showed a pressure loss nearly twice as big as the reduction offered by the double thread screws. A particularly low level of reduction was observed for those *SFS* screws which presented the higher initial pressure-gain. *HBS 10x300* screws (thread length = *100 mm*) showed half of the pressure loss (*CoV = 13 %*) registered for the other single thread screws of similar size.

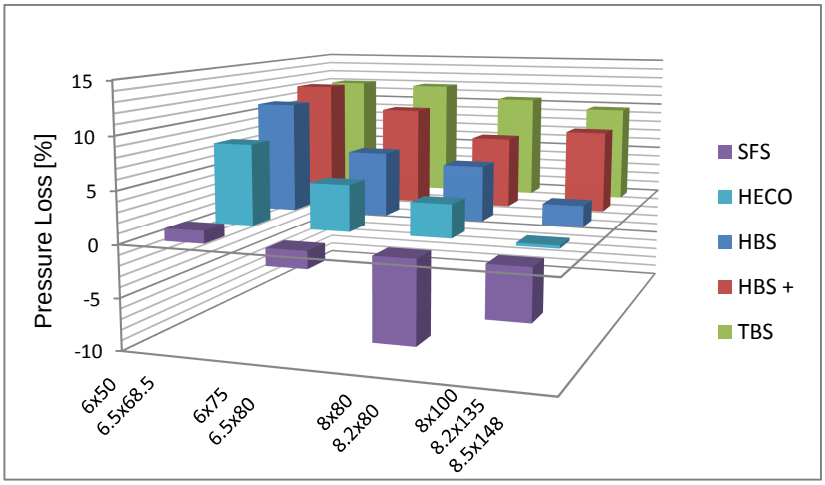

Fig. 8.12 Short term (30 min) pressure loss

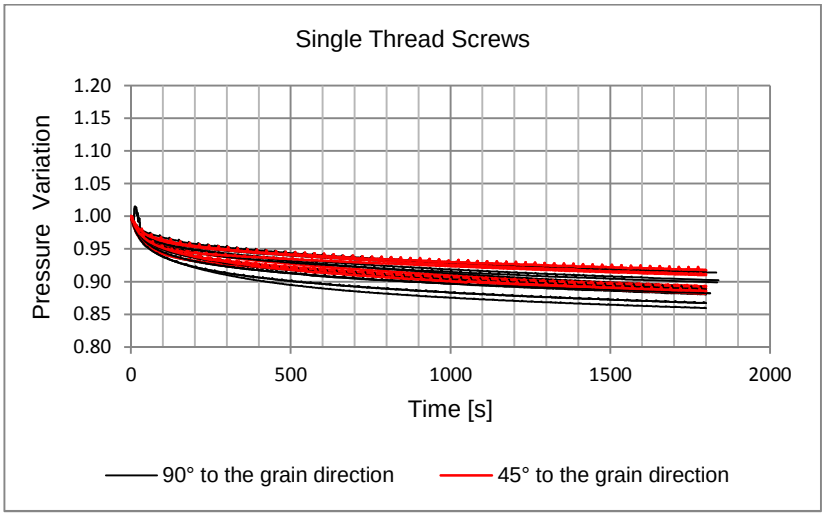

Fig. 8.13 Short term pressure variation: single thread screws (curves normalized to the clamp release moment)

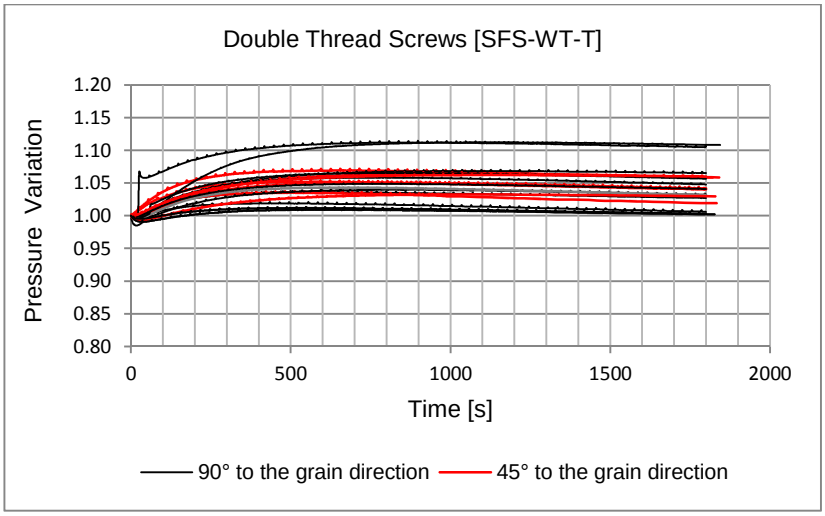

Fig. 8.14 Short term pressure variation: double thread screws

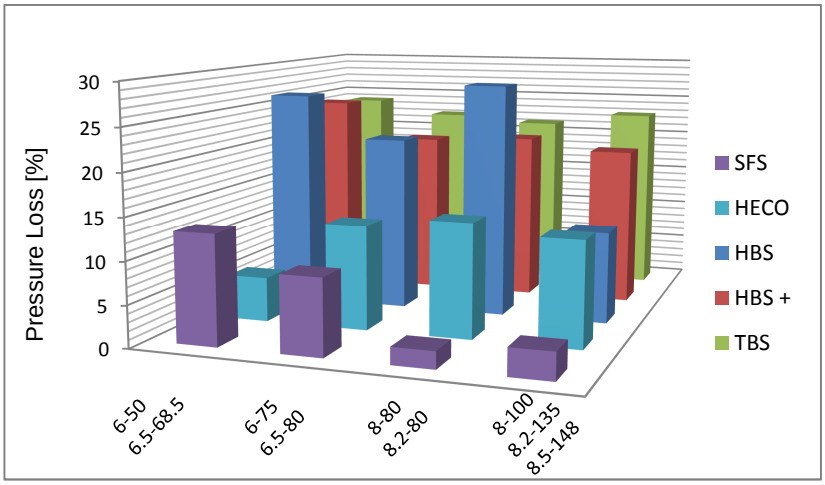

Fig. 8.15 Long term (15 h) pressure loss

8.6 Pressure prediction formula

An experimental formula to predict the screw pressure[10] was determined. The general structure of the formula is:

[10] Measured 10 min after the clamp removal

$$T = \gamma \left(d \cdot l_{th} \right)^{\alpha} \rho^{\beta} \cdot \varphi \qquad \textit{(Eq. 7.43)}$$

Where T is the resultant pressure generated by the fastener [N], d is the connector diameter [mm], l_{th} is the threaded part length [mm] (for double-threaded screws l_{th} is the length of one of the threads), ρ is the wood density and α, β, γ are experimental parameters ($\alpha = 3/5$, $\beta = 20/7$, $\gamma = 2.67 \cdot 10^{-6}$). φ is a parameter depending on the screw typology (Tab. 8.4).

	φ
Heco Topix CC	1
SFS WT	0.95
HBS	0.63
HBS+	0.52
TBS	0.39

Tab. 8.4 φ values

For single-thread screws, in case of washer presence, the φ value has to be doubled. Tab. 8.5 shows the comparison between the experimental values of T and those obtained through (Eq. 7.43) for the various connector typology. It can be noted how (Eq. 7.43) is able to predict the resultant pressure with sufficient accuracy. The maximum error obtained was in fact about 12.5%.

Screw Typology	diameter x length	T - Experimental [KN]	T - Analytical [KN]	Err. [%]
HBS	6x120	1.027	1.108	7.9
	6x260	1.330	1.189	-10.6
	8x260	1.711	1.861	8.8
	8x300	2.402	2.394	-0.3
	10x260	2.737	2.744	0.3
	10x300	2.568	2.549	-0.7
	8x260/washer	4.946	4.788	-3.2
HBS Plus	6x120	1.629	1.591	-2.3
	6x260	2.686	2.449	-8.8
	8x260	2.721	2.854	4.9

	8x300	3.102	3.298	6.3
	8x300/washer	7.086	6.595	-6.9
TBS	6x120	2.096	1.978	-5.6
	6x200	2.613	2.407	-7.9
	8x260	3.264	3.671	12.5
	8x300	3.388	3.602	6.3
SFS-WT-T	6.5x190	4.919	4.608	-6.3
	6.5x220	4.175	3.861	-7.5
	8.2x220	3.782	4.152	9.8
	8.2x330	8.042	8.125	1.0
HECO-Topix-CC	6.5x190	3.923	3.748	-4.5
	6.5x215	3.684	3.957	7.4
	8.5x215	5.209	4.648	-10.8
	8.5x350	9.202	9.157	-0.5

Tab. 8.5 Comparison between experimental data and analytical values

8.7 Conclusions

From the analysis of the test results, it appears that screw fasteners can exert a considerable compression force on the timber elements that they are connecting. The observed pressure values ranged from nearly *1 kN* to about *9 kN*, accordingly to the connector size and typology. By showing the highest resultant pressure values and the smallest losses, double thread screws proved to be the most effective fasteners. Single thread screw performance, on the other hand can be improved by the employment of washers. The inclination to the grain direction did not show a significant influence on the results. It should be kept in mind that, despite an elevated number of tests, the "population" such considerations are based on is relatively small (considered the result variability), owing to the several parameters investigated.

The research is still ongoing and further study has certainly to be carried out. Particular regard should be paid to the determination of the "load diffusion area" at the interface between the two timber elements. Considering the new cambering method proposed in chapter *7*, additional tests are suggested to deepen the understanding of pressure evolution at really long term.

The proposed experimental formulation, seems to be able to estimate the resultant pressure obtained through the different screws, with sufficient accuracy. Future developments will involve the possibility of taking into account the wood species and a precise time-dependent relation.

8.8 References

EN 1993-1-8:2005 (E), (2005), *Eurocode 3: Design of steel structures - Part 1-8: Design of joints*

EN 1995-1-1:2004, (2004), *Eurocode 5: Design of timber structures - Part 1-1: General - Common rules and rules for buildings*

ETA-11/0030, (2011), *Self-tapping screws for use in timber structures*, European Technical Approval

Z-9.1-472, (2006), *Viti di fissaggio SFS WT-T-6,5, WT-T-8,2 e WR-T-8,9 come elementi di fissaggio per legno* Deutsches Institut fűr Bautechnik, DIBt Kolonnenstraße 30, Berlin

Z-9.1-665, (2007), *Viti HECO-TOPIX-CC CombiConnect come elementi di collegamento per legno*, Deutsches Institut fűr Bautechnik, DIBt Kolonnenstraße 30, Berlin

9 CONCLUSIONS

The pushover analysis of a traditional URM building modeled through the equivalent frame method, showed that as-built square sheathed timber diaphragms behave quite poorly and prevent masonry structures from developing their full capacity in terms of strength and “ductility”. Therefore the stiffening and strengthening of wood floors is a crucial issue in the process of reducing the seismic vulnerability of heritage masonry buildings. It appears though, that the choice of the retrofit technique is not fundamental, as long as a certain stiffness-threshold is reached. Since the capacity curves appeared to be influenced by the masonry modeling method (macro-element based), a different approach (continuum based) was studied.

A linear elastic procedure which allowed take into account masonry low tensile strength was proposed. This method also permitted a rough evaluation of the damage evolution with the advantage of being extremely simple and “user-friendly”. From the results it seems that the importance of modeling a realistic diaphragm stiffness becomes significant only when a remarkable eccentricity between the mass center and the stiffness center is present. It should be noted that in ancient masonry buildings, the center of mass is related to the center of stiffness because the timber diaphragm seismic mass is very small compared to the masonry skeleton mass. Obviously it has to be remembered that second mode failure mechanisms were not analyzed in the present thesis. It was also observed that passing from a nonlinear modeling of the timber diaphragm to a linear one (provided the correct target point) does not affect the prediction of the global seismic response of a masonry building.

To deepen the understanding of timber floor in-plane behavior a parametric analysis was conducted focusing on single square sheathed diaphragms, by calibrating a finite element model. As expected, nails proved to be the governing parameter in determining the floor deformations. The floorboard disposition appeared to be a quite important factor as well. When subjected to lateral loads corresponding to different seismic acceleration levels, timber floor diaphragms exhibit a nonlinear response. Consequently, even if floors might be treated as linear materials in a full-scale model of the building, it is necessary to have a nonlinear formulation, in order to be able to predict the correct value of the equivalent secant stiffness. To this purpose, an analytical formula was proposed.

An *in-situ* experimental campaign on full-scale 100 year old timber diaphragms was performed during a 4 month exchange period at the University of Auckland. Both quasi-static and dynamic tests were conducted thanks to an *ad-hoc* test setup. Besides the as-built condition, different retrofit solutions were also tested. The test results were compared to the suggestions provided by the relevant standards and guidelines on seismic assessment of existing vintage timber diaphragms. It appears that NZSEE suggests stiffness values for single straight sheathed diaphragm that are very close to those registered experimentally, while FEMA and ASCE tend to overestimate the diaphragm stiffness because they do not consider the orthotropic behavior of diaphragms. Once the plywood panel overlay is applied, the response is governed by the plywood and consequently the values provided in FEMA and ASCE are similar to the experimental ones.

The “re-nailing” method proved to be a valid strengthening solution. In fact, with a very low cost-effectiveness ratio, it permitted an increase in stiffness of up to 30%, which ensured that the tested floor section had the capacity to transfer shear loads corresponding to severe seismic events within acceptable drift levels. An extremely stiff response was achieved through the installment of a plywood panel overlay directly onto the existing floorboards. Such behavior was maximized by the peculiar panel disposition which also allowed a very fast installation procedure. The natural period evaluation approach proposed in Chapter 5 proved to be a helpful guidance when determining the shear load transfer. Considering the material property variability (e.g. conservation status, wood species, element dimensions), further testing need to be performed to make the outcomes of the campaign presented in the present thesis more representative. The test setup designed for this experimental campaign was shown to be non-invasive, easy to install and versatile (adaptable to different-sized specimens).

Poor in-plane mechanical properties of timber diaphragms are often accompanied by inadequate out-of-plane strength and stiffness and vice versa. Therefore, to comply with recent standards, particular care has to be paid to the refurbishment of vintage wood floors. An experimental campaign on timber-to-timber strengthening solutions, all realized by using screw fasteners, was carried out. The adopted fastener configurations permitted to reach extremely high levels of connection efficiency under service loading. Solutions with fasteners inclined at 45° showed higher collapse loads. It was observed that the approach embodied in EN 1995 when a suitable stiffness calculation method is adopted, is able to accurately predict the midspan deflection with no need of finer modeling.

To address the problem of sagged timber floors (which sometimes cannot be buttressed due to heritage issues), an innovative method to camber a timber beam by just superposing a “dry reinforcement element” was presented. The results obtained from preliminary tests conducted on new timber beams showed the possibility to achieve significant values of upward deflection. The method proved to be more effective when the assembly procedure starts from the center of the beam. To help study the cambering phenomenon a numerical model was calibrated on the experimental data. An analytical cambering prediction formula was also proposed. Because a close solution to the nonlinear problem governing the cambering process was found, the analytical expression is relatively simple and easy to handle. Certainly further testing has to be performed in order to investigate the effect that the internal stress state induced by the cambering procedure has on vintage timber beams. Particular attention should also be paid to the method effectiveness in case of unclear boundary conditions.

The cambering method described in Chapter 7 relies on the possibility of introducing an axial stress into the beam by using an inclined screw fastener. Consequently, the definition of the pressure that screws are able to exert is a crucial point. Therefore a wide experimental campaign was conducted. Double thread screws have shown to be the most effective fasteners, yielding remarkable resultant pressure values. It was observed that that the inclination to the grain direction have a small influence on the pressure level. Because of the many parameters investigated, further testing is suggested to increase the “statistical population”.